

# **Comprehending Neural Networks**

via Translation to And-Inverter Graphs

**Jarren Briscoe**

A thesis submitted for the degree of  
Master of Science of Computer Science



**WEBER STATE  
UNIVERSITY**

Department of Computer Science  
Weber State University  
United States of America  
January 9, 2021

## Supervisory Committee

**Signature:** *Robert Ball*

**Email:** robertball@weber.edu

Jan 29, 2021

---

Committee Chair, Dr. Robert Ball

**Signature:** *Kyle Feuz*

**Email:** kylefeuz@weber.edu

Jan 29, 2021

---

Committee Member, Dr. Kyle Feuz

**Signature:** *Brian Rague*

**Email:** brague@weber.edu

Jan 29, 2021

---

Committee Member, Dr. Brian Rague

## Author

**Signature:** *Jarren Briscoe*

**Email:** jarrenbriscoe@mail.weber.edu

Jan 29, 2021

---

Student, Jarren Briscoe

# Contents

|           |  |           |
|-----------|--|-----------|
| <b>I</b>  | <b>Introduction</b>                          | <b>11</b> |
| 1         | Abstract, Format, and Purpose                | 13        |
| 2         | Introduction                                 | 15        |
| 2.1       | Background Summary . . . . .                 | 15        |
| 2.2       | A Comprehensible Medium . . . . .            | 16        |
| 2.3       | Neural Networks Considered . . . . .         | 16        |
| 2.4       | Converting Neural Networks to AIGs . . . . . | 17        |
| 2.5       | Reasoning and Results . . . . .              | 18        |
| <b>II</b> | <b>Background</b>                            | <b>19</b> |
| 3         | Neural Networks                              | 21        |
| 3.1       | Structure . . . . .                          | 21        |
| 3.2       | Types of Activation Functions . . . . .      | 25        |
| 4         | Graphs                                       | 29        |
| 4.1       | Graphs . . . . .                             | 29        |
| 4.2       | ABC Software . . . . .                       | 32        |
| 5         | Comprehension                                | 35        |
| 5.1       | Understanding . . . . .                      | 35        |
| 5.2       | Quantifying Comprehensibility . . . . .      | 38        |
| 5.2.1     | Quantified Definition . . . . .              | 38        |
| 5.2.2     | AIG versus Neural Network . . . . .          | 39        |
| 5.3       | Inputs . . . . .                             | 41        |
| 5.4       | Tips and Further Reading . . . . .           | 43        |

|   |               |
|---|---------------|
| <b>6 Other Influential Works</b>                        | <b>45</b>     |
| 6.1 Chatterjee . . . . .                                | 45            |
| 6.2 Brudermueller et al. . . . .                        | 46            |
| 6.2.1 ABC and AIGs . . . . .                            | 47            |
| 6.3 Shi et al. . . . .                                  | 47            |
| <br><b>III Methods</b>                                  | <br><b>49</b> |
| <b>7 XORNN</b>  | <b>53</b>     |
| 7.1 Definitions . . . . .                               | 53            |
| 7.2 Creating XORNNs . . . . .                           | 55            |
| 7.2.1 XORNN Code . . . . .                              | 55            |
| 7.2.2 Rationale for Algorithm 2 . . . . .               | 59            |
| 7.2.3 Time Creating XORNN . . . . .                     | 60            |
| 7.3 Understanding XORNN . . . . .                       | 61            |
| 7.4 Learning XORNN . . . . .                            | 64            |
| 7.4.1 Creating a Decision Tree Network . . . . .        | 64            |
| 7.5 Understand the Decision Tree Network . . . . .      | 66            |
| <br><b>8 Importance</b>                                 | <br><b>73</b> |
| 8.1 Weights . . . . .                                   | 73            |
| 8.2 Monotonic Functions . . . . .                       | 74            |
| 8.2.1 Proving a Function is Monotonic . . . . .         | 76            |
| 8.3 Generalizing to More Activation Functions . . . . . | 77            |
| 8.4 Application to $\mathcal{B}$ . . . . .              | 82            |
| <br><b>9 Parsing the Neural Network</b>                 | <br><b>85</b> |
| 9.1 Brute Force . . . . .                               | 86            |
| 9.2 Binary Decision Tree ( $\mathcal{B}$ ) . . . . .    | 88            |
| 9.2.1 Order . . . . .                                   | 89            |
| 9.2.2 $\mathcal{B}$ Defined . . . . .                   | 89            |
| 9.2.3 Complexity . . . . .                              | 94            |
| 9.3 Traversing the Neural Network . . . . .             | 95            |
| 9.4 Additional Ideas . . . . .                          | 97            |
| 9.4.1 Maximum Tree Depth . . . . .                      | 97            |
| 9.4.2 Subtrees and Dynamic Programming . . . . .        | 99            |
| 9.5 Alternatives . . . . .                              | 99            |

|  |            |
|--|------------|
| <b>CONTENTS</b>  | <b>5</b>   |
| 9.5.1 Linear Algebra . . . . .                               | 99         |
| 9.5.2 A Table-Based Approach . . . . .                       | 100        |
| <b>10 Empirical Complexity of <math>\mathcal{B}</math></b>   | <b>105</b> |
| 10.1 Node Complexity . . . . .                               | 105        |
| 10.1.1 Average Node Complexity . . . . .                     | 106        |
| 10.1.2 Worst-Case Node Complexity . . . . .                  | 109        |
| 10.1.3 Exhaustive Case . . . . .                             | 112        |
| 10.2 Time Complexity . . . . .                               | 112        |
| 10.2.1 Average Time Complexity . . . . .                     | 112        |
| 10.2.2 Worst-Case Time Complexity . . . . .                  | 115        |
| 10.2.3 Brute-Force Complexity . . . . .                      | 117        |
| 10.2.4 Average, Worst, and Brute Time Ratios . . . . .       | 120        |
| 10.3 Conclusion . . . . .                                    | 120        |
| <b>11 Don't-Care Variables</b>                               | <b>121</b> |
| 11.1 Red is Stop . . . . .                                   | 121        |
| 11.2 Binarization and Limitations . . . . .                  | 124        |
| 11.2.1 Real to Binary Inputs . . . . .                       | 124        |
| 11.2.2 Illustrating the Limitations of Algorithm 9 . . . . . | 124        |
| 11.3 Versicolor or Setosa . . . . .                          | 129        |
| 11.4 Ensemble of Neural Networks and AIGs . . . . .          | 139        |
| 11.4.1 Developing and Subtle Relationships . . . . .         | 139        |
| 11.4.2 Neural Network and AIG Ensemble Accuracy . . . . .    | 139        |
| <b>IV Results</b>  | <b>147</b> |
| <b>12 Results and Moving Forward</b>                         | <b>149</b> |
| 12.1 Conclusion . . . . .                                    | 149        |
| 12.2 Future Work . . . . .                                   | 150        |
| <b>V Appendix</b>  | <b>153</b> |
| <b>A Definitions</b>   | <b>155</b> |
| A.1 Abbreviations . . . . .                                  | 155        |
| A.2 Mathematical Symbols . . . . .                           | 156        |
| A.3 Complexity Symbols . . . . .                             | 156        |

|                          |     |
|--------------------------|-----|
| A.4 Vocabulary . . . . . | 157 |
|--------------------------|-----|

# List of Figures

|     |  |    |
|-----|--|----|
| 3.1 | A visual for the feedforward walkthrough . . . . .   | 24 |
| 3.2 | What is linearly separable data? . . . . .   | 25 |
| 4.1 | Binary Decision Diagram (BDD) . . . . .  | 32 |
| 4.2 | AIG as illustrated by ABC [1] . . . . .  | 33 |
| 5.1 | Understanding $n^{th}$ -order meta-cognition using mathematical induction. . . . .           | 36 |
| 5.2 | Using mathematical induction to understand an AIG. . . . .                                   | 37 |
| 5.3 | Comprehensibility comparison . . . . .   | 41 |
| 5.4 | Visualization of dimension reduction . . . . .   | 42 |
| 6.1 | The neural network to AIG pipelines contrasted in [2] . . . . .                              | 46 |
| 7.1 | Topology of a XORNN . . . . .  | 54 |
| 7.2 | Contour plots of a XORNN’s predictions . . . . .   | 58 |
| 7.3 | Bar graph of neural networks’ accuracy given the XOR data set                                | 59 |
| 7.4 | Scatterplot of training time versus epochs . . . . .   | 60 |
| 7.5 | Node sensitivity of a XORNN . . . . .  | 63 |
| 7.6 | Decision tree trained on XOR . . . . .   | 64 |
| 7.7 | Decision tree network trained on a XORNN . . . . .   | 65 |
| 7.8 | AIG representations of a XORNN . . . . .   | 71 |
| 8.1 | Graphs satisfying the diagonal quadrants property . . . . .                                  | 78 |
| 8.2 | Monotonic activation functions satisfy the diagonal quadrant property . . . . .              | 79 |
| 8.3 | Other functions satisfying the diagonal quadrant property given a decent threshold . . . . . | 80 |

|  |     |
|--|-----|
| 8.4 Activation functions that are conditional or not recommended for $\mathcal{B}$     | 81  |
| 9.1 Weight matrix format   | 88  |
| 9.2 Graphs for $\mathcal{B}$ 's worst and best cases                                   | 95  |
| 9.3 Illustrations of decision-tree networks given a maximum depth                      | 98  |
| 10.1 Graphs of average node complexities   | 107 |
| 10.2 The average increase of nodes over n weights                                      | 108 |
| 10.3 Graphs of worst-case node complexities  | 110 |
| 10.4 Average increase of worst-case nodes over n weights                               | 111 |
| 10.5 Graphs of $\mathcal{B}$ 's average time complexity                                | 114 |
| 10.6 Graphs of $\mathcal{B}$ 's worst-case time complexity                             | 116 |
| 10.7 Graphs of the brute-force time complexities                                       | 119 |
| 11.1 AIG representations of RYG  | 123 |
| 11.2 Line plots for the Iris data set  | 128 |
| 11.3 Optimal AIG for Versicolor or Setosa  | 130 |
| 11.4 An AIG for the Iris data set  | 131 |
| 11.5 An AIG from a separately trained neural network on the binarized Iris data subset | 134 |
| 11.6 An AIG from a larger neural network trained on the binarized Iris data subset     | 135 |
| 11.7 AIG abstractions with varying maximum depths in $\mathcal{B}$                     | 138 |
| 11.8 Distribution plot of AIG accuracy for the smaller neural network                  | 144 |
| 11.9 Distribution plot of AIG accuracy for the larger neural network                   | 145 |

# List of Tables

|      |   |     |
|------|---|-----|
| 7.1  | XOR's truth table . . . . .   | 53  |
| 7.2  | A XORNN as an LUT . . . . .   | 61  |
| 9.1  | A brute-force alternative for $\mathcal{B}$ . . . . .   | 86  |
| 9.2  | An example of step two in Section 9.5.2 (a less efficient alternative to $\mathcal{B}$ ) . . . . .    | 103 |
| 10.1 | Average node complexities of $\mathcal{B}$ . . . . .  | 106 |
| 10.2 | Worst-case node complexities . . . . .  | 109 |
| 10.3 | Node complexity of the exhaustive case . . . . .  | 112 |
| 10.4 | Average time complexity of $\mathcal{B}$ . . . . .  | 113 |
| 10.5 | $\mathcal{B}$ 's worst-case time complexity . . . . .   | 115 |
| 10.6 | Brute-force time complexities . . . . .   | 118 |
| 10.7 | Approximate ratios of the time complexities . . . . .   | 120 |
| 11.1 | A network of LUTs for RYG . . . . .   | 122 |
| 11.2 | A binary data set with all possibilities . . . . .  | 125 |
| 11.3 | Unique rows for the binarized Iris data subset . . . . .  | 130 |
| 11.4 | Weight values of a neural network trained on the binarized Iris data subset . . . . .                 | 133 |
| 11.5 | AIG accuracy over many samples . . . . .  | 140 |
| 11.6 | Average neural network probabilities and AIG predictions for a 4X3X3X1 neural network . . . . .       | 141 |
| 11.7 | Average neural network probabilities and AIG predictions for a 4X8X8X8X8X8X1 neural network . . . . . | 142 |



# **Part I**

## **Introduction**



# Chapter 1

## Abstract, Format, and Purpose

**Abstract** This thesis gives a novel algorithm  $\mathcal{N}$  that helps users understand neural networks (NNs) via abstraction to and-inverter graphs (AIGs). I find that AIGs are more comprehensible than NNs due to their conciseness. For small NNs,  $\mathcal{N}$  consistently creates AIG abstractions with perfect accuracy. However, translating large NNs to AIGs introduces the memorization versus generalization problem. Memorization elicits noise and reduces the comprehensibility of the AIG. To improve generalization and comprehensibility, I consider only the most important weights (using a maximum depth for the binary decision tree  $\mathcal{B}$ ). Furthermore, I survey the accuracy of the ensemble method for further noise mitigation. This work successfully creates a single AIG that is a concise, generalized, and accurate NN abstraction. However, the AIGs are not always as comprehensible as one would like. Future work can further investigate noise reduction techniques such as the ensemble method.

**Format** I divide this thesis into five parts: introduction (Part I), background (Part II), methods (Part III), results (Part IV), and the appendix (Part V). Part I gives a summary of the thesis. Part II clarifies definitions and surveys related work. I present the fine details of my work in Part III. Part IV gives a conclusion and suggests future work. Finally, refer to Part V for a reminder of common abbreviations, mathematical symbols, and other definitions.

**Purpose** This thesis was funded by the AFRL Research Grant FA8650-20-F-1956 with co-directors Dr. Robert Ball and Joshua Jensen, M.S. to

research explainable artificial intelligence. Moreover, this thesis coincides with my ambition to understand complex structures, create novel algorithms, research the philosophies of comprehension, and further artificial intelligence.

**Distribution** See <https://github.com/jbroot/ThesisPublic> for an electronic copy of this thesis, the defense presentation, and the copyright notice.

# Chapter 2

## Introduction

### 2.1 Background Summary

Neural networks (NNs) are powerful machine learning techniques, yet they are exceptionally difficult to understand due to their intricate structure. From the many techniques analyzing NNs [3, 4], three generic categories are derived: decompositional, eclectic, and pedagogical.

Decompositional techniques consider individual weights, activation functions, and the finer details of the network. For example, learning each node in the NN is a decompositional technique.

On the other hand, a pedagogical approach learns by an oracle or teacher—allowing a relatively facile change in underlying machine learning structures. For example, a simple pedagogical approach may be a decision tree whose training inputs are fed into a NN, and the decision tree’s learned class values are the output of the NN. This simple pedagogical approach can easily transition from the NN black box to another machine learning algorithm.

Finally, eclectic approaches consider the neural networks as a gestalt—a figure whose sum (big picture) is more valuable than the individual parts (details). Namely, the eclectic approach combines the decompositional and pedagogical approaches. An example of an eclectic approach is directing a learning algorithm over neural nodes (decompositional) while omitting inputs negligible to the final product (pedagogical). In this paper, I take an eclectic approach with localized learning of each neuron (a decompositional technique) with directions given by the latter layers (partly pedagogical).

## 2.2 A Comprehensible Medium

In Chapter 5, I argue that a comprehensible structure must be concise and that AIGs are more concise than NNs. As such, this thesis understands NNs via translation to AIGs.

**AIGs** AIGs (And-Inverter Graphs) are formally verifiable (provable with formal methods) and legacy white box structures. The AIG is a directed, acyclic graph that consists of an input layer, a finite or null amount of intermediate layers, and an output layer. Besides the input nodes, every node in an AIG is binary and performs logical conjunction upon its two in-edges. Additionally, every edge in an AIG can invert inputs (perform a logical NOT), hence the term “And-Inverter Graph”. I further explain AIGs in Section 4.1.

**Software** Fortunately, open-source implementations of AIGs with active maintenance already exist. I use mockturtle from the EPFL’s Logic Synthesis Library [5] to translate the intermediate representation (a network of lookup tables) to an AIG. Additionally, I use Brayton and Mischenko’s ABC software [1] to simplify and visualize the AIGs.

## 2.3 Neural Networks Considered

As described in Chapter 3, NNs have many forms. This thesis will only consider a subset of all possible NNs.

**Types Allowed** The intended NN is a feed-forward, sequentially layered, fully connected, multi-layer perceptron (a traditional NN). Meaning if and only if some node A is in a layer  $i$  (a hidden layer), then each node in layer  $i-1$  has a directed edge ending at A and A begins a directed edge to a node if and only if the node is in layer  $i+1$ .

**Formal Definition** Let the transition set be  $\delta$  and each sequential layer be expressed as  $L_i$ . Then this algorithm allows any NN with the property

$$i \in L_{l-1}, j \in L_l \longleftrightarrow (i \rightarrow j) \subseteq \delta$$

for any output or hidden layer  $L_l$ .

If a NN meets the requirements above except for being fully connected, one can create pseudo-edges with a weight of zero for it to become a fully connected NN.

## 2.4 Converting Neural Networks to AIGs

This section describes how I convert NNs to a network of sum of products (SoP) that is easily translated to an AIG.

**Definitions** Let the traversal over the NN be called  $\mathcal{N}$  (Algorithm 4), the optimized binary decision tree that approximates activation functions (Section 3.1) be  $\mathcal{B}$  (Section 9.2), and the network of SoPs be  $\mathcal{T}$ . The feature space is already binarized (Section 11.2.1) and the neural network is trained.

**Decision Tree ( $\mathcal{B}$ )** Traditional decision trees that use information gain or Gini impurity are too powerful and computationally expensive than what is required. I present  $\mathcal{B}$ —a linear and optimized binary decision tree that accurately finds the SoP for a neural node. See Section 8.2 and Section 8.3 for details on the activation functions  $\mathcal{B}$  can approximate. Furthermore,  $\mathcal{B}$  had the same predictions as the traditional decision trees for these activation functions (see Section 7.4). Since  $\mathcal{B}$  creates the network of SoPs  $\mathcal{T}$  ad hoc,  $\mathcal{B}$  is never stored.

**Complexity**  $\mathcal{B}$  is in  $\Omega(n)$  and  $O(2^n)$  with an average of  $\Theta(2^{0.5n})$  where  $n$  is the amount of in-degree weights for the given node (Chapter 10). Note: after I created  $\mathcal{B}$ , Shi et al. found an older algorithm that computes what  $\mathcal{B}$  does in  $O(2^{0.5n}n)$  time [6].

**Parsing ( $\mathcal{N}$ )**  $\mathcal{N}$  traverses the neural layers in reverse—from the output layer ( $L_n$ ) to the first hidden layer ( $L_1$ ). Traversing  $L_i$  before  $L_{i-1}$  allows any negligible nodes in  $L_{i-1}$  to be skipped entirely. Nodes within a layer are independent of each other and can be naively parallelized. Each neural node is only parsed over once (and possibly skipped).

**Translation Summarized** Succinctly,  $\mathcal{N}$  parses over the NN in reverse and employs  $\mathcal{B}$  to find the sum of products as needed. Then an AIG is produced.

## 2.5 Reasoning and Results

**Comprehensibility** The esoteric nature of the neural network is due to the complexity of and vast amount of nodes, weights, summations, multiplications, and activation functions. Since AIGs are simpler and more concise than neural networks, they are relatively comprehensible. In Chapter 5, I provide further analysis on comprehensibility considering the overall complexity of the neural network and how interpretable the basis (input names and values) is.

**Practicality and Results**  $\mathcal{N}$  successfully translates simple NNs to concise AIGs with perfect accuracy. However, the translation of large NN suffers from the memorization versus generalization problem and elicits noise. Employing a maximum depth on  $\mathcal{B}$  improves the AIG’s conciseness with little or no reduction in accuracy down to a certain maximum depth. Additionally, I investigate an AIG ensemble’s accuracy and potential to reintroduce generalization in Section 11.4. A concise and accurate AIG provides another tool for machine learning experts to use in debugging, analyzing, and understanding the complex NNs and their corresponding data. Notably, AIGs cannot abstract some functions found by NNs enough to be comprehensible as some functions are inherently complex and difficult to understand. Furthermore, the AIG can be translated to a circuit for computationally limited systems.

## Part II

# Background



# Chapter 3

## Neural Networks

Traditional neural networks train on a data set containing inputs and classifications (supervised learning). After training, the neural network predicts classifications for new inputs.

Neural networks in machine learning originated from the McCulloch and Pitts paper that modeled how neurons might work [7]. A major milestone of the neural network was overcoming the XOR problem [8] that was solved by backpropagation [9]. See [10] for a survey on the theory of neural networks and [11] for a survey on deep neural network architectures and their applications.

### 3.1 Structure

A lack of formal definitions for neural networks hindered formal proofs in the neural network's early decades. E. Fiesler gave a flexible hierarchical and a universal mathematical definition to give the field a solid and formal foundation [12]. Below is a summary of his hierarchy with some added research.

- **Topology**
  - **Framework**
    - \* **Number of clusters** (i.e. layers or slabs). Layers and slabs are both subsets of neurons with the same hierarchical level. However, layers are ordered while slabs need not be. Not enforcing order means that the neurons in a slab can be rearranged.

- \* Number of neurons in each cluster
- Inter-connection scheme
  - \* Connection types
    - **Interlayer connections** are connections between adjacent layers and are the most common connection type.
    - **Intralayer connections** connect neurons of the same layer. A self-connection is a type of intralayer connection where the neuron connects to itself.
    - **Supralayer connections** connect a neuron to a layer that is neither adjacent nor in the same layer.
  - \* **Connectivity** defines how dense the connections are among the neurons. A fully interlayered-connected network is commonly shortened as a fully connected network—this thesis will use this shorthand version. A plenary neural network is a neural network with all possible connections in the interlayer, intralayer, and supralayer domains.
  - \* **Symmetry versus asymmetry.** A symmetric connection uses the same weight for both directions (i.e backpropagation and forward feeding). An asymmetric connection uses one weight for both directions.
  - \* **Order.** Higher-order connections combine the outputs of several neurons as a single input—usually by multiplication. Specifically, a higher-order connection that combines  $N$  outputs is called an  $N^{th}$ -order connection. Furthermore, the highest-order connection determines the order of the entire network. Most neural networks are first order.

- Constraints

- **Weight value range** is the set of values an output may be amplified or diminished by.
- **Local threshold value range** holds the values allowed for an offset for each neuron’s activation. This is often perpetuated with a bias node (neuron) at each hidden layer.
- **Activation range** is the set of values a neuron may output.

- Initial state

- **Initial weights.** These should be created with random numbers to break symmetry and mitigate the potential null space. Intuitively, allowing the initial weights to be in a substantial subset of the weight value range would further rupture symmetry; however, larger initial weights may result in exploding values during propagation [13].
- **Initial local thresholds.** The bias nodes can be set with heuristically chosen constants (often the constant equals one). The weights attached to the bias node are chosen as described for initial weights.
- **Initial activation functions.** Commonly, the initial activation functions are unchanged throughout the training process.
- **Transition functions** update the state of the neural network.
  - **Activations functions** (neuron functions) translate the inputs of a neuron to its respective output given some function  $a(x)$ .
  - **Learning rules** dictate how weights will be updated.
    - \* **Cost functions** (also called loss functions or error functions) determine the magnitude of a penalty given a miss. A correct prediction suffers no penalty [13].
    - \* **Optimizer functions** use the cost found in the cost function to update the weights.
  - **Clamping functions** decide if a neuron will consider incoming information.
  - **Ontogenetic functions** change the neural network’s topology.

**Neural Networks Considered** This thesis will focus on the most common neural networks. Specifically, they will be fully interlayered-connected, symmetric, first-order neural networks with some finite amount of layers and nodes. The networks are trained on a binary data set so binary cross-entropy will be the loss function. The Adam optimizer (a stochastic gradient-based optimization algorithm [14]) is used throughout this thesis unless mentioned otherwise. Despite training on a binary data set, the activation functions are real-valued. The types of activation functions recommended are discussed in Section 8.3 and Section 8.2. The initial weights are randomly initialized to

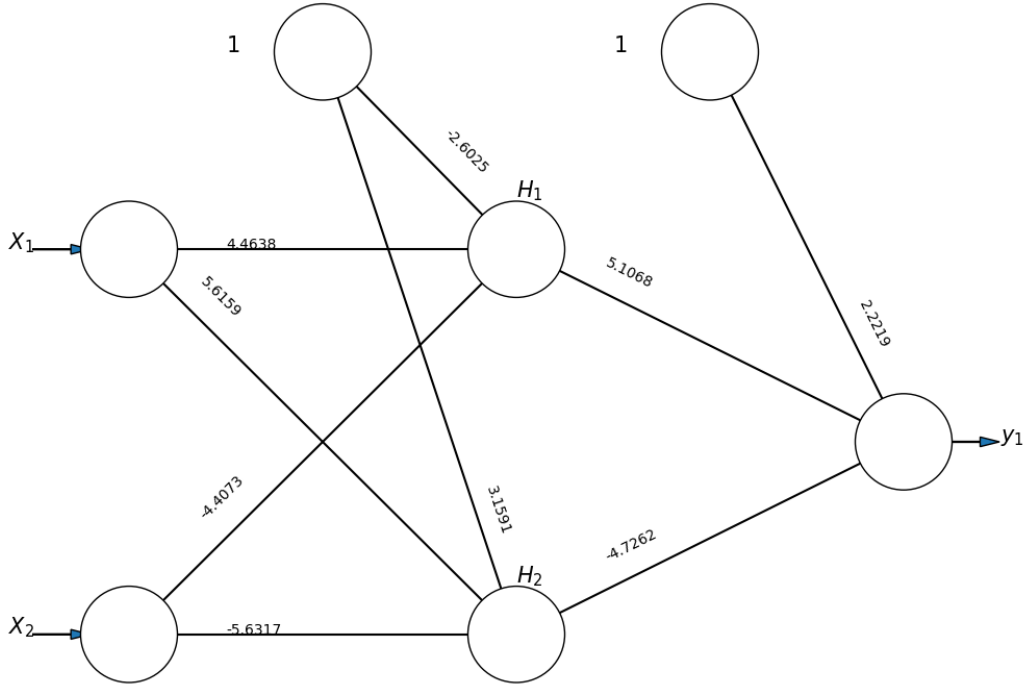


Figure 3.1

small values. Bias nodes with a value of one are used in every layer except the output layer unless stated otherwise. Activation functions will not change over time. Furthermore, the clamping and ontogenetic functions will not be considered.

**Feedforward** Some examples in this thesis use matrix notation to describe part of the feedforward process. Simply,  $\vec{x}$  is the vector of inputs and  $\vec{w}$  is the vector of weights. Furthermore,  $\vec{x} \cdot \vec{w}^T = \theta$  where  $\theta$  is the dependent variable for some activation function  $f$ . For example, when computing the activation function  $f(\theta)$  for  $H_1$  in Figure 3.1,  $\vec{w} = (X_1 \rightarrow H_1, X_2 \rightarrow H_1, \text{bias\_node} \rightarrow H_1) = (4.4638, -4.4073, -2.6025)$  and  $\vec{x} = (X_1, X_2, 1)$ . So if  $X_1 = X_2 = 0$ , then  $\theta = -2.6025$  and  $H_1$  will output  $f(-2.6025)$ .

## 3.2 Types of Activation Functions

**Identity Function** The identity or linear activation function is  $f(x) = cx$  where  $c$  is a predefined constant. If a neural network only consists of identity activation functions, it can only discriminate linearly separable data (see Figure 3.2 for an example). The linear function is sometimes used for the output neuron to allow a prediction of any real number (given the constraints of the system).

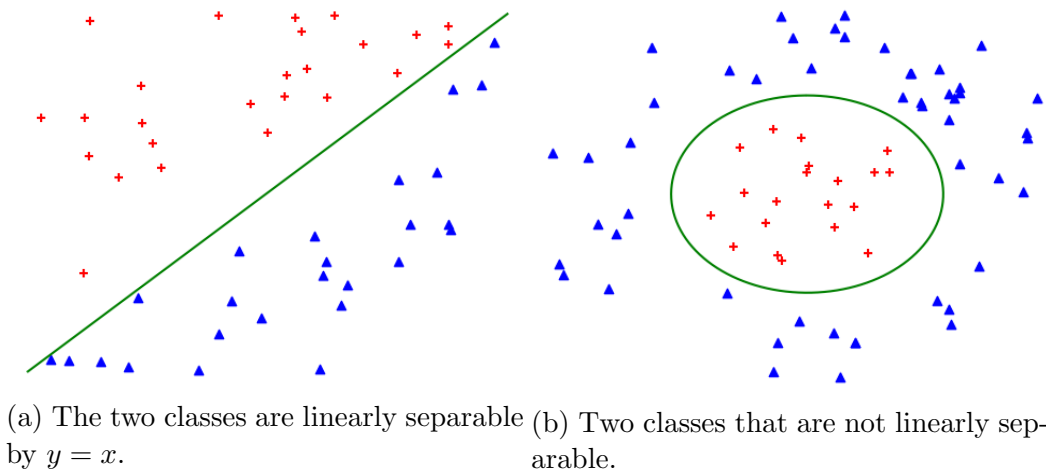


Figure 3.2

**ReLU** The Rectified Linear Unit function (ReLU) is  $f(x) = \max(0, x)$ . ReLU is the simplest nonlinear activation function and is commonly used in deep learning for its simple derivatives [13]. To remedy the loss of information in the  $\max(0, x)$  cast, leaky ReLUs ( $f(x) = \max(cx, x)$  for  $0 < c < 1$ ) are a similar function that still allow negative values to propagate. Swish is a differentiable function similar to the ReLU [15].

**Sigmoids** Sigmoid functions take the shape of an “s” and are commonly used for binary classification. Examples of sigmoid activation functions and their output range ( $\mathcal{R}$ ) include

- $f(x) = \frac{1}{1+e^{-x}}$ .  $\mathcal{R} \in (0, 1)$ , exclusively.
- $f(x) = \tanh(x) = \frac{e^x - e^{-x}}{e^x + e^{-x}}$ .  $\mathcal{R} \in (-1, 1)$ , exclusively.

- $f(x) = 1.7159 \tanh(\frac{2x}{3})$ .  $\mathcal{R} \in (-1.7159, 1.7159)$ , exclusively.

Since the hyperbolic tangent ( $\tanh$ ) can be computationally expensive, LeCun et al. recommend using  $f(x) = 1.7159 \tanh(\frac{2x}{3})$  which allows for an approximation with a ratio of polynomials [16]. Symmetric or odd sigmoids (sigmoid functions that do not change when reflected across the line  $y = -x$ ) often converge faster than the logistic function  $f(x) = \frac{1}{1+e^{-x}}$  [17]. This is partially due to symmetric sigmoids allowing negative activations. In neuroscience, positive and negative activations are called inhibitory and excitatory, respectively. As negative activations can help neural networks, inhibitory neurons help the human cortex [18].

**Softmax** While sigmoid functions can be described as a probability distribution over a binary classification, softmax activations give a probability distribution over  $n$  classifications. Essentially, each class is given a log probability similar to the logistic function above. Each log probability is then normalized by dividing the log probability by the sum of all log probabilities. By performing normalization, all probabilities in the vector sum up to one [13] (see Algorithm 1 for an algorithmic description). After the softmax is computed, the input with the highest probability is predicted.

---

**Algorithm 1:** The softmax function.

---

**Input:**  $\vec{a}$ , the input array.  
**Output:**  $P$ , an array of probabilities.  
**forall**  $a_i \in a$  **do**  

$$\quad \left[ P[i] \leftarrow \frac{e^{a_i}}{\sum_{a_j \in a} e^{a_j}}; \right]$$
  
**return**  $P$

---

### Summary of the Common Activation Functions

$$\text{ReLU: } f(x) = \begin{cases} x, & \text{if } x > 0, \\ 0, & \text{if } x \leq 0. \end{cases}$$

$$\begin{aligned}
 \text{Leaky ReLU: } f(x) &= \begin{cases} x, & \text{if } x > 0, \\ cx, & \text{if } x \leq 0. \end{cases} \\
 \text{Swish: } f(x) &= \frac{x}{1 + e^{-x}} \\
 \text{Logistic: } f(x) &= \frac{1}{1 + e^{-x}} \\
 \text{tanh: } f(x) &= \frac{e^x - e^{-x}}{e^x + e^{-x}} \\
 \text{Softmax: } \max(P) \text{ for } P(a_i \in Z) &= \frac{e^{a_i}}{\sum_{a_j \in Z} e^{a_j}}
 \end{aligned}$$

Since Keras allows many of these activation functions, custom activation functions, and granular control and inspection of neural networks, Keras (with the Tensorflow backend) is used to create neural networks throughout this thesis. More research on activation functions can be found in [19].



# Chapter 4

## Graphs

### 4.1 Graphs

Graphs are abstract data types from graph theory that are defined as the pair  $(V, E)$ , where

- $V$  is a set of vertices (or states).
- $E$  is a set of edges (transitions between vertices). Edges may be directed (one-way) or undirected (two-way).

**Circuits** Circuits are specialized types of graphs where each node is called a gate and computes some function. Formally, a circuit is a triple  $(M, L, G)$ , where

- $M$  is a set of values.
- $L$  is a set of gate functions (or labels) that maps n-ary input to a single output:  $M^i \mapsto M$ .
- $G$  is a directed acyclic graph labeled with  $L$ .

**AIGs** And-Inverter Graphs (AIGs) are Boolean circuits with

- $M = \mathbb{B} = \{0, 1\}$ .
- $L = \{AND, NOT\}$ .

- $G$  is finite.

Despite AIGs being structurally inefficient at a hardware level, AIGs excel in abstractions with their effective manipulations of complex Boolean functions and simple design. This thesis is only concerned with comprehensibility so the abstraction is essential, and any hardware inefficiency is irrelevant. Furthermore, simplification and visualization of AIGs have been implemented in free software such as “ABC: An academic industrial-strength verification tool” [1].

**MIGs** Formally, Majority-Inverter Graphs (MIGs) are Boolean circuits with

- $M = \mathbb{B} = \{0, 1\}$ .
- $L = \{MAJ, NOT\}$ , where  $MAJ$  is the majority gate.
- $G$  is finite.

Amarú et al. introduced MIGs in 2014 with two basis operations: majority (MAJ) and inversion (NOT). According to Amarú et al., a set of five primitive transformations creates a complete axiomatic system. By definition, a complete axiomatic system can prove any valid statement in the theory true or false. Therefore, the five primitive transformations allow a simple traversal of the entire MIG representation space. On average, MIG optimization reduces the logic levels by 18% when compared to AIGs optimized by the state-of-the-art ABC tool [1]. Furthermore, Amarú et al. proved MIGs to be a superset of AIGs [20].

While the reduced levels of MIGs would make the graph more concise than AIGs, MAJ gates are not as intuitive as AND gates to some people. Future work can investigate this trade-off.

**AOIGs** And-Or-Inverter Graphs (AOIGs) are Boolean circuits with

- $M = \mathbb{B} = \{0, 1\}$ .
- $L = \{AND, OR, NOT\}$ .
- $G$  is finite.

AIGs use De Morgan's law

$$\neg(\neg a \wedge \neg b) = a \vee b$$

to illustrate an OR. While AIGs may require more NOTs than an AOIG, the optimized AOIG has the same amount of nodes as an optimized AIG for any Boolean formula.

**Comprehensibility** As discussed in Chapter 5, comprehensibility can be defined as conciseness. From this, it stands to reason that MIGs are more comprehensible than AIGs. Furthermore, conciseness can be improved by converting subgraphs in the MIG to OR or AND nodes if doing so does not increase the total amount of nodes. Future work can investigate the comprehensibility of Majority-And-Or-Inverter Graphs further. See Amarú et al.'s work for information on how conversion may be done [20].

**BDDs** Binary Decision Diagrams (BDDs) are rooted, directed, acyclic graphs that consist of terminal and binary decision nodes (see Figure 4.1). BDDs were used by Shi et al. to illustrate activation functions that were converted to step functions [6]. Future work may investigate if BDDs are more comprehensible than AIGs.

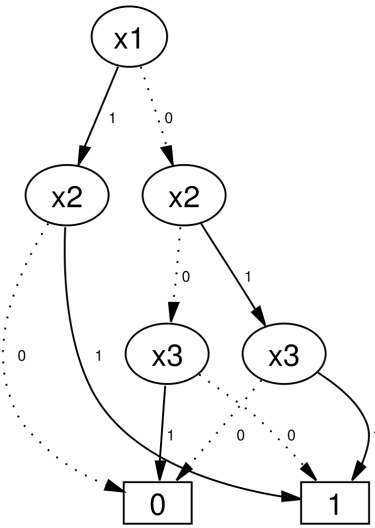


Figure 4.1: A binary decision diagram (BDD) for  $f(x_1, x_2, x_3) = \neg(x_1x_2x_3) + x_1x_2 + x_2x_3$ . This picture is from [Wikipedia](#).

## 4.2 ABC Software

This thesis uses ABC software [1] to illustrate and simplify AIGs. See Figure 4.2 for an example and below for the legend.

### Legend for ABC's AIG

- Inputs: up-right triangles ( $\triangle$ ).
- Outputs: upside-down triangles ( $\nabla$ ).
- AND gates: oval nodes ( $\circ$ ).
  - Labels: ABC labels nodes numerically; the numbers have no logical value.
- NOT gates: a dashed arrow ( $--\rightarrow$ ).

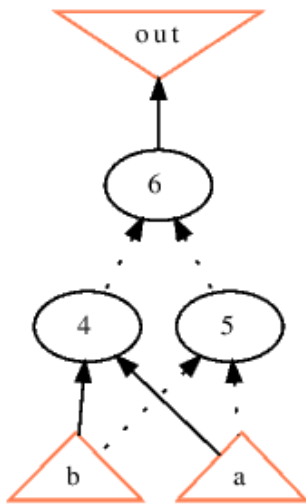


Figure 4.2: An AIG for the XOR function:  $\text{out} = \neg ab \vee \neg ba$ .

- Transitions: an arrow that is solid for transitions without a NOT gate ( $\rightarrow$ ) and dashed for transitions with a NOT gate ( $--\rightarrow$ ).

**File Formats** To write AIGs to the disk, I used the AIGER format (a highly-compressed format intended for AIGs) [21] with the Python library pyAiger [22] when coding in Python. However, writing AIGER files is not implemented in EPFL’s library (a C++17 library for logic synthesis) [5]. I use the BENCH format (a public format that can encode AIG equivalents) [23] since it produces the smallest file size of the intersection between what EPFL’s library can write and ABC [1] can read.<sup>1</sup>

**ABC Commands** ABC has a simple command-line integration with the “-c” option—example: “abc -c ‘commands\_here’”. After  $\mathcal{N}$  and mockturtle wrote the BENCH file, I ran a bash script with the below command to read the file, translate it into an AIG, refactor (simplify) the AIG, and then finally illustrate the AIG.

```
abc -c "read ${file}; strash; refactor; show;"
```

---

<sup>1</sup>As of November 20, 2020, EPFL’s library has implemented writing AIGER files in the mockturtle submodule.



# Chapter 5

## Comprehension

In this chapter, comprehension is analyzed and quantified. Later, I show that an AIG is more comprehensible than a neural network due to its conciseness (fewer and simpler operations). Finally, I give some tips to understand AIGs.

### 5.1 Understanding

**A Complete Understanding** Comprehension is a loaded term, yet the strongest form of comprehension can be expressed well by parts of Descartes’ “Rules for the Direction of the Mind” [24]. Essentially, one must intuit each basic fact (input) before understanding the relations among the inputs. Furthermore, this extends to relationships of relationships: one must intuit the first-order relationships before understanding second-order relationships. Descartes’ philosophy on comprehension is a bottom-up approach (start from the primitives and work to the more abstract).

**First-Order Logic (FOL)** In formal logic, FOL is defined as quantifying over propositional logic with the existential or universal quantifiers. However, this thesis defines first-order relationships as the innermost relationship to be understood, and  $n^{th}$ -order relationships are relationships of the  $(n - 1)^{th}$ -order ones.

#### N<sup>th</sup>-Order Relationship Example

$$\phi = (a \wedge b) \wedge (\neg c \wedge b)$$

Here, the zeroth-order relationships are the atomic values  $a$ ,  $b$ , and  $c$ . First-order relationships are  $a \wedge b$  and  $\neg c \wedge b$ . The entire property,  $\phi$ , is a second-order relationship. This definition is not strict. For example, one could consider the NOT operator as another level; I just use  $n^{th}$ -order relationships to loosely articulate how nested a relationship is.

**A General understanding** While a complete understanding is optimal, a disciplined intuition may be impractical in cases with a high-order relationship. For example, consider the unary operator “meta”. “meta” transcends its operand using self-reference so “cognition” (thinking) would become “meta-cognition” (thinking about thinking). Extending this concept to  $n^{th}$ -order meta-cognition (thinking about  $(n-1)$ -order meta-cognition), it is time-consuming to intuit each lower-order meta-cognition, but our understandings of “cognition” and “meta” give us a general feel for what an  $n^{th}$ -order meta-cognition would mean<sup>1</sup>. Section 5.1 uses mathematical induction to articulate this arching principle (or pattern).

1. Basis step: The initial (first-order) state of  $n^{th}$ -order meta-cognition is meta-cognition. Since cognition (zeroth-order) means thinking and “meta” is a self-referential operator, meta-cognition means to think about thinking.
2. Induction step:  $N^{th}$ -order meta-cognition is thinking about  $(N - 1)^{th}$ -order meta-cognition.

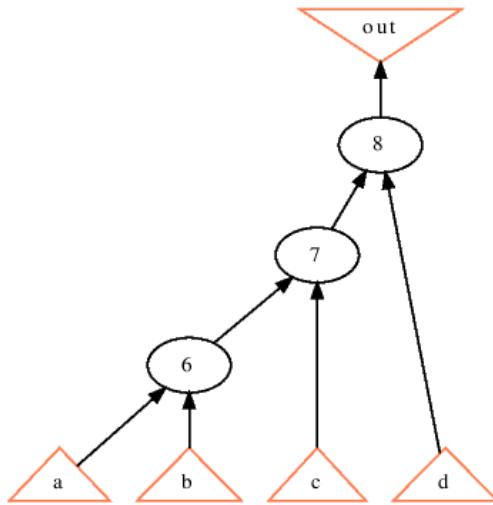
Figure 5.1: Understanding  $n^{th}$ -order meta-cognition using a type of “arching principle” called mathematical induction.

**AIG Example** Consider a Boolean function that is the conjunction of all its atoms (example in Figure 5.2a). For people that have previously intuited the conditional of universal truth (i.e. all elements must be true),

---

<sup>1</sup>Following the argument that metascience applies reflectively to itself [25], one can argue that metacognition encompasses  $n^{th}$ -order metacognition since metacognition is a type of cognition. However, assume that is not the case for this example.

they can quickly understand this graph. Others can understand the graph with mathematical induction (see Figure 5.2b).



(a) AIG for  $\text{out} = a \wedge b \wedge c \wedge d$ .

1. Basis step:  $a$  must be true and the first-order relationship  $a \wedge b$  must be true.
2. Induction step: traversing the graph, the  $(n - 1)^{\text{th}}$ -order relationship and the  $n^{\text{th}}$ -order relationship must be true.

(b) Understanding Figure 5.2a by mathematical induction.

Figure 5.2: Understanding an AIG that represents the universal truth conditional.

**Boolean Logic Example** Consider the property  $\phi$  over the atoms `fight` (to contend in physical conflict) and `flight` (to flee from physical conflict):

$$\phi = (\text{fight} \wedge \neg\text{flight}) \vee (\neg\text{fight} \wedge \text{flight})$$

After reading the inputs' definitions, start by understanding the innermost relations.

- $\neg\text{flight}$  must mean “to not flee from physical conflict.”
- $\neg\text{fight}$  must mean “to not contend in physical conflict.”

Next, we intuit the two conjunctions.

- $(\text{fight} \wedge \neg\text{flight})$ : to contend in physical conflict and to not flee from physical conflict.

- ( $\neg \text{fight} \wedge \text{flight}$ ): to not contend in physical conflict and to flee from physical conflict.

Finally, apply the final disjunction and understand  $\phi$  is satisfied in one of two scenarios: 1) where one fights and does not flee, or 2) where one does not fight and flees.

## 5.2 Quantifying Comprehensibility

This section begins with a basic definition of comprehensibility and extends that definition to allow the comprehensibility of similar graphs to be determined without human subjects. Later, the comprehensibility of a neural network is contrasted with the AIG.

### 5.2.1 Quantified Definition

**Basic Definition:** comprehensibility scales by the inverse of the average time it takes one to understand it (e.g.  $\frac{1}{1 \text{ second}}$  is larger and more comprehensible than  $\frac{1}{100 \text{ seconds}}$ ).

**Conditional Conclusion:** If each input and operation of two graphs take approximately equal time to intuit, then the graph with more inputs and operations is less comprehensible. Additionally, if the graph with more inputs and operations also takes longer to intuit each part, then this graph is still less comprehensible than the other.

**Derived Definition** This definition allows us to quickly determine how understandable an AIG is to another. While I will not explicitly calculate the formula in every AIG, know that when I contrast the comprehensibility of graphs that satisfy the above condition, I will use the derived definition:

$$\text{Comprehensibility} = \frac{1}{\|I\| + \|O\|}$$

where  $\|I\| + \|O\|$  is the sum of the magnitudes of inputs and operations.

**Future Work** If one takes Descartes' bottom-up approach, then the number of nodes and operations should convey comprehensibility as seen in the derived definition. However, recall from Figure 5.2a that a top-down approach may be quicker than and elicit approximately the same understanding as a bottom-up approach. I will leave ideas such as this to future work for a comprehensive quantification of comprehension.

### 5.2.2 AIG versus Neural Network

See Section 4.1 and Chapter 3 for the definitions of AIGs and neural networks respectively.

If one were to attempt intuition of a traditional and neural network, each activation function would be seen as a classifier with some real-valued range for the given weighted inputs. Analogous to earlier terms, each neural node in the first hidden layer is a first-order relationship, and each node in the  $n^{th}$  layer is an  $n^{th}$ -order relationship. For hidden sigmoid activation functions, this relationship is the probability that the given set of weighted  $(n - 1)^{th}$ -order relations indicate some intermediary binary classification.

Furthermore, intuiting a trained neural network would require people to intuit each activation function,  $(n - 1)^{th}$ -order relation, each bias constant and weight vector, multiplication, and addition over the real numbers. In contrast, AIGs have fewer elements to consider and simpler gates—people must simply understand the inputs, AND-gates, and NOT-gates over Boolean values.

**Contrasting NN and AIG Comprehensibility** Each operation in the neural network is at least as complex as an AND gate which is more complex than a NOT gate. However, let us assume that every operation is the same complexity as an AND gate. Then we can compute each complexity by counting the number of operations.

**Neural Network Comprehensibility** A neural network's comprehensibility is a summation of its layers' comprehensibility (each layer is denoted as  $L_i$ ). An input layer of size  $n$  has comprehensibility  $n$ . The comprehensibility of a hidden or output layer ( $L_i$ ) is found by

$$\text{Complexity}(L_i) = n_i(2n_{i-1} + 1)$$

where  $n_i$  is the size of  $L_i$  and  $n_{i-1}$  is the size of  $L_{i-1}$ .

*Proof.* Assume a fully-connected neural network with bias nodes. Each node in  $L_i$  is a dot product with vectors of size  $n_{i-1}$ . This amounts to  $n + 1$  multiplications and  $n$  additions. However, the bias constant is always one in this case so we can omit one multiplication. This means each dot product takes  $n_{i-1} + n_{i-1} = 2n_{i-1}$  operations. The dot product ( $\theta$ ) is then fed into the activation function ( $f(\theta)$ ). Granted this can contain numerous operations, however let us just consider the activation function as one operation. Then, each neural node in  $L_i$  takes  $2n_{i-1} + 1$  operations.  $L_i$  has  $n_i$  nodes so  $L_i$  has  $n_i(2n_{i-1} + 1)$  operations.  $\square$

**AIG Complexity** The AIG only contains two operations: AND and NOT. The number of operations is simply the addition of its AND and NOT gates.

**Example** Consider the neural network Figure 5.3a and its binary equivalent Figure 5.3b. Figure 5.3a has  $n_0$  inputs and  $n_1(2n_0 + 1) + n_2(2n_1 + 1)$  operations—where  $n_0$  is the size of layer 0 ( $n_0 = 2$ ),  $n_1$  is the size of layer 1 ( $n_1 = 2$ ), and  $n_2$  is the size of layer 2 ( $n_2 = 2$ ). So the comprehensibility of Figure 5.3a is

$$\frac{1}{2 + 2(2 \times 2 + 1) + 1(2 \times 2 + 1)} = \frac{1}{17}.$$

Figure 5.3b has 2 inputs, 3 nodes (AND gates), and 4 dotted transitions (NOT gates).  $2 + 3 + 4 = 9$  so Figure 5.3b's comprehensibility is  $\frac{1}{9}$ .

Since  $\frac{1}{17} < \frac{1}{9}$ , Figure 5.3b is more comprehensible than Figure 5.3a. Recall that each operation in the neural network is more complex than the most complex operation in an AIG (the AND gate). This comparison is heavily biased towards neural network comprehensibility; even so, the AIG is often more comprehensible. Improvements to the AIGs comprehensibility are given in Figure 11.7, Section 11.4, and Section 12.2.

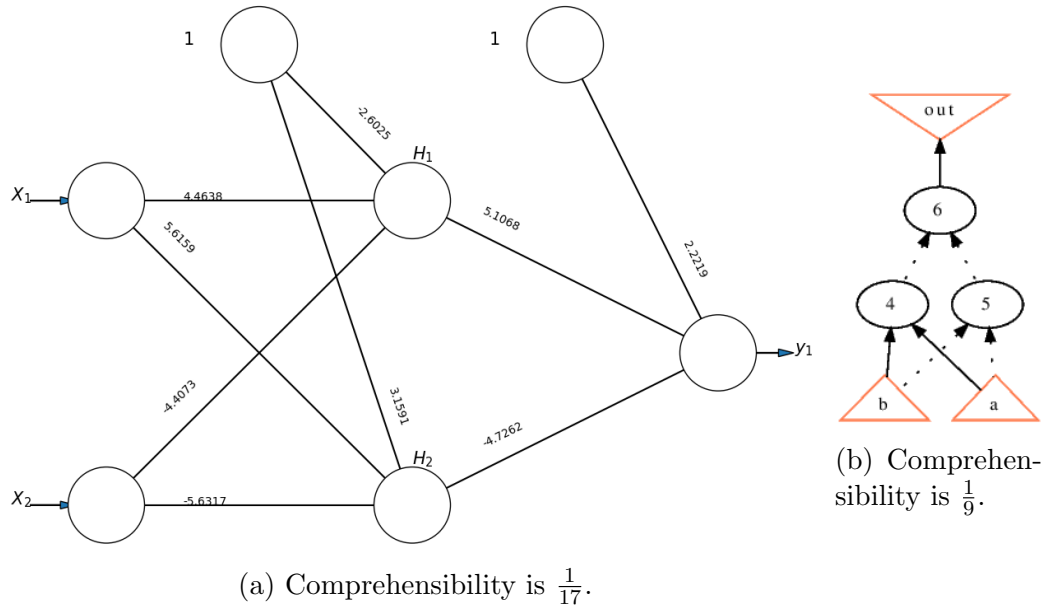


Figure 5.3: Comprehensibility comparison of two models that both represent the XOR function.

### 5.3 Inputs

**Understanding Inputs** Consider if Figure 5.2a stood for some fictional female's (Ashley's) preference in men where  $(a, b, c, d)$  stood for (confident, humble, masculine, gentle). To cultures where masculine is antonymous with gentle or for people who believe that confidence cannot coexist with humility, Figure 5.2a would make no sense to them despite its simplicity. In this case, no structure can help the individual understand what is being articulated—the inputs must be better defined or understood.

**Reducing Inputs** Additionally, Ashley may have considered confidence to be a trait of masculinity ( $\therefore$  confidence  $\subseteq$  masculinity). Now, the input basis is not optimized for comprehension (it is not minimized) since the information is duplicated in the confidence and masculinity axes. Future work can investigate the optimal ways to reduce the input space while remaining comprehensible.

**Dimension Reduction** While there exist dimension reduction techniques such as PCA (see Figure 5.4) that reduce the input space, these techniques may not be facilely understandable. For example, PCA casts  $m$  inputs into  $n$  components ( $PCA : i^m \mapsto c^n$  for  $m \geq n$ ) by combining information from inputs and omitting other information. Each component in the component-space is likely to be more difficult to understand than each input.

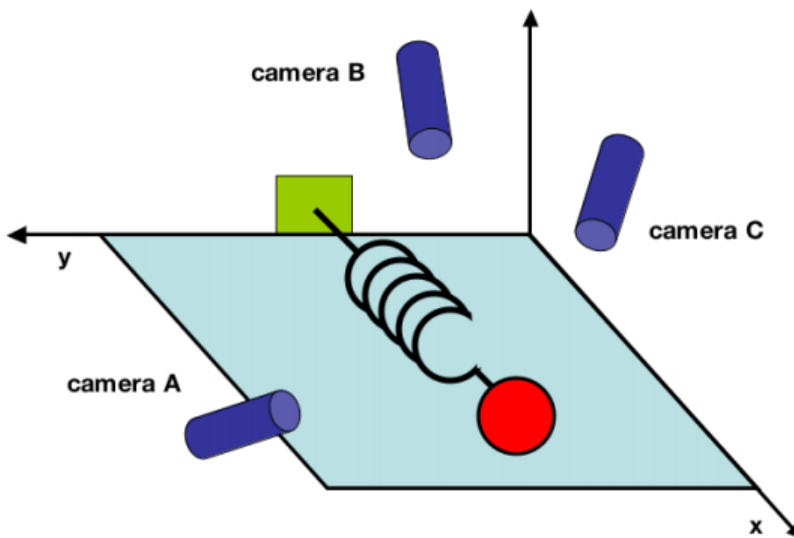


Figure 5.4: Shlen's PCA tutorial used this example of data duplication [26]. Only one camera is needed to predict the spring's position at any given time, yet multiple cameras give us variants of the same data. Dimension-reduction techniques such as PCA help alleviate duplicated information such as this.

## Many Inputs

While comprehension is possible by unconscious or conscious means, both ways are impractical for a human to learn large data sets or intricate graphs.

**Unconscious Comprehension** Consider MNIST [27]: this problem is to predict hand-written digits using numerous pixel values. One might reason that since humans can decipher digits given by dots, people can also interpret a digit from a series of numeric dot values. As shown by BrainPort

(a computer to brain interface that sends signals to a blind person’s tongue from a camera allowing them to see [28]), it may be possible for our unconscious minds to reorganize the relationships seen by numeric pixel values to visualize a digit, but for the sake of facile comprehension, this is eccentric and difficult [28, 29]. Furthermore, cognitive psychologists have coined this type of learning as “implicit learning” which our conscious mind cannot fully acknowledge nor articulate [30]. Even if one could intuit large data sets this way, the person could not articulate the findings to another.

**Conscious Comprehension** As for our conscious brain, we can only hold a small, finite amount of information in our working memory at a time [31]. Intuiting a concept means that the concept is stored into a longer-term portion of our memory from our working memory, and this process takes time for each concept to be stored. Therefore, there exist concepts with such intricacy that will take too much time to be realistically intuited.

**Patterns** However, a multitude of inputs and operations does not necessitate complexity. Elucidation can occur if one recognizes groups or patterns in the mass of information. For example, the numerous pixels in the MNIST input space can be understood by aligning shaded pixels (not numeric values) as the original images. Then one can correlate lines and curves from the original data to pixel values in the data set.

**Patterns via Machine Learning** Alternatively, one can employ a convolutional neural network (CNN) to highlight patterns of massive data. Given many inputs, CNNs learn patterns independent of location and create a feature-map of these patterns. One can then learn which features are associated with which types of curves and/or lines. Tools such as saliency masks can help humans understand the patterns learned [3].

## 5.4 Tips and Further Reading

**Tips** Understanding the entire AIG may still be a daunting task—even taken one relationship at a time. For the more complex AIGs, it may be better to consider individual sequences as they come about. Realize that a zero input to AND forces that gate to become zero, no matter what the other input is. Since this other variable is considered a “don’t care”, you can skip

all nodes which create the “don’t-care” variable for this input sequence. See Theorem 11.3.2 for an example.

**Final Notes** The user must understand that the AIG model is an abstraction of the neural network that approximates the possibly biased data set. According to Descartes’, believing in false relationships makes one less knowledgeable than if one did not know any relationship exists [24].

**Further Reading** Human comprehension is at the intersection of several subjects including philosophy, cognitive psychology, neuroscience, anthropology, and more. An emergent field called “cognitive science” attempts to unite computer science and mathematical models with these many subjects. Furthermore, machine learning and artificial intelligence attempt to capture comprehension using mathematical models. For those interested in truth and axioms, I recommend reading Tarski’s theories of truth and satisfiability [32] and Gödel’s incompleteness theorems [33]. While Tarski argued that truth is problematic, but the satisfaction of properties are obtainable, this thesis uses truth as defined in a Boolean context. For philosophies of comprehension and cognitive systems, there exists associationism [34] and connectionism [35, 36] among many others. For more research into self-referential logic and paradoxes, investigate Alan Turing’s work in [37]. To research interactions and strategies among two or more agents, read into game theory [38–40].

# Chapter 6

## Other Influential Works

A major problem in converting neural networks to a Boolean structure is the memorization versus generalization problem. Boolean structures such as AIGs are logical structures that are commonly used for memorization. One of the few works done that elicited generalization from logical operations (specifically factoring) is “Learning and Memorization” by Chatterjee [41]. Later, Brudermueller et al. used LogicNet and random forests to mitigate the memorization problem when converting neural networks to AIGs [2]. After I had completed the  $\mathcal{B}$  and  $\mathcal{N}$  algorithms (Section 9.2.2 and Algorithm 4), Shi et al. [6] published a paper that used Chan and Darwiche’s algorithm [42] to solve the problem  $\mathcal{B}$  does in  $O(2^{0.5n}n)$  time.

### 6.1 Chatterjee

Lookup tables (LUTs) save previously calculated results in an array-structure. For Boolean functions, an N-bit LUT has a fan-in of N and  $2^N$  possible entries. Chatterjee arranged LUTs in successive layers to mimic a fully connected neural network. However, unlike a neural node in a fully connected neural network, each LUT only receives inputs from a random subset of the previous layer of LUTs during training. This is done to mitigate complexity and has precedents in deep-learning architectures such as convolutional neural networks. Chatterjee describes these random inputs as a memorization process with noise. Furthermore, each LUT is globally trained on the entire network’s output (helping elicit generalization).

In related work, Chatterjee and Mishchenko discover clues on how neural

networks generalize (not by brute-force but by finding common patterns) while illustrating how circuit-based simulations can detect overfitting [43].

While parsing the neural network in  $\mathcal{N}$ , I took the idea of global training from LogicNet (see Algorithm 4). However, the final algorithm for  $\mathcal{N}$  is not a traditional machine learning technique since there is no explicit training. To consider the final output, I created  $\mathcal{N}$  to parse the neural network in reverse. This allowed  $\mathcal{N}$  to skip negligible neural nodes and to prevent islands in the final AIG.

## 6.2 Brudermueller et al.

In 2020, Brudermueller et al. published an article contrasting three pipelines (see Figure 6.1) that converted neural networks to AIGs using ABC [2]. To binarize the inputs, Brudermueller et al. cast the numbers into their lossless binary representations.

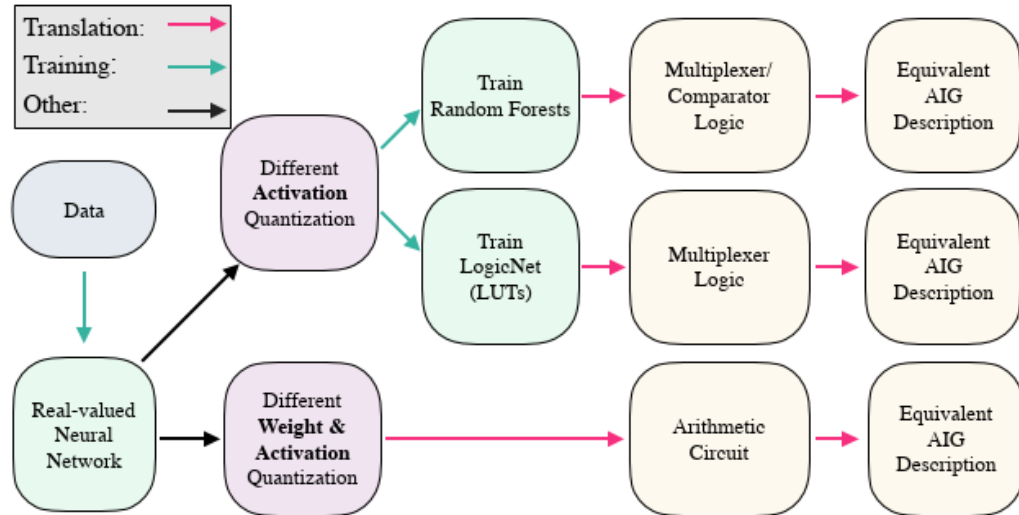


Figure 6.1: The pipelines contrasted in Brudermueller et al. [2].

In their direct translation, the researchers directly create an arithmetic circuit using multipliers, comparators, adders, multiplexers, and shifters. Each input and weight is allowed  $m$  bits, clipping and binning is done throughout their activation function circuit to keep inputs and weights at  $m$  bits. They found this pipeline elicited noise and that the AIGs were less accurate

than the pipelines that used dependency elimination ad-hoc (throughout the circuit) (see Section 4.3 of [2]).

The other two pipelines tested included random forests and LogicNet. To evoke generalization, the outputs of each activation node were trained on the global activation to eliminate “unimportant” features or relations in each of these pipelines. In my work, I realize these “unimportant” features or relations were likely tentative or developing relationships of the neural network. Section 11.4 suggests an ensemble of neural networks to and-inverter graphs would also elicit generalization. Future work can discover which way is more effective.

While Brudermueller et al. note that there is little work done on using logical operations to find generalization, one article that researches this topic is “Learning and Memorization” by Chatterjee [41]. Here, Chatterjee used factoring to elicit generalization. Furthermore, these simplified structures allow one to test the sensitivity of the inputs.

### 6.2.1 ABC and AIGs

**AIGs** The idea to use an AIG (which can represent any Boolean function) as the comprehensible output came from Brudermueller et al. Furthermore, freely-available software called “ABC” can take AIGs as input and provide powerful transformations such as redundancy removal to make the AIG more comprehensible [1].

**Satisfiability** The Boolean satisfiability problem (SAT) asks if there exists a set of inputs (given some restraints) that invokes a true output. SAT solvers can have  $O(n)$  complexity—where  $n$  equals the number of variables [44–46]. Fortunately, ABC includes an SAT solver called MiniSAT [1] which can be used to test the properties of AIGs abstracted from neural networks. Additionally, AIGs are formally verifiable (properties of AIGs can be proven or disproven).

## 6.3 Shi et al.

In “On Tractable Representations of Binary Neural Networks”, Shi et al. [6] trained a neural network with sigmoid activations which were later transformed into step activations to allow an easier translation to an ordered

binary decision diagram (OBDD or BDD) [6]. For BDDs, variable ordering is essential to create the most concise BDD. Furthermore, this paper connected finding the truth table of a neural node with an analogous problem Chan and Darwiche had solved with  $O(2^{0.5n}n)$  complexity [42]. While Shi et al. also convert activation functions to a binary step function based on some threshold, I extend this research by exploring which activation functions are best suited for the binary function cast in Section 8.2. Shi et al. partially overlap the novel work I had done and came out after I had completed much of my experiments.

# **Part III**

## **Methods**



Part III articulates the work and thoughts that went into compiling an AIG from a neural network. Chapter 7 shows a prototype created in Python using Keras sequential neural models, Sklearn’s decision tree, and other Python tools that empirically produce an AIG with a ludicrous  $O(5^n)$  time complexity. Chapter 8 recognizes the extensive computation time required to elicit the XORNN (XOR Neural Network) prototype and lays the groundwork for an optimized binary decision tree ( $\mathcal{B}$ ) in Chapter 9. Chapter 9 also defines how the network is parsed ( $\mathcal{N}$ ). Finally, Chapter 11 introduces AIG construction with real data sets—including those with “don’t-care” variables. Chapter 10 in Part IV gives supporting evidence that  $\mathcal{B}$  reduced the worst-case complexity to  $O(2^n)$  and the average case to  $O(2^{0.5n})$ .



# Chapter 7

## XORNN

This chapter investigates neural networks that can solve the XOR problem as a prototype to construct AIGs. Efficient algorithms and other examples are introduced in Chapter 9 and Chapter 11 respectively.

### 7.1 Definitions

**XOR Definition** For the prototype, I used the simple, nonlinear data set XOR. Formally, XOR can be defined as  $f(a, b) = (a \vee b) \wedge \neg(ab)$ .  $f(a, b)$  gives us this truth table for XOR (Table 7.1).

Table 7.1

| $a$ | $b$ | $f(a, b)$ |
|-----|-----|-----------|
| 0   | 0   | 0         |
| 0   | 1   | 1         |
| 1   | 0   | 1         |
| 1   | 1   | 0         |

**XOR Problem** The simplest neural network that can solve the nonlinear, XOR problem poised by Minksy and Papert [8] requires three layers. The first layer (the input layer) is composed of two input nodes and one bias node. The second layer (a hidden layer) has two nodes and one bias node.

The final layer (the output layer) is a single node. The hidden nodes and the output node are equipped with the sigmoid activation function.

**XORNN defined** Let AllXORNN be the set of all neural networks that perfectly fit the XOR data set and have the topology as described above and as visualized in Figure 7.1. A specific neural network in AllXORNN is referred to as XORNN. An initialized neural network will be trained on the data found in Table 7.1; if 100% accuracy is obtained, the neural network becomes a XORNN. Since all possibilities of the XOR data set are known and trained upon, perfect accuracy is attainable and generalization is not a concern—that is, XORNN cannot be overfitted. However, I found that XORNN’s created with the code given in Section 7.2.1 often reached a local minimum of 75% accuracy for at least a million epochs. If the neural network had less than 100% accuracy after about 5000 epochs, it is better to reset the weights and start again.

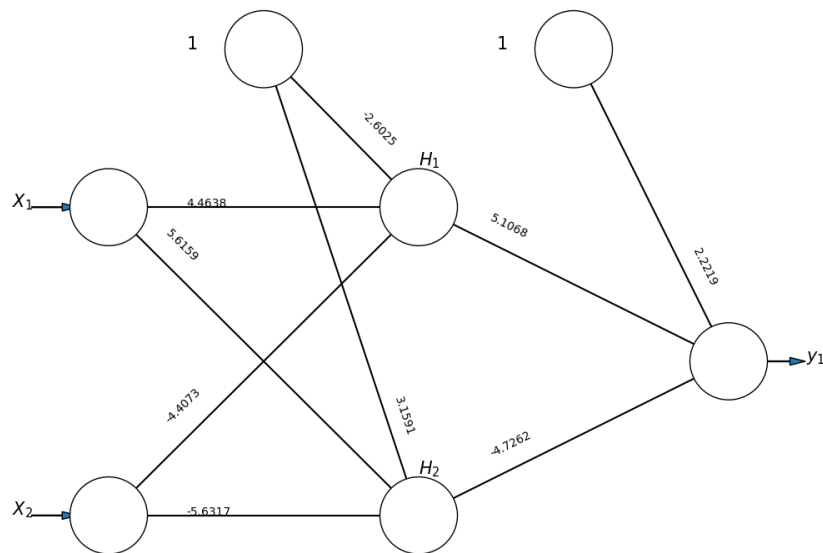


Figure 7.1: Every XORNN has the same topology—only the weights differ.

## 7.2 Creating XORNNS

I highlight how to make XORNNS efficiently in this section. Efficiency is important since the more XORNNS that are produced, the larger our sample data is.

### 7.2.1 XORNN Code

The pseudo-code in Algorithm 2 surveys how a XORNN is created—the corresponding Python script is in Section 7.2.1. An example of the boundaries drawn by a XORNN is given in Figure 7.2. Section 7.2.2 explains how and why this algorithm is refined.

---

**Algorithm 2:** Pseudocode for the Python script in Section 7.2.1.

---

```

Output: XORNN
for  $i = 0 \dots 49$  do
    Initialize an XOR neural network (XORNN) with the topology
    illustrated in Figure 7.1.
    Train XORNN on the XOR data set (Table 7.2).
    if Accuracy is 100% then
         $\downarrow$  return XORNN
    throw “A XORNN could not be produced. Statistically, this is
        unlikely to occur given 50 attempts.”
return
```

---

Review of the Python libraries used in Section 7.2.1.

- Keras is an API for creating neural networks with the user’s choice of Theano or Tensorflow for the backend.
- NumPy is advertised as “[t]he fundamental package for scientific computing.” NumPy provides high-level functions to manipulate C-style arrays.
- Scikit-learn (also called sklearn) is a general machine learning library with a broad choice of machine learning algorithms and metrics to measure these algorithms.

**Python code corresponding to Algorithm 2.**

```

import numpy as np
from keras.models import Sequential
from keras.layers import Dense
from sklearn import metrics

def create_xor_nn(numEpochs=5000, numAttempts=50):
    inputs, outputs = np.array([[0,0],[0,1],[1,0],[1,1]])
        , np.array([0,1,1,0])
    #build a new neural net (with new random weights) and
    train it until the neural net can reach 100%
    accuracy.
    #Gives up after numAttempts=50 tries.
    #Most of the time, three or fewer tries are needed.
    for _ in range(numAttempts):
        #Create a sequential neural network model with
        Keras
        xorModel = Sequential()
        #Dense() is a Keras object for a fully connected
        layer
        #the first add() includes the input layer and the
        first hidden layer
        xorModel.add(Dense(2, input_dim=len(inputs[0]),
                          activation='sigmoid'))
        xorModel.add(Dense(1, activation='sigmoid'))
        xorModel.compile(
            loss='binary_crossentropy', optimizer='adam', metrics
            =[ 'binary_accuracy' ]
        )

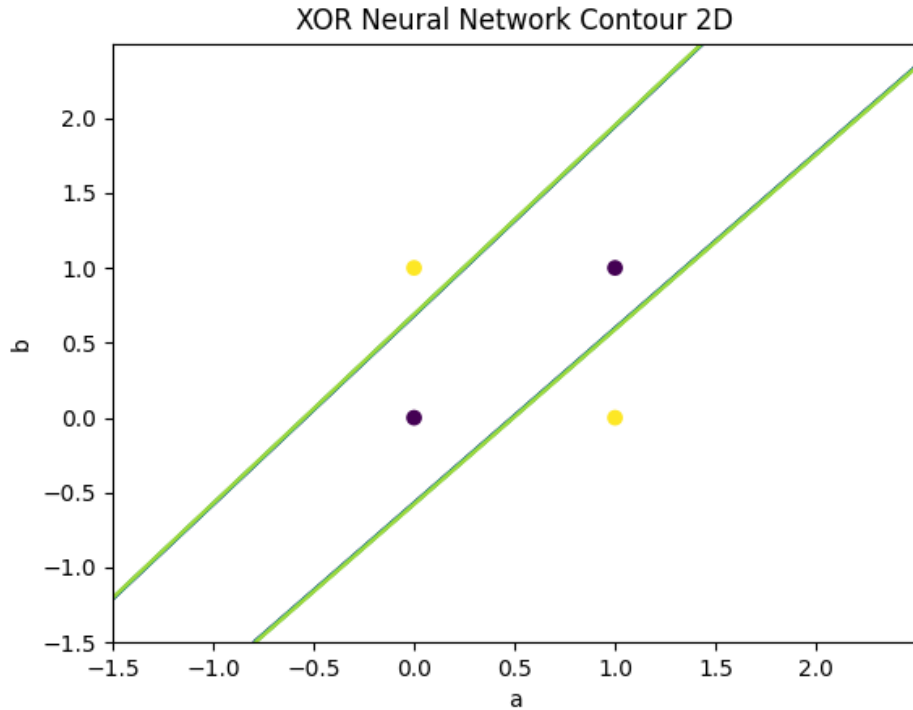
        #train the neural net
        history = xorModel.fit(inputs, outputs, epochs=
            numEpochs, verbose=0)
        predictions = xorModel.predict_classes(inputs)
        accuracy = metrics.accuracy_score(predictions,
                                           outputs)
        print("Accuracy: ‘‘, accuracy)
        #stop trying for new neural networks once we
        achieve perfect accuracy

```

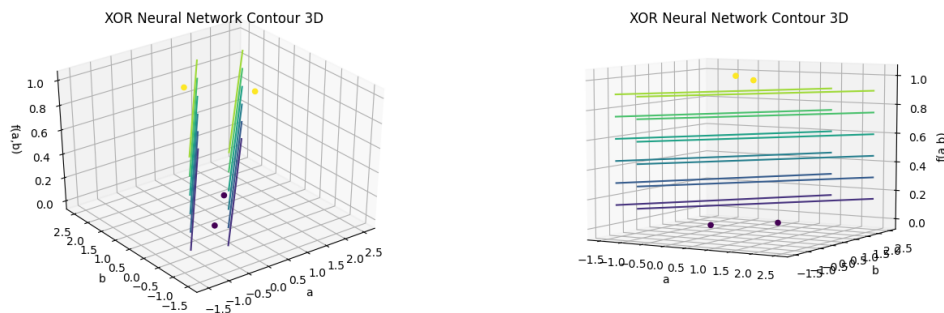
```
if accuracy == 1:  
    break  
if accuracy != 1:  
    #Statistically , this error is very unlikely given  
    # 50 attempts.  
    raise RuntimeError('A XORNN was not produced after  
        ' + str(numAttempts) + ' attempts.')  
return xorModel  
  
xorModel = create_xor_nn()  
#once we create the model, we can save it for  
    # persistence across sessions  
saveToThisPath = '/tmp/xor.kerasModel'  
xorModel.save(saveToThisPath, overwrite=True,  
    include_optimizer=True)
```

After saving our XORNN as done above, we can load the saved model with this script:

```
import keras  
loadedXor = keras.models.load_model('filePathHere')
```



(a) A 2D contour plot of XORNN predictions with the XOR data set plotted. The slope is so steep, all of the contour lines have agglomerated together.



(b) A 3D contour plot of the same XOR neural network in Figure 7.2a.

(c) A side view of Figure 7.2b.

Figure 7.2: Graphs of a XORNN boundary (lines) compared with the XOR data set (dots).

### 7.2.2 Rationale for Algorithm 2

**Local Minima** As illustrated in Figure 7.3, I discovered that the neural networks with suboptimal accuracy after 5000 epochs would often remain suboptimal for at least 1,000,000 epochs. To remedy being stuck in this local minima, I reinitialized the neural network with random weights after 5000 epochs. Future work can investigate if there is an epoch threshold where suboptimal NNs will never become a XORNNS and the basis of original weights that elicit this phenomenon.

**Degeneracy** Figure 7.3 shows that a few XORNNS’ accuracies decreased (therefore losing status as a XORNNS) as the epochs surpassed 50,000. 64.4% of all NNs are XORNNS at 50,000 epochs while training with 100,000 epochs only yields XORNNS 58.4% of the time. Using the Adam optimizer algorithm (refer to Section 3.1 for a review on optimizer functions), I consistently found neural networks to remain in a local minimum about 42% of the time. Preliminary results indicate that the SGD (stochastic gradient descent) optimizer that Adam was based on also stalls in these local minima. I created the code in Section 7.2.1 with this experiment in mind.

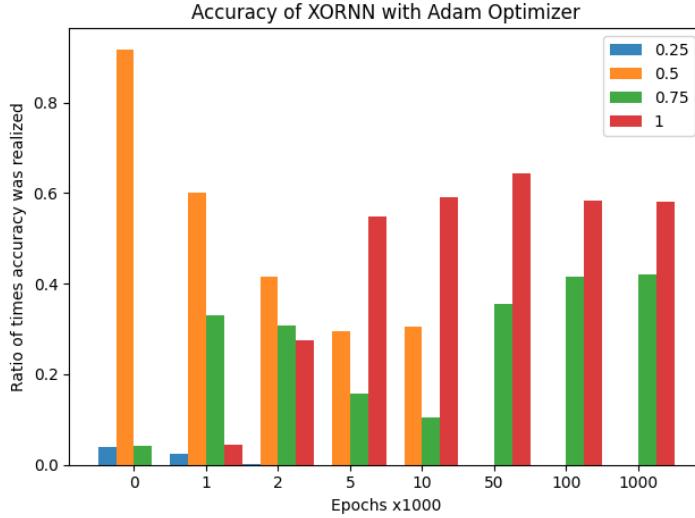
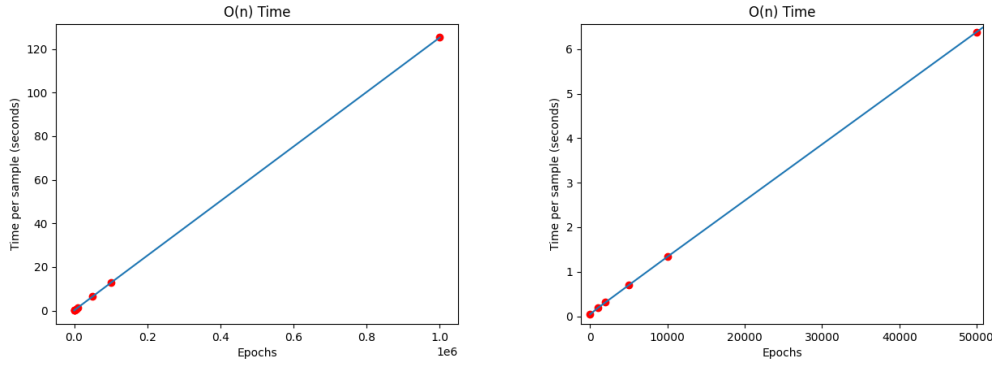


Figure 7.3: The accuracy is differentiated by color. Epochs 0 through 100,000 had 500 samples each. 1,000,000 epochs had 100 samples. No sample was reused and tested with the code in Section 7.2.1.

### 7.2.3 Time Creating XORNN

Experiments were done with six threads on a six-core Intel i5-9600K CPU and aggregated into Figure 7.4. To prevent threads from obtaining the same pseudo-random weights, a short lock guarded the critical section that initialized weights with a random seed. This lock and child-process spawn times are negligible compared to the training time of the model.



- (a) The training time is linear with the number of epochs.  
 (b) Figure 7.4a zoomed in by omitting the two largest epochs.

Figure 7.4

**GPU Training** I did not implement GPU training due to the small size of the matrices. GPUs excel at multiplying large matrices. And matrix size increases proportionally to the number of nodes in the fully connected neural network. My XORNN topology (Figure 7.1), with a total of seven nodes, trains slower on an RTX 2070 with CUDA than on the Intel i5-9600K CPU.

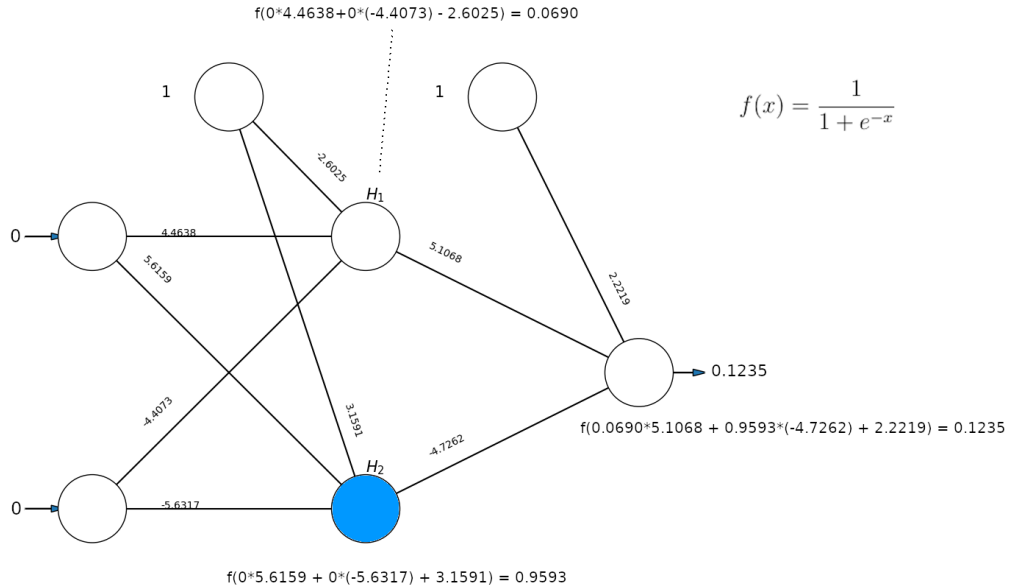
**CPU-Level Parallelism** While implementing CPU-level parallelism, I found Keras' backend Theano was throttled by Theano's locks and switched to the Tensorflow backend to solve the throttling problem.

Table 7.2: The logic of the XORNN in Figure 7.5.

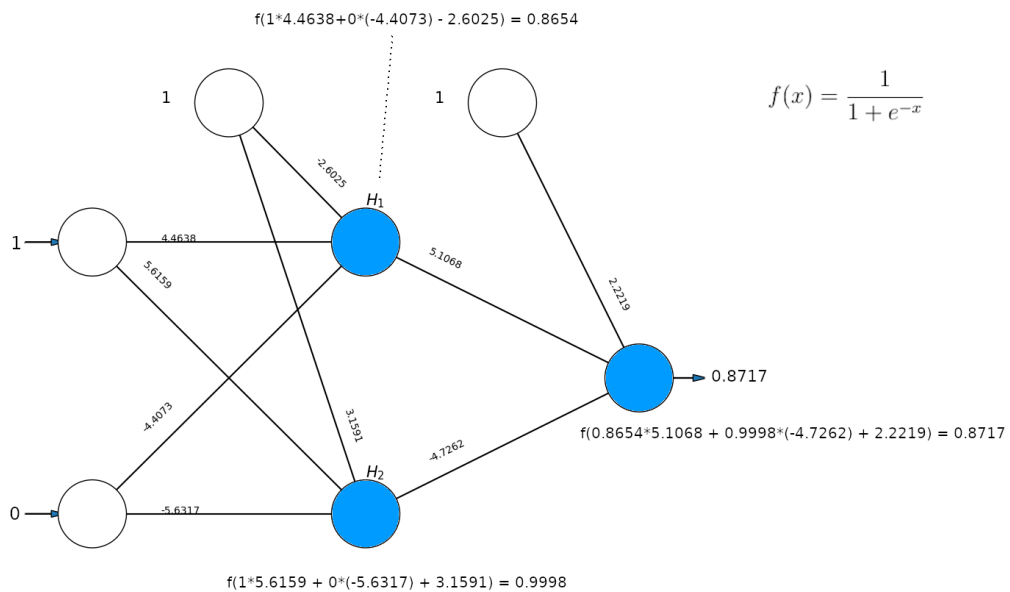
| $x_1$ | $x_2$ | $h_1(x_1, x_2)$ | $h_2(x_1, x_2)$ | $out(h_1, h_2)$ |
|-------|-------|-----------------|-----------------|-----------------|
| 0     | 0     | 0               | 1               | 0               |
| 1     | 0     | 1               | 1               | 1               |
| 1     | 1     | 0               | 1               | 0               |
| 0     | 1     | 0               | 0               | 1               |

### 7.3 Understanding XORNN

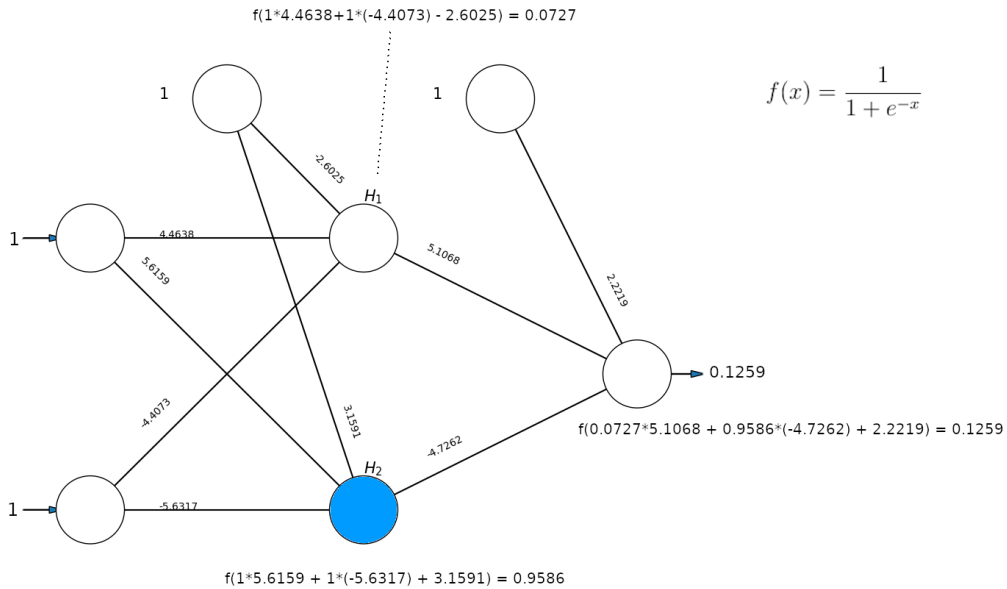
To gain a better understanding of the rule extraction techniques, let us exhaustively traverse and illustrate the XOR data set with a specific XORNN in Figure 7.5. Using the activation function  $f(x) = \frac{1}{1 + e^{-x}}$ , the blue nodes indicate an activation greater than 0.5. Table 7.2 converts Figure 7.5 into a more comprehensible truth table.



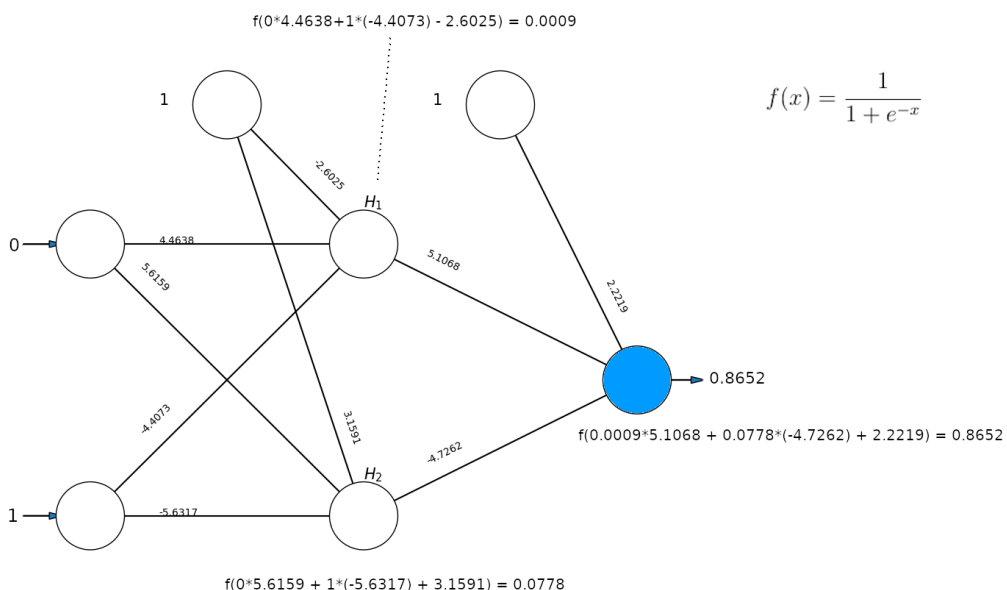
(a) A walkthrough with inputs = {0,0}.



(b) A walkthrough with inputs = {1,0}.



(c) A walkthrough with inputs = {1,1}.



(d) A walkthrough with inputs = {0,1}.

Figure 7.5: Exhaustive walkthroughs of a XORNN.

## 7.4 Learning XORNN

This section investigates using a network of decision trees (called XORD) to approximate a XORNN.

### 7.4.1 Creating a Decision Tree Network

**Tree Graphs** The tree graphs in this section use sklearn's [47] built-in graphing function which uses Graphviz [48] and several other libraries. Consider the optimal decision tree for the XOR data set as illustrated in Figure 7.6. Each of the parent (white) nodes contain five lines of text. The first line is the conditional of the node that dictates which branch to take (left is true and right is false). The second line shows the Gini impurity of the conditional. The third line represents the number of samples the node was given at this point, and the fourth line shows how many samples of each class were given. Finally, the last line is the tree's best guess of a class given its current path. The color of the nodes signifies the class prediction.

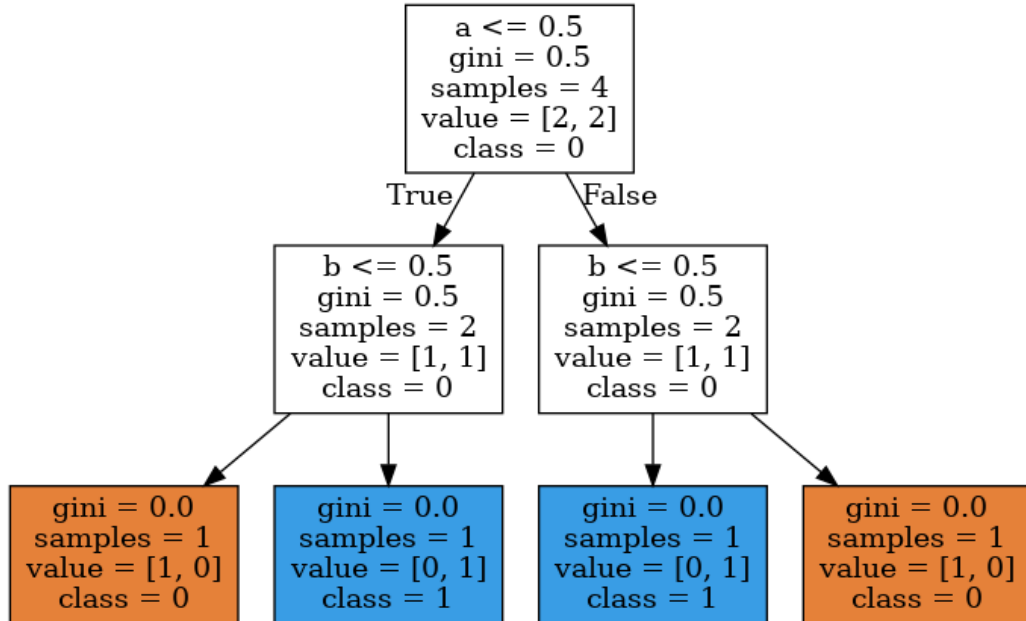


Figure 7.6: The optimal decision tree for the XOR data set created with Sklearn [47].

**Learning the Neural Nodes** To approximate and extract logic from a XORNN, a simple decompositional technique is employed: learn each node with a decision tree then layer the decision trees according to their respective nodes (see Figure 7.7). Finally, Section 7.5 analyzes the logic of the decision-tree network.

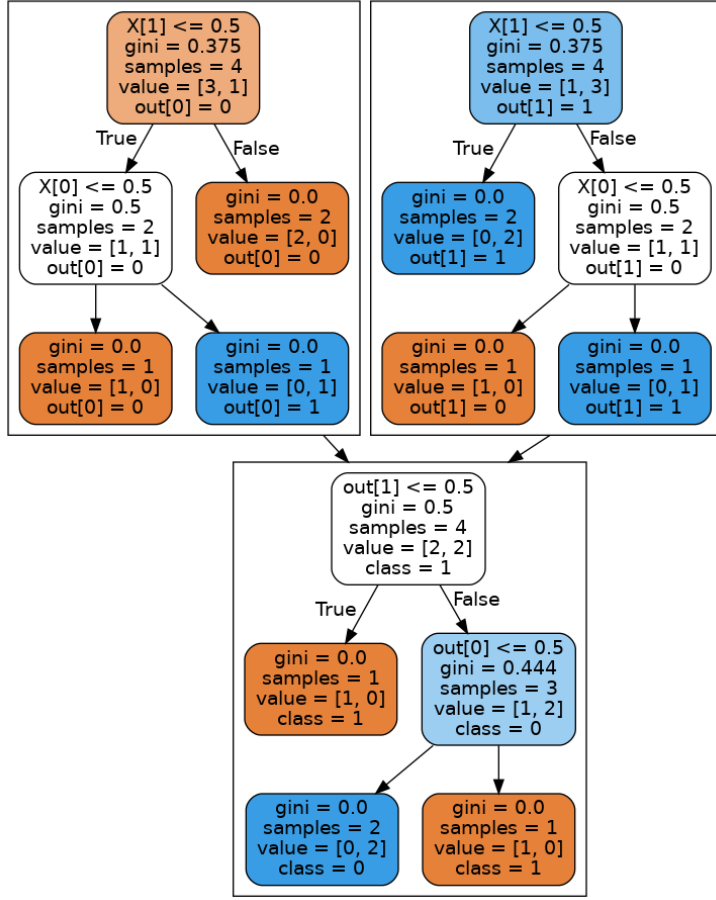


Figure 7.7: A decision tree network learned from the binarized activations of the XORNN pictured here Figure 7.5. The top left decision tree learned the activation from node  $H_1$ , the top right decision tree's activation function was from  $H_2$ , and the final decision tree at the bottom represents the activation from the output node. As one can see, this decision tree network requires reorganizing to be shown as Figure 7.6.

## 7.5 Understand the Decision Tree Network

This section translates Figure 7.7 to a Python function by nesting the conditionals of the decision tree. After the Python code is tested to correctly model Figure 7.7, I convert the Python to Boolean algebra to prove it correctly approximates XORNN and the XOR data set.

**XORD to Python** Since all inputs in the decision tree are binary, it is known that “ $x[1] \leq 0.5$ ” means “ $x[1] == 0$ ” and “ $x[1] > 0.5$ ” means “ $x[1] == 1$ ”. After this realization, I recreated the conditionals in my Python code below.

```
def xord(x):
    #initialize the output node's input to impossible
    #values
    out = [-1,-1]
    #H1 (Hidden node 1) (also the top-left decision tree)
    #produces x[0] (here we call it out[0]) for the
    #out node
    if x[1] == 0: #gini = 0.375
        if x[0] == 0: #gini = 0.5
            out[0] = 0 #samples = 1
        else:
            out[0] = 1 #samples = 1
    else:
        out[0] = 0 #samples = 2

    #H2 (top-right decision tree) produces out[1]
    if x[1] == 0: #gini = 0.375
        out[1] = 1 #samples = 2
    else:
        if x[0] == 0: #gini = 0.5
            out[1] = 0 #samples = 1
        else:
            out[1] = 1 #samples = 1

    #Output node (bottom decision tree)
    if out[1] == 0: #gini = 0.5
```

```

    return 1 #samples = 1
else:
    if out[0] == 0: #gini = 0.444
        return 0 #samples = 1
    else:
        return 1 #samples = 2

#x can be any of the four data points in XOR
allInputs = [[0,0],[0,1],[1,0],[1,1]]
for x in allInputs:
    print(x, ' returned ', xord(x))

```

Running the script in Section 7.5 confirms the decision-tree network in Figure 7.7 is correct.

```
[0, 0] returned 0
[0, 1] returned 1
[1, 0] returned 1
[1, 1] returned 0
```

**Conditionals to SoP** Now let us simplify Figure 7.6 further by translating each if-else chain to a sum of products (SoP) (shown in my Python code below). Simply begin with the outer-most if, then create a product for each path (following the logic of each conditional). If class 1 is reached during the traversal, write the current product in the sum of products. Any paths that end with a class 0 are omitted. The final SoP will fully encompass the space of our if-else blocks. This idea of only including class 1 in the sum of products was tested and implemented in  $\mathcal{B}$  in Section 9.2.

```

#Goal: change all comparisons and assignments to
      Boolean logic.

#Conjoin each conditional with each conditional within
      it.
#Add the conjunction (product) to the sum of products
      only if an assignment of True is found.
#If the False assignment is found, backtrack the
      product in a tree-like fashion.

```

```

def xord_simplified(x):
    #initialize the output node's input
    out = [False, False]
    #H1 (Hidden node 1) and top-left decision tree
    #produces out[0] for the out node's input
    out[0] = (not x[1] and x[0])
    # if not x[1]: # add not x[1] to our product
    #     if not x[0]: #add not x[0] to the product
    #         out[0] = False
    #     else: #x[0] is true #remove not x[0] and add x
    [0]
    #             out[0] = True #add our first product 'not x
    [1] and x[0]'
    # else: #x[1] is true
    #     out[0] = False

    #Begin with a new empty product with each outermost
    if block.
    #H2 and top-right decision tree produces out[1]
    out[1] = not x[1] or (x[0] and x[1])
    # if not x[1]: #product = not x[1]
    #     out[1] = True #add product.
    # else: # x[1] is true #flip the final conditional.
    product = x[1]
    #     if not x[0]: #product = x[1] and not x[0]
    #         out[1] = False
    #     else: # x[0] is true #product = x[1] and x[0]
    #         out[1] = True #SoP = not x[1] or (x[0] and
    x[1])

    #Output node and bottom decision tree
    return not out[1] or (out[0] and out[1])
    # if not out[1]:
    #     return True
    # else: #out[1] is true
    #     if not out[0]:
    #         return False
    #     else: #out[0] is true

```

```
#           return True
```

In Python, “and” operators take precedence over “or” operators, so the parentheses are not needed but help with cohesion for those less attenuated to Python’s parsing. Without comments, the function is now the following:

```
def xord_simplified(x):
    out = [False, False]
    out[0] = (not x[1] and x[0])
    out[1] = not x[1] or (x[0] and x[1])
    return not out[1] or (out[0] and out[1])
```

**Identical Logic** With this simplification, we can see that  $\text{out}[1]$  (node  $H_2$ ) and the return (output node) share the same simplified logic. Indeed, the ordered weights going into the respective nodes in Figure 7.1 share similar ratios ( $3.1591 : 5.6159 : -6.6317 \approx 2.2219 : 5.1068 : -4.7262$ ). This is due to  $x$  being a linear function of its dependent variables which are scaled with their respective weights. This concept is further explored in Section 8.2 and brings the idea of identifying equivalent subtrees in Section 9.4.2.

Using substitution, I redefine the function below.

```
def xord_simplified(x):
    return (not (not x[1] or (x[0] and x[1]))) or ((not x
        [1] and x[0])
        and (not x[1] or (x[0] and x[1])))
```

This substitution evokes a complicated expression. Using Boolean algebra, the function is simplified to the definition of XOR below.

```
def xord_simplified(x):
    return (x[1] and not x[0]) or (not x[1] and x[0])
```

### Proving the Derived Code Correct

**Theorem 7.5.1.** *The Python code  $(\text{not } (\text{not } x[1] \text{ or } (x[0] \text{ and } x[1]))) \text{ or } ((\text{not } x[1] \text{ and } x[0]) \text{ and } (\text{not } x[1] \text{ or } (x[0] \text{ and } x[1])))$  is equivalent to  $(x[1] \text{ and not } x[0]) \text{ or } (\text{not } x[1] \text{ and } x[0])$ .*

*Proof.* Let  $x[0] = a$  and  $x[1] = b$ . Then our return statement is:

$$\neg(\neg b + ab) + (\neg ba(\neg b + ab)) \quad (7.1)$$

Change the first product using De Morgan's laws.

$$\neg(\neg b + ab) = b \neg(ab) \quad (7.2)$$

Again, use De Morgan's laws.

$$b \neg(ab) = b(\neg a + \neg b) \quad (7.3)$$

Use the distributivity of AND over OR.

$$b(\neg a + \neg b) = b \neg a + b \neg b \quad (7.4)$$

Use a law of complementation (b and not b must be a false statement).

$$b \neg a + b \neg b = b \neg a + 0 \quad (7.5)$$

Removing the 0 of the logical sum, return the simplified first product.

$$\neg(\neg b + ab) + (\neg ba(\neg b + ab)) = b \neg a + (\neg ba(\neg b + ab)) \quad (7.6)$$

Use the distributive property on the second product.

$$(\neg ba(\neg b + ab)) = \neg b \neg ba + \neg ba ab \quad (7.7)$$

Remove clear redundancies using the laws of idempotence.

$$\neg b \neg ba + \neg ba ab = \neg ba + \neg bb \quad (7.8)$$

Use a law of complementation.

$$\neg ba + \neg bb = \neg ba + 0 \quad (7.9)$$

Remove the 0 from the logical sum and return the second product back to the original equation.

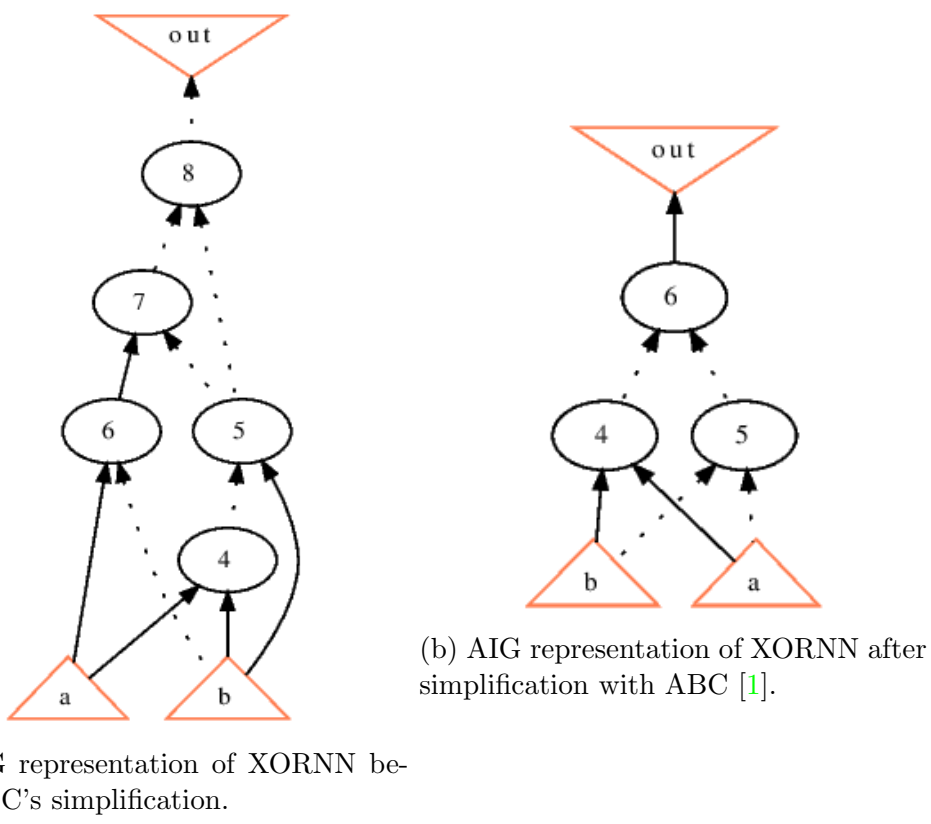
$$\neg(\neg b + ab) + (\neg ba(\neg b + ab)) = b \neg a + (\neg ba(\neg b + ab)) \quad (7.10)$$

$$= \neg ab + \neg ba \quad (7.11)$$

□

**Python to AIG** Using AIGER [21,22] and ABC [1], the logic of the neural network is expressed with an and-inverter graph (AIG) in Figure 7.8. See Section 4.2 for details on ABC's AIGs.

**Comprehensibility** By the logic in Section 5.2.2, the AIG in Figure 7.8 is more comprehensible than the original XORNN (see Figure 5.3 for a side-by-side visual).



(a) AIG representation of XORNN before ABC's simplification.

(b) AIG representation of XORNN after simplification with ABC [1].

Figure 7.8: Equivalent AIG representations of XORNN.



# Chapter 8

## Importance

The importance of an input is the input’s influence on class prediction. While importance can be evaluated with Gini impurity or information gain, this chapter finds a more computationally efficient way to determine importance specifically for neural nodes.

Furthermore, this chapter discusses why only weights and some scalar threshold ( $\theta_t$ ) need to be considered in  $\mathcal{B}$ . Section 8.1 briefly discusses why weights are the “important” factor. Furthermore, Section 8.2 and Section 8.3 explains how  $\mathcal{B}$  does not have to compute the activation function.

**Binarization** Regarding quantization, I cast all input values (values from the initial data set) into  $\{0, 1\}$ . This works fine for some inputs; however, other inputs have a non-monotonic relationship with the output and too much information is lost with the 0,1 cast. In the latter case, single inputs can be read as two or more inputs that can effectively maintain information (further addressed in Section 11.2.2).

### 8.1 Weights

Each activation function,  $f$  has a single dependent variable,  $\theta$ .  $\theta$  is found by the dot product of the weight ( $\vec{w}$ ) and input ( $\vec{x}$ ) vectors.

Lemma 8.1.1 and Theorem 8.1.2 shows that the importance of each  $x_i \in \vec{x}$  is exactly the absolute value of the corresponding  $w_i \in \vec{w}$ . This is the discovery that allows  $\mathcal{B}$  to skip the computationally expensive information gain or Gini impurity that are often used in decision trees.

**Lemma 8.1.1.** *For every  $x_i \in \vec{x}$ ,  $\frac{\delta\theta}{\delta x_i} = w_i$ .*

*Proof.*

$$\theta = \vec{x} \cdot \vec{w}^T = w_0x_0 + w_1x_1 + \cdots + w_{n-1}x_{n-1} + 1 \times w_bb \quad (8.1)$$

$$\frac{\delta\theta(\vec{w}, \vec{x})}{\delta x_i} = w_i \quad (8.2)$$

□

**Theorem 8.1.2.** *The importance of  $x_i \in \vec{x}$  is the absolute value of the corresponding  $w_i \in \vec{w}$ .*

*Proof.* Since each input ( $x_i \in \vec{x}$ ) has the same range and is scaled by its respective weight (see Lemma 8.1.1) in the linear function  $\theta(\vec{w}, \vec{x})$ , the portion of contribution each  $x_i$  has towards  $\theta$  can be found by taking the ratio of  $w_i$  to the absolute sum of all  $|w| \in \vec{w}$ .

$$\text{importance}(x_i) = \frac{|w_i|}{\sum_{w_j \in \vec{w}} |w_j|}$$

Removing the common denominator among all  $\text{importance}(x_i) \in \text{importance}(\vec{x})$  yields:

$$\text{importance}(x_i) = |w_i| \quad (8.3)$$

□

Because of Theorem 8.1.2,  $\mathcal{B}$  sorts all weights in a given node by its absolute value then iterates from the largest (most important) to the smallest (least important).

## 8.2 Monotonic Functions

This thesis uses a threshold to approximate a real-valued function as a binary function. To binarize a real function into two classes, Lemma 8.2.1 can be used. The third case can be decided in the respective algorithm that is created. For example, I chose whichever value would stop  $\mathcal{B}$  from further traversal in the  $\mathcal{B}$  algorithm. Figure 8.1b provides a visual example.

**Lemma 8.2.1.** *Given a function  $f(\theta)$  and a threshold  $\alpha \in \mathcal{R}$*

$$g(\alpha, f(\theta)) = \begin{cases} 1 & f(\theta) > \alpha \\ 0 & f(\theta) < \alpha \\ 0 \vee 1 & f(\theta) = \alpha \end{cases}$$

Alternatively, one can find the independent variable  $\theta$  instead of  $\alpha$  for  $f(\theta) = \alpha$ . Then, any relaxed or strictly monotonic function does not need to compute  $f$  for every class decision and instead can use Lemma 8.2.2. Theorem 8.2.3 proves non-decreasing monotonic functions can use a threshold on the domain, and a similar proof can be made for non-increasing monotonic functions. See Section 8.3 for examples of non-monotonic functions that can be used.

**Lemma 8.2.2.** *A threshold is  $\theta_t$  in the function:*

$$g(\theta_t, x) = \begin{cases} 1 & x > \theta_t \\ 0 & x < \theta_t \\ 0 \vee 1 & x = \theta_t \end{cases}$$

$0 \vee 1$  depends on the algorithm.  $\mathcal{B}$  takes whichever value renders a quicker computation (a greedy approach).

**Theorem 8.2.3.** *For any non-decreasing monotonic function  $f$  and any given threshold  $\alpha$  on the dependent axis, the corresponding independent value  $\theta_t$  for  $f(\theta_t) = \alpha$  may be used as the threshold without any loss in accuracy. That is,  $g(f(\theta_t), f(x)) = g(\theta_t, x)$ .  $g$  is defined in Lemma 8.2.2.*

*Proof.* By definition, non-decreasing monotonic functions must satisfy the property:

$$\forall(x, y) : x \leq y \longleftrightarrow f(x) \leq f(y) \quad (8.4)$$

Therefore, if  $f(\theta_t) = \alpha$ , then each case in  $g(\alpha, f(x))$  is identical to  $g(\theta_t, x)$ .

$$f(x) > \alpha \longleftrightarrow x > \theta_t \quad (8.5)$$

$$f(x) < \alpha \longleftrightarrow x < \theta_t \quad (8.6)$$

$$f(x) = \alpha \longleftrightarrow x = \theta_t \quad (8.7)$$

Therefore,

$$g(f(\theta_t), f(x)) = g(\theta_t, x) \quad (8.8)$$

□

**Non-Increasing Monotonic Functions** Usually, activation functions do not satisfy the *non-increasing* monotonic property:

$$\forall(x, y) : x \leq y \longleftrightarrow f(x) \geq f(y)$$

However, if an activation function does, then

$$g(\alpha, f(x)) = \neg g(\theta_t, x)) \quad (8.9)$$

since the function's slope changes from positive to negative.

### 8.2.1 Proving a Function is Monotonic

To prove a function is monotonic and that the logic above can therefore be applied to it, one can prove its first derivative is always non-positive or always non-negative. An example is given in Theorem 8.2.4.

**Theorem 8.2.4.** *One of the most common activation functions,  $f(\theta) = \frac{1}{1 + e^{-\theta}}$ , is a non-decreasing monotonic function.*

*Proof.* This is done by proving  $f(\theta)$ 's first derivative is always non-negative.

Using the chain rule, we find  $\frac{df}{d\theta}$ .

$$f(\theta) = (1 + e^{-\theta})^{-1} \quad (8.10)$$

$$\frac{df}{d\theta} = -(1 + e^{-\theta})^{-2} \cdot -e^{-\theta} \quad (8.11)$$

$$\frac{df}{d\theta} = \frac{e^{-\theta}}{(1 + e^{-\theta})^2} \quad (8.12)$$

$e^{-\theta}$  is positive since e is positive and a real-valued exponent cannot change the positivity of its base nor yield 0 from a non-zero base.

$$e^{-\theta} > 0 \quad (8.13)$$

Any square of nonzero, real-valued numbers must always yield a positive real value. To prove the denominator is nonzero, see that  $1 > 0$  and  $e^{-\theta} > 0$  by Equation (8.13). Since both values are positive and real, their summation must also be positive and real.

$$(1 + e^{-\theta})^2 > 0 \quad (8.14)$$

Of course, dividing a positive real number by another positive real number results in a positive real number. Therefore,

$$\frac{df}{d\theta} = \frac{e^{-\theta}}{(1 + e^{-\theta})^2} > 0 \geq 0 \quad (8.15)$$

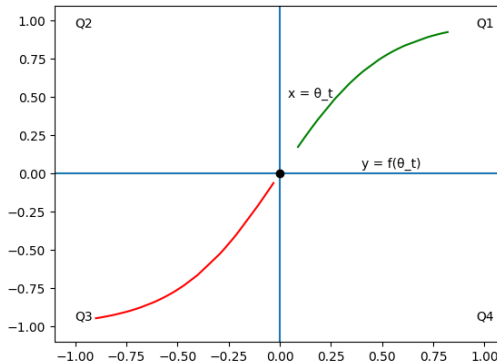
□

### 8.3 Generalizing to More Activation Functions

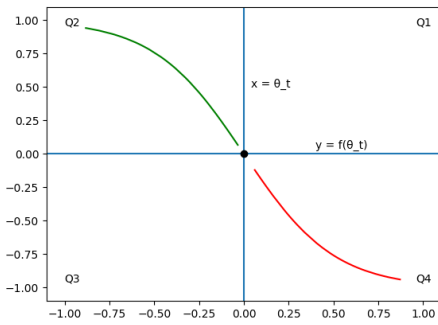
Section 8.2 relies on the monotonicity of the activation function. This section generalizes the principle of using a threshold in the domain instead of the range.

**Diagonal Quadrants** Using the domain to find the threshold instead of the range assumes that the range’s threshold corresponds to the domain’s threshold. This occurs when two perpendicular lines (one horizontal and one vertical) are drawn intersecting  $(\theta, f(\theta))$  and the function only resides on the lines of or inside two diagonal quadrants (see an illustration in Figure 8.1). For monotonic functions, any threshold satisfied this property.

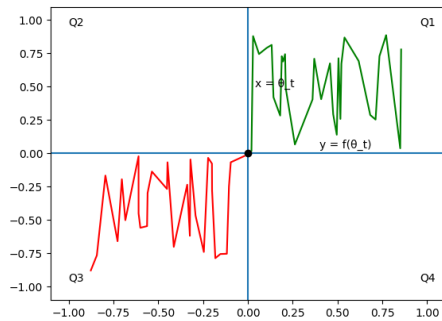
**Decent Threshold Choices** Besides satisfying the diagonal-quadrants property, a threshold must also be a “decent” choice. A formal analysis of “decent” choices for the threshold  $\theta_t$  will be left for future work, but factors such as  $\theta_t$  being a mean, median, point of inflection, drastic change in slope (ReLU), or an intersection with the y-axis are valid arguments that the threshold is “decent”. For odd (symmetric with respect to the origin), monotonic functions, Figure 8.2 shows a good strategy to find suitable thresholds. Figure 8.3 shows examples of finding a decent threshold for functions that are not odd. Finally, Figure 8.4 shows some uncommon activation functions where  $\mathcal{B}$  is not guaranteed to do well with.



(a) A function which is in diagonal quadrants Q1 and Q3.

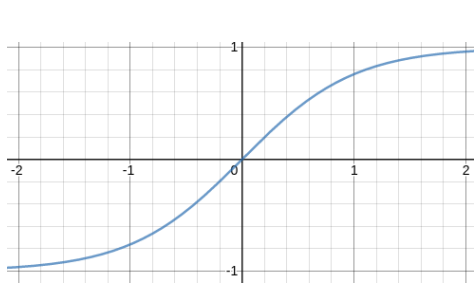


(b) A function which is in diagonal quadrants Q2 and Q4. Notice how the positive class (green) is for values less than  $\theta_t$ . Accordingly,  $\mathcal{B}$  must flip which products (summations of weights) which are considered true and false (see Section 8.2).

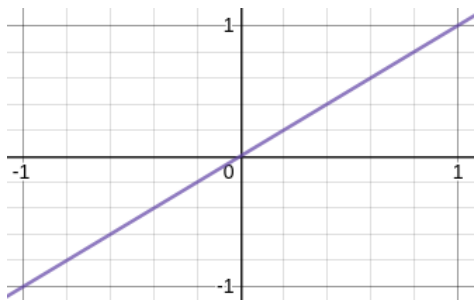


(c) The function does not need to be monotonic.

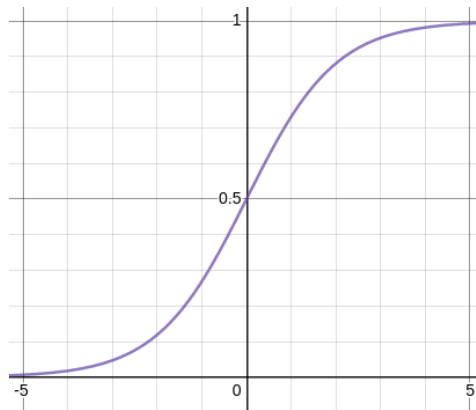
Figure 8.1: Examples of graphs which satisfy the diagonal quadrants property.



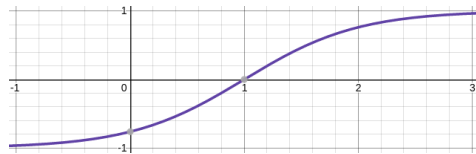
(a) In  $\tanh(\theta) = \frac{2}{1+e^{-2\theta}} - 1$ ,  
 $(a, b) = (0, 0)$  so  $\theta_t = 0$ .



(c) The identity function  $f(\theta) = \theta$   
has  $(a, b) = 0$  and  $\theta_t = 0$ .

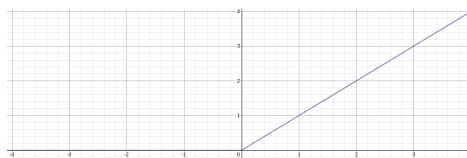


(b) In  $\frac{1}{1+e^{-\theta}}$ ,  $(a, b) = (0, 0.5)$  so  
 $\theta_t = 0$ .

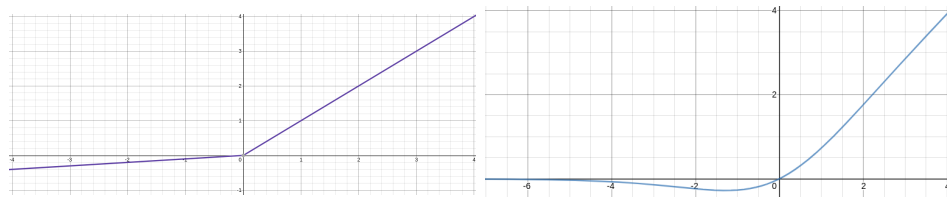


(d) Most activation functions center around  $\theta = 0$ . This function  $\tanh(\theta-1)$  is a translation of  $\tanh(\theta)$  which yields  $(a, b) = (1, 0)$  and  $\theta_t = 1$ . While not recommended as an activation function, this example is to illustrate the uncommon case of  $\theta_t \neq 0$ .

Figure 8.2: If a monotonic function  $f(\theta)$  can be translated to an odd function by a constant pair  $(a, b)$  in  $f(\theta - a) + b$ , then  $f(\theta)$  has a suitable threshold at  $\theta_t = a$ .



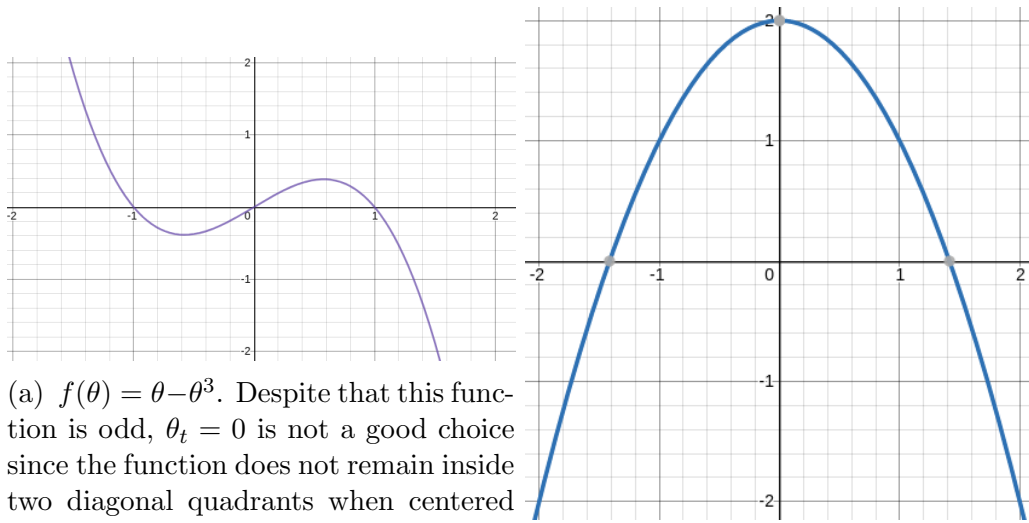
(a) For the ReLU activation function  $f(\theta) = \max(0, x)$ , we see a drastic change in slope at  $(0, 0)$ . Furthermore, ReLU was purposely designed with this sudden change at  $\theta = 0$ .  $\theta_t = 0$  is a quality choice.



(b) The leaky ReLU activation function  $f(\theta) = \max(0.1x, x)$  was made with similar intentions as ReLU. For similar reasons,  $\theta_t = 0$  is a decent choice.

(c) The Swish activation function  $f(\theta) = \theta \cdot \text{sigmoid}(\beta x)$  models a differentiable ReLU activation function [15]. Like ReLU, Swish has a great choice of  $\theta_t = 0$ .

Figure 8.3: These functions will not be odd even if translated by any constant pair. However, they still have a decent choice of  $\theta_t = 0$  since the function remains one the lines of or in two diagonal quadrants.



(a)  $f(\theta) = \theta - \theta^3$ . Despite that this function is odd,  $\theta_t = 0$  is not a good choice since the function does not remain inside two diagonal quadrants when centered on  $\theta_t = 0$ . However, if the frequency of weight summations inside  $-1 < \theta < 1$  is small,  $\mathcal{B}$  can still give accurate results.

(b)  $f(\theta) = -\theta^2 + 2$ . Even functions have no possible threshold where the function is contained in two quadrants. Therefore, even functions are unsuitable for  $\mathcal{B}$ .

Figure 8.4: Activation functions where the accuracy of  $\mathcal{B}$  will be low or conditional on the weights.

**Unsuitable Activation Functions** For uncommon activation functions such as Figure 8.4a, a single threshold is unsuitable. While  $\mathcal{B}$  can work with any threshold, the results will be less accurate as less of the function is contained within two diagonal quadrants. To regain the lost accuracy, a set of ranges could be implemented such as  $\theta_R = \{(-\infty, -1], [0, 1]\}$ ; however, this would likely make  $\mathcal{B}$  more computationally expensive on average. Considering the infrequent use and impracticality of such activation functions on  $\mathcal{B}$ , I will leave them to future work.

## 8.4 Application to $\mathcal{B}$

For functions that are contained in quadrants one and three (see Figure 8.1),  $\mathcal{B}$  translates weight summations that are greater than  $\theta_t$  as a product in the sum of products, and weight summations that are less than  $\theta_t$  are forgotten. For functions contained in quadrants two and four, the opposite can be done.

**Algorithm 3** Since each activation function has been binarized, the outputs of previous functions ( $\vec{x}$ ) can be considered as a bitmask. Now  $\mathcal{B}$  searches for every possible bitmask of  $\vec{x}$  whose dot product with the weight vector  $\vec{w}$  is greater than the threshold  $\theta_t$ . The domain threshold  $\theta_t$  can be used instead of a range threshold because most activation functions satisfy the diagonal quadrant property for suitable choices of  $\theta_t$ . Chapter 9 investigates this problem thoroughly.

---

**Algorithm 3:**

---

**Input:**

- $\vec{w} \in \mathbb{R}^n$ , the weight vector.
- $\theta_t$  the threshold.

**Output:**  $P \in \mathbb{B}^{m \times n}$  for  $0 \leq m \leq 2^n$ .  $P$  is a table of products that consist of every product in the sum of products which represents this given node.

```

 $P \leftarrow \emptyset$ 
/* The set  $\mathbb{B}^n$  can also be described as an n-ary Cartesian
   power of  $\{0,1\}$ .
forall  $\vec{x} \in \mathbb{B}^n$  do
  if  $\vec{x} \cdot \vec{w}^T \geq \theta_t$  then
     $P \leftarrow P \cup \vec{x}$ 
return  $P$ 

```

---



# Chapter 9

## Parsing the Neural Network

To parse the neural network, each layer is traversed, then  $\mathcal{B}$  converts each node in the current layer to a sum of products; finally, I construct an AIG . First, a computationally expensive brute-force attempt is shown in Section 9.1. Next, ideas from Section 8.2 are implemented into the optimized binary decision tree ( $\mathcal{B}$ ) which is presented in  $\mathcal{B}$ .  $\mathcal{B}$  converts a neural node to a sum of products (SoP) ad hoc. Next, Algorithm 7 describes the layer parsing. See Algorithm 4 for an overview of the neural network parsing and when  $\mathcal{B}$  is implemented.

---

**Algorithm 4:** A brief algorithmic description of Chapter 9.

---

**Input:**  $N[1 \dots L]$  and  $\theta_t$ .  $N$  is an array representing the layers of a neural network, and each layer is an array of in-degree weights.  $\theta_t$  is the threshold.

**Output:** AIG

Let SoP be a two-dimensional table where each element is a sum of products.

**forall**  $l_i \in N$  **do**

**forall**  $n_j \in l_i$  **do**  
   $SoP_{i,j} \leftarrow \mathcal{B}(n_j)$

$AIG \leftarrow table\_sop\_to\_aig(SoP)$

**return**  $AIG$

---

After I explain the algorithm, I give supplemental ideas and future work for  $\mathcal{B}$  in Section 9.4. Finally, I mention alternative algorithms to  $\mathcal{B}$  in Section 9.5.

|                           | $w_1 = 3$ | $w_2 = -6$ | $w_3 = -2$ | $w_{act} = \overrightarrow{mask}_i \cdot \vec{w} + 3$ | $w_{act} \geq 0$ |
|---------------------------|-----------|------------|------------|---|------------------|
| $\overrightarrow{mask}_0$ | 0         | 0          | 0          | 3   | 1                |
| $\overrightarrow{mask}_1$ | 0         | 0          | 1          | 1   | 1                |
| $\overrightarrow{mask}_2$ | 0         | 1          | 0          | -3  | 0                |
| $\overrightarrow{mask}_3$ | 0         | 1          | 1          | -5  | 0                |
| $\overrightarrow{mask}_4$ | 1         | 0          | 0          | 6   | 1                |
| $\overrightarrow{mask}_5$ | 1         | 0          | 1          | 4   | 1                |
| $\overrightarrow{mask}_6$ | 1         | 1          | 0          | 0   | 1                |
| $\overrightarrow{mask}_7$ | 1         | 1          | 1          | -1  | 0                |

Table 9.1: A truth table finding all  $2^3$  linear combinations of  $\vec{w} = [3 \ -6 \ -2]$  which satisfy  $w_{act} \geq 0$ . 3 is the bias constant and 0 is the threshold. Section 9.5.1 gives a linear algebra implementation for this brute force approach.

## 9.1 Brute Force

In this section, I give an example of a brute-force for-loop approach in Algorithm 5. Examples of bitmask vectors ( $\overrightarrow{mask}$ ) are illustrated in Table 9.1 where each variable is defined and  $w_{act} \geq 0$  is the conditional.

**Preamble for Algorithm 5** Let  $n$  = the number of dimensions in  $\vec{x}$ ,  $SOP = \text{false}$  be the sum of products, and  $P$  be the current product. Let  $\mathbb{L}$  be the ordinal set of layers in the neural network. Each  $l \in \mathbb{L}$  is a double (W, B) where W is a matrix of weights with the ordinal of the previous layer's node found by the column number, and the current layer's node ordinal found by the row number. In other words, the weight  $w_{i,j}$  in matrix W is yielded by the transition function  $prev_j \rightarrow_w curr_i$ . See Figure 9.1 for an illustration. B is the vector of bias weights for each node in the layer. Finally, “|” and “>>” are binary AIG operators for parallel composition and sequential composition, respectively [22].

Let the layers in NeuralNetwork be ordered as  $\{1, 2, 3, \dots\}$ . Since the input layer's ( $L_0$ ) out-degree weights are remembered by  $L_1$ 's in-degree weights, the algorithm will extract the input layer ( $L_0$ ) from the first layer ( $L_1$ ) in the neural network array and its nodes will be defined as  $\{node_{0,1}, node_{0,2}, \dots, node_{0,n}\}$ .

---

**Algorithm 5:** Converting a neural network to an AIG with brute force and for loops.

---

**Input:**

- NeuralNetwork, a two-dimensional array of weights following Figure 9.1.
- $\theta_t \in \mathcal{D}$  of  $f(x)$ , the threshold ( $\theta_t$ ) of the activation function  $f(x)$  as a domain value ( $\mathcal{D}$ ). See Section 8.2 and Section 8.3 for why  $\theta_t \in \mathcal{D}$ .

**Output:** NNAIG, the AIG representation of NeuralNetwork

NNAIG  $\leftarrow null$

**foreach**  $layer_l \in NeuralNetwork$  **do**

```

    layerAIG  $\leftarrow null$ 
    /*  $\overrightarrow{row}_i$  is a row vector that consists of all in-degree
       weights (except the bias weight) for the  $i^{th}$  node in
       layer  $l$ . */
    foreach  $\overrightarrow{row}_i, bias \in layer$  do
        /* The SoP representing the  $i^{th}$  node of the  $l^{th}$  layer
           will be saved to  $node_{l,i}$  */
         $node_{l,i} \leftarrow false$ 
        /* Iterate over every possible bitmask */
        forall  $\overrightarrow{mask} \in (false, true)^{length(\overrightarrow{row})}$  do
            if  $\overrightarrow{row} \cdot \overrightarrow{mask} + bias \geq \theta_t$  then
                product  $\leftarrow true$ 
                forall  $b_i \in \overrightarrow{mask}$  do
                    /*  $node_{l-1,i}$  is the  $i^{th}$  node from the
                       previous layer. */
                    if  $b_i = 0$  then
                        product  $\leftarrow product \wedge \neg node_{l-1,i}$ 
                    else
                        product  $\leftarrow product \wedge node_{l-1,i}$ 
                     $node_{l,i} \leftarrow node_{l,i} \vee product$ 
             $layerAIG \leftarrow layerAIG | SoP$ 
    NNAIG  $\leftarrow NNAIG >> layerAIG$ 
return NNAIG

```

---

$$\begin{array}{cccc}
 prev_1 \rightarrow_w curr_1 & prev_2 \rightarrow_w curr_1 & \dots & prev_n \rightarrow_w curr_1 \\
 prev_1 \rightarrow_w curr_2 & \ddots & \ddots & \vdots \\
 \vdots & \ddots & \ddots & \vdots \\
 prev_1 \rightarrow_w curr_m & \dots & \dots & prev_n \rightarrow_w curr_m
 \end{array}$$

- (a) The layer  $l$  represented by a matrix of one-way transition functions  $\rightarrow_w$  with operands of two nodes in adjacent layers where  $prev_j$  is the prior layer.

$$\begin{array}{cccc}
 w_{1,1} & w_{1,2} & \dots & w_{1,n} \\
 w_{2,1} & \ddots & \ddots & \vdots \\
 \vdots & \ddots & \ddots & \vdots \\
 w_{m,1} & \dots & \dots & w_{m,n}
 \end{array}$$

- (b) A simplified version of Figure 9.1a. For consistency with matrix notation, weights are labeled as  $w_{curr_i, prev_j}$ .

Figure 9.1

## 9.2 Binary Decision Tree ( $\mathcal{B}$ )

The classes of neural nodes are true, false, and mixed. For example, a neural node with all positive weights must always be true (hence the class “true”). However, many nodes are in the mixed class since they may be true or false.  $\mathcal{B}$  determines each neural node’s class and proceeds to find the sum of products if the node is in the mixed class. If the node is true or false,  $\mathcal{B}$  labels it as such in  $\Theta(n)$  time. Otherwise,  $\mathcal{B}$  has an average complexity of  $O(2^{0.5n})$  and a worst-case complexity of  $O(2^n)$  (see Chapter 10).

During the node’s parsing,  $\mathcal{B}$  keeps track of which node in the previous layer is considered in this sum of products. If every node in the current layer does not use some node X from the previous layer, then X is given a “negligible” class. The parsing algorithm,  $\mathcal{N}$ , directs  $\mathcal{B}$  to approximate a node and skips the negligible nodes.

As proven in Section 8.1, ordering weights by importance is the same as ordering weights by the greatest absolute value—this is why  $\mathcal{B}$  sorts the weight vector. Furthermore, recall the activation function is not computed due to Section 8.2 and Section 8.3. Lemma 8.2.2 defines a threshold. Furthermore,  $\mathcal{B}$  takes advantage of knowing that trained neural networks often

have sparse weight matrices [49].

### 9.2.1 Order

To list the inputs from the greatest importance to the least importance I used the C++ standard library's (STL) `std::sort` that has a time complexity of  $O(n \log(n))$ . However, the ordinal value (position) of the weight is used to determine which node in the previous layer the weight came from. This ordinality is destroyed by sorting. To compensate, create a simple struct called “ordinal\_weight.”

```
struct ordinal_weight {
    unsigned short const ordinal;
    float const weight;
    ordinal_weight(unsigned short const o, float const w)
        : ordinal(o), weight(w){}
    inline bool absGreaterThan(ordinal_weight const& rhs)
        const{
        return std :: fabs(weight) > std :: fabs(rhs.weight);
    }
};
```

Then STL's sort function allows for an easy sort.

```
std :: sort(
    ordinalWeightsArr.begin(),
    ordinalWeightsArr.end(),
    [](ordinal_weight const& lhs, ordinal_weight const&
        rhs){
        return lhs.absGreaterThan(rhs);
    }
);
```

### 9.2.2 $\mathcal{B}$ Defined

As described before,  $\mathcal{B}$  is an optimized, binary decision tree which finds the sum of products (SoP) approximating a neural node. Section 9.2.2 illustrates  $\mathcal{B}$  in pseudo-code.

To summarize,  $\mathcal{B}$  keeps track of the current summation of weights (current), the minimum possible summation (min), and the maximum possible

summation (max). If min is ever greater than or equal to zero, then any combination of future weights will yield true—therefore these weights are “don’t-cares” for this product. In the second case, if max is ever less than or equal to zero, then any combination of future weights will yield false (early termination). Finally, if neither case is true, the tree continues traversing. Note that both cases include equals in their conditional; this is the greedy approach as foreshadowed in Lemma 8.2.2.

**Definitions** Let  $\pi$  be the current path in  $\mathcal{B}$  and binaryNodeArgs be a tuple  $(currentSum, maxSum, minSum, node_{l,j}, i, product, SoP, prevNodesMatter)$  where

- currentSum is the summation of weights given  $\pi$ .
- maxSum is the maximum possible summation of weights given  $\pi$ .
- minSum is the minimum possible summation of weights given  $\pi$ .
- $node_{l,j} = (w_0, o_0), (w_1, o_1), \dots, (w_n, o_n)$  is an array of weight\_ordinal pairs (see Section 9.2.1) which consists of the in-degree weights for the  $j^{th}$  node of the  $l^{th}$  layer.
- $(w_i, o_i)$  is the current weight\_ordinal pair in  $node_{l,j}$
- product is a truth array that will be updated and joined with the sum of products.
- SoP is the table of products.
- prevNodesMatter is a Boolean array which  $\mathcal{B}$  uses to tell the network parser which nodes from the previous layer are used in  $node_{l,j}$ .

---

**Procedure**  $\text{root}(\text{node}_{l,j}, b, \theta_t)$ .

---

**Input:**

- $\text{node}_{l,j} = [(w_0, o_0), (w_1, o_1), \dots, (w_n, o_n)]$ , a vector of weight-ordinal pairs.
- $b$ , a bias constant.
- $\theta_t$ , the  $\theta$ -threshold (see Section 8.3).
- negligible, a Boolean variable. If  $\text{node}_{l,j}$  was not used for any node in the sequential layer,  $\mathcal{B}$ , which approximates the node, is skipped entirely.
- prevNodesMatter, as described in Section 9.2.2.

**Output:**

- $SoP$ , a sum of products describing  $\text{node}_{l,j}$ .
- prevNodesMatter is manipulated and passed by reference.

```

if negligible is true then
    return
/* Check if this node is always true or always false. */
 $b \leftarrow b - \theta_t;$ 
 $currentSum \leftarrow b;$ 
 $minSum \leftarrow b;$ 
 $maxSum \leftarrow b;$ 
for  $i \leftarrow 0 \dots n$  do
    if  $w_i \geq 0$  then
        |  $maxSum \leftarrow maxSum + w_i$ 
    else
        |  $minSum \leftarrow minSum + w_i$ 
if  $maxSum < 0$  then
    | return false
else if  $minSum \geq 0$  then
    | return true
/* Sorted by weight value. */*
 $node_{l,j} \leftarrow sort(node_{l,j});$ 
/* Initialize values */*
 $product \leftarrow true;$ 
 $SoP \leftarrow false;$ 
/* Begin the algorithm */*
 $binaryNodeArgs \leftarrow$ 
 $(currentSum, maxSum, minSum, node_{l,j}, 0, product, SoP, prevNodesMatter);$ 

if  $w_0 \geq 0$  then
    | pos_true(binaryNodeArgs);
    | pos_false(binaryNodeArgs);
else
    | neg_true(binaryNodeArgs);
    | neg_false(binaryNodeArgs);
return  $SoP$ 

```

---

---

**Procedure** atomize( $l, o$ ) –a name mangling function that labels each given node from the neural network.

---

**Input:**

- $l$ , the layer number.
- $o$ , the node's ordinal value.
- prevNodesMatter, as defined in Section 9.2.2.

**Output:** A unique name for  $node_{l-1,o}$  to be used in labeling AIG nodes.

```
prevNodesMatter[o] ← true;
/* The ordinal value, o, is referring to the previous
   layer; hence, the name-wrangling does “l-1”.           */
return "L" + string(l-1) + "N" + string(o)
```

---



---

**Procedure** directions(*binaryNodeArgs*)

---

**Input:** *binaryNodeArgs*

```
i ← i + 1;
if  $w_i \geq 0$  then
    posTrue(binaryNodeArgs);
    posFalse(binaryNodeArgs);
else
    negTrue(binaryNodeArgs);
    negFalse(binaryNodeArgs);
return
```

---

---

**Procedure** posTrue(binaryNodeArgs). The true case of a positive weight.

---

**Input:** binaryNodeArgs  
 $product \leftarrow product \wedge atomize(o_i);$   
 $current \leftarrow current + w_i;$   
 $minSum \leftarrow minSum + w_i;$   
**if**  $minSum \geq 0$  **then**  
  |  $SoP \leftarrow SoP \vee product$   
**else**  
  | directions(binaryNodeArgs)  
**return**

---



---

**Procedure** posFalse(binaryNodeArgs). The false case of a positive weight.

---

**Input:** binaryNodeArgs  
 $product \leftarrow product \wedge \neg atomize(o_i);$   
 $max \leftarrow max - w_i;$   
**if**  $max \geq 0$  **then**  
  | directions(binaryNodeArgs)  
**return**

---



---

**Procedure** negTrue(binaryNodeArgs). The true case of a negative weight.

---

**Input:** binaryNodeArgs  
 $product \leftarrow product \wedge atomize(o_i);$   
 $current \leftarrow current + w_i;$   
 $max \leftarrow max + w_i;$   
**if**  $max \geq 0$  **then**  
  | directions(binaryNodeArgs)  
**return**

---

---

**Procedure** negFalse(binaryNodeArgs). The false case of a negative weight.

---

**Input:** binaryNodeArgs  
 $product \leftarrow product \wedge \neg atomize(o_i);$   
 $min \leftarrow min - w_i;$   
**if**  $min \geq 0$  **then**  
  |  $SoP \leftarrow SoP \vee product$   
**else**  
  | directions(binaryNodeArgs)  
**return**

---

### 9.2.3 Complexity

$\mathcal{B}$ 's time complexity is in  $\Omega(n)$  and  $O(2^n)$  with an average complexity of  $\Theta(2^{0.5n})$  (see Chapter 10).

**Best-Case of  $\mathcal{B}$**  Consider the case where all the weights (including the bias's weight) are positive and the threshold is zero.  $\mathcal{B}$  will iterate over each weight (costs  $\Theta(n)$ ) to find the maximum and minimum sums possible. Since every weight and the bias are positive, the minimum sum will be equal to the bias's weight that is greater than zero.  $\mathcal{B}$  ends here and notes that this neural node is always true. The  $O(n \times \log_2(n))$  sort nor the tree traversal are needed. Therefore,  $\mathcal{B}$ 's best case is  $\Theta(n)$ . See Figure 9.2b for an example.

**Worst-Case of  $\mathcal{B}$**   $\mathcal{B}$ 's worst case is  $\Theta(2^n)$  and occurs when all of the weights have equal magnitudes and are distributed as evenly as possible between the positives and negatives bins. Figure 9.2a illustrates this case. However, Section 10.2.4 shows that  $\mathcal{B}$ 's worst case is still approximately twice as fast as the brute-force approach.

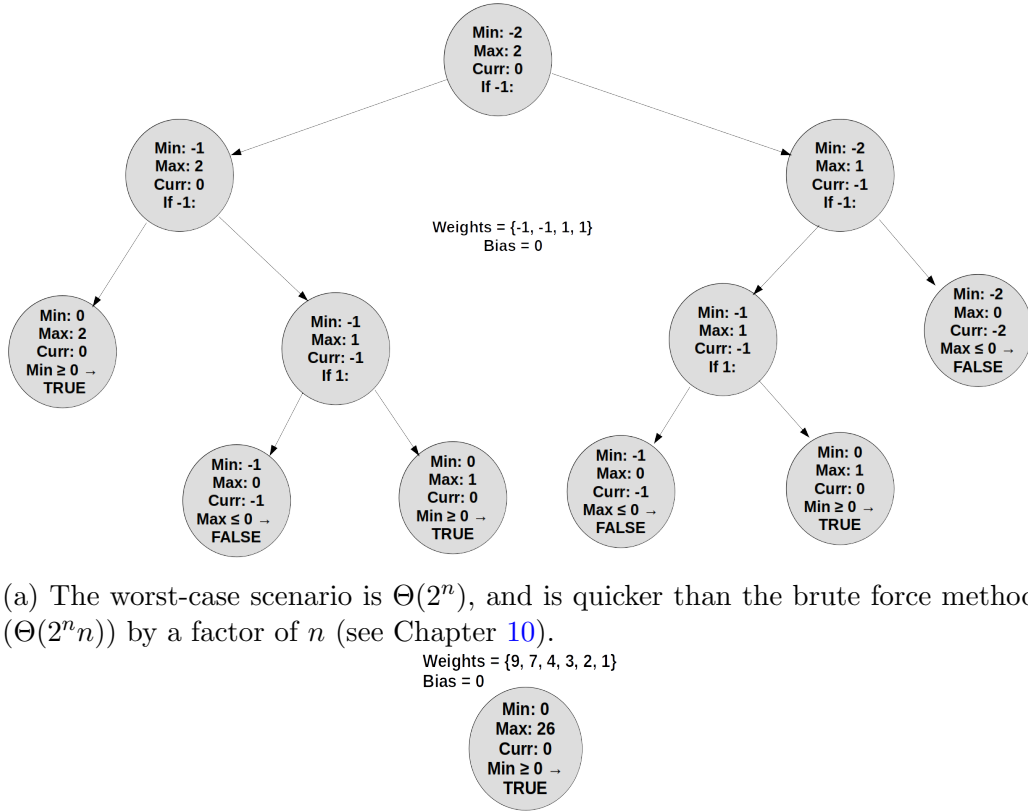


Figure 9.2: Visualization of the possible complexity extremes.

### 9.3 Traversing the Neural Network

The neural network's reversed traversal allows the algorithm to decide if a neural node must be predicted by  $\mathcal{B}$  as defined in  $\mathcal{B}$  or if the neural node is negligible and subsequently skipped. This is tracked by the `prevNodesMatter` argument in  $\mathcal{B}$ . Algorithm 6 describes a problematic forward traversal which calculates  $\mathcal{B}$  for every node while Algorithm 7 is the optimized reverse traversal.

**Forward Traversal** Algorithm 6<sup>1</sup> can be naïvely parallelized by node or by layer. However, Algorithm 6 can also produce islands (graph components that do not include an input node and an output node) or dead ends (a non-output node with an out-degree of zero) in the final AIG. For example, if no sum of products produced by layer 2 include  $node_{1,i}$  from layer 1, then the AIG will have a dead-end representing  $node_{1,i}$ . An island may occur if a node is determined to be constant (always true or always false) and is negligible (not used in any SoP for the subsequent layer). Algorithm 7 modifies Algorithm 6 by omitting negligible nodes from computation and the AIG output.

---

**Algorithm 6:** Forward Traversal

---

**Input:**  $NN = [l_1, l_2, \dots, l_m]$ . Each  $l_i \in NN$  is a vector of nodes  $[node_0, node_1, \dots, node_n]$ . Each  $node_j \in l_i$  is a vector of weight-ordinal pairs  $(w_k, o_k)$  where  $o_k$  is the placement of  $w_k$  in the original input vector for  $node_j$ . The original placement signifies the associated node from the previous layer. The function  $root$  is as defined in  $\mathcal{B}$  and begins  $\mathcal{B}$ .

**Output:** AIG approximation of the neural network.

```

for  $i = 1 \dots m$  do
    forall  $node_j \in l_i$  do
         $SoP_{i,j} \leftarrow root(node_{i,j}, bias, \theta_t);$ 
        Label the output of  $SoP_{i,j}$  as  $atomize(i, o_j);$ 
         $ParallelAIG_i \leftarrow SoP_{i,0}|SoP_{i,1}| \dots |SoP_{i,n};$ 
    endfor
     $CompleteAIG \leftarrow ParallelAIG_1 >> ParallelAIG_2 >> \dots >>$ 
     $ParallelAIG_m;$ 
return  $CompleteAIG$ 

```

---

**Reverse Traversal** Algorithm 7 reduces the computation needed by omitting the negligible neural nodes that also prevents dead ends and islands.

---

<sup>1</sup>Recall that “|” and “>>” are binary operators that take AIG as operands and denote parallel and sequential compositions, respectively [22].

---

**Algorithm 7:**  $\mathcal{N}$ : Reverse traversal

---

**Input:**  $NN = [l_1, l_2, \dots, l_m]$  as described in Algorithm 6.

**Output:** AIG approximation of the neural network.

Let  $length(l_i)$  return the number of nodes in  $l_i$ ;

$DoCurrentInputsMatter \leftarrow [true_0, true_1, \dots, true_{length(l_m)}]$ ;

**for**  $i = m, m - 1, \dots, 1$  **do**

$DoPrevInputsMatter \leftarrow [false_0, false_1, \dots, false_{length(l_{i-1})}]$ ;

**forall**  $node_{i,j} \in l_i$  **do**

$SoP_{i,j} \leftarrow$

$root(node_{i,j}, bias, \theta_t, DoCurrentInputsMatter[j], DoPrevInputsMatter);$

$DoCurrentInputsMatter \leftarrow DoPrevInputsMatter;$

$ParallelAIG_i \leftarrow SoP_{i,0}|SoP_{i,1}| \dots |SoP_{i,n};$

$CompleteAIG \leftarrow ParallelAIG_1 >> ParallelAIG_2 >> \dots >>$

$ParallelAIG_m$ ;

**return**  $CompleteAIG$

---

## 9.4 Additional Ideas

### 9.4.1 Maximum Tree Depth

$\mathcal{B}$  enforces an optional maximum depth ( $d$ ) to reduce the worst-case complexity and to increase the AIGs comprehensibility. The worst-case complexity will become  $O(2^d)$  and the average case will be  $O(2^{0.5n})$  (recall  $n$  is the size of the input vector) if  $d > 0.5n$  else the average complexity will be  $O(2^d)$ . However, the maximum depth may give some loss in accuracy for instances where  $\mathcal{B}$  would normally surpass  $d$ . See Figure 11.7 for AIG illustrations using maximum depth.

Recall the XORNN from Chapter 7 is only composed of three layers. If we change the first two layers from two to ten inputs, the average amount of nodes in the decision trees increases exponentially. Figure 9.3a does not enforce maximum depth. However, the optimal solution's depth cannot exceed the size of the previous layer (10 in this case); the proof is in Chapter 8 and  $\mathcal{B}$  enforces this concept.

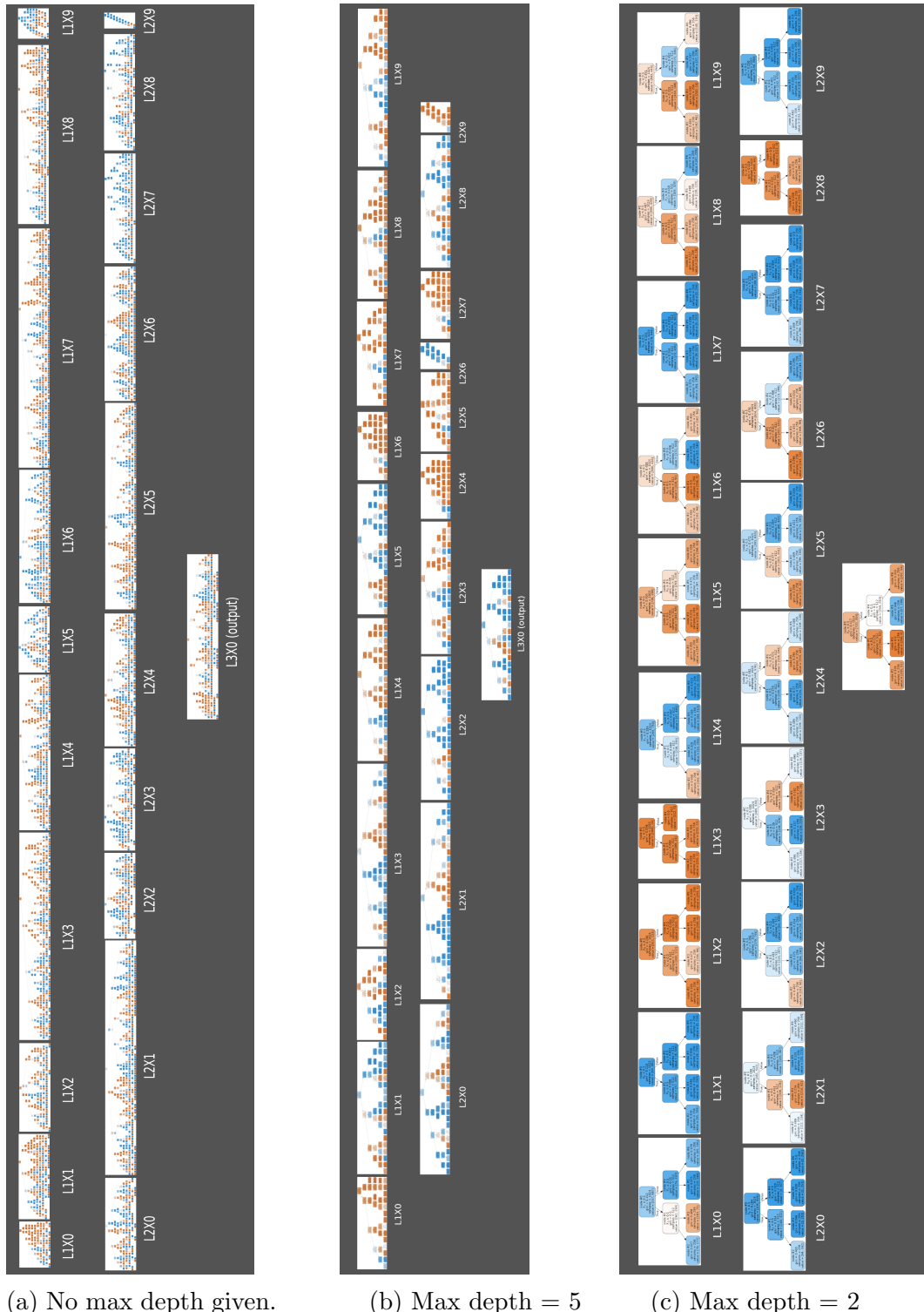


Figure 9.3: Three decision tree networks each representing a 10-10-10-1 (inputs, hidden layer 1, hidden layer 2, output) layered neural network. The input layer is inserted into the first layer of decision trees, then the network proceeds through the layers in the same fashion a neural network predicts input—the only difference being  $\mathcal{B}$  is now the activation function.

### 9.4.2 Subtrees and Dynamic Programming

Since  $\theta = \vec{x} \cdot \vec{w}^T$  is a linear combination, coefficients (weights) with similar ratios and positivity yield similar activations. This causes some subtrees in  $\mathcal{B}$  to be identical. Future work may determine how to recognize these repeated structures.

## 9.5 Alternatives

### 9.5.1 Linear Algebra

Alternatively, one can use linear algebra to obtain the sum of products for a node. Below is the Python source code that can be used to compute an entire layer (all input weight sizes are the same since the network is fully connected).

```
import numpy as np
from itertools import product
sizeOfPrevLayer = 10
sizeOfThisLayer = 1
#columns are the weights from the previous layer to the
#ith (row) node of the current layer
weights = np.random.uniform(-10, 10, (sizeOfPrevLayer,
    sizeOfThisLayer))
inputs = np.asarray(list(product([0,1], repeat=
    sizeOfPrevLayer))) #2^n possibilities
outputs = np.matmul(inputs, weights) >= 0
#Construct truth tables by concatenating inputs and
#outputs. A layer of nodes expressed as a layer of
#sum of products can be derived from this.
...
```

The iterative algorithm of matrix multiplication places this algorithm at  $\Theta(2^n \times n \times \text{sizeOfLayer})$ . However, Raz that proved the lower bound for matrix multiplications of two **square** matrices is  $\Omega(n^2 \log_2 n)$  [50]. Currently, there exists no algorithm with this low complexity—Alman and Williams published the current best complexity of  $O(n^{2.37286})$  in October 2020 [51].

**Theorem 9.5.1.** *Let  $s$  be the size of the current layer and  $n$  be the size of the weight array (equal the size of the previous layer). Then, the matrix approach has a lower bound of  $\Omega(2^n n \log_2 n)$  if  $n \leq s$  and  $\Omega(2^n s \log_2 s)$  if  $n \geq s$ .*

*Proof.* If  $n \leq s$ , then let's assume the matrix product  $M = 2^n \times n \cdot n \times s$  is instead  $C = 2^n \times n \cdot n \times n$  which is a quicker computation than the original.

Split the left-hand side of  $C$  ( $2^n \times n$ ) into  $\frac{2^n}{n}$  submatrices each with size  $n \times n$  and having no overlap. Then the product of each submatrix with the reduced RHS ( $n \times n$ ) has a lower bound of  $\Omega(n^2 \log_2 n)$  by Raz's theorem. Since there are  $\frac{2^n}{n}$  submatrices,  $C$  is therefore in

$$\Omega\left(\frac{2^n}{n} n^2 \log_2 n\right) = \Omega(2^n n \log_2 n)$$

Since  $M$  is more computationally expensive than  $C$ ,  $M$  is also in  $\Omega(2^n n \log_2 n)$ .

Alternatively,  $n > s$ . Like the prior proof, I reduce  $M$  to a less expensive  $C$  matrix. Let  $C = 2^n \times s \cdot s \times s$ .

Following the same logic as before, split  $2^n \times s$  into  $\frac{2^n}{s}$  submatrices. Then,  $C$  is in

$$\Omega(2^n n \log_2 n)$$

Since  $M$  is more computationally expensive than  $C$ ,  $M$  is also in  $\Omega(2^n n \log_2 n)$ .  $\square$

**Corollary 9.5.1.1.** *With a worst-case complexity of  $O(2^n)$  per node,  $\mathcal{B}$  is still more computationally efficient when computing an entire layer  $O(s \times 2^n)$  than the theoretical optimal algorithm for the linear algebra approach of  $\Omega(2^n n \log_2 n)$ .*

### 9.5.2 A Table-Based Approach

First and foremost, this algorithm has a worse memory complexity and average time complexity than  $\mathcal{B}$ . This approach attempted to exploit tables to reduce the worst case of  $O(2^n)$  to  $O(2^{0.5n}n)$  which occurs when the weights are approximately equal in absolute value and distribution of positive and negative weights. Unfortunately, this algorithm's time complexity is  $\Theta(2^n n)$  and the memory complexity is in  $\Omega(2^{\frac{n}{2}} n)$  and  $O(2^n n)$ . In comparison,  $\mathcal{B}$  has a time and space complexity of  $\Omega(n)$  to  $O(2^n)$  with an average of  $O(2^{0.5n})$  (see the complexity of nodes in Section 10.1).

This algorithm was appealing due to the potential  $\Omega(2^{\frac{n}{2}})$  memory-bound (see Table 9.2) and the binary search shown in step 4. This algorithm's best-case occurs exactly in the worst cases of  $\mathcal{B}$  and was intended to only be used in those cases.

**Step 0:** Begin with a set of weights,  $W$ .

**Step 1:** Divide  $W$  into sorted negative and positive bins; negligible weights (0 plus or minus the machine epsilon or greater if the user desires) can be omitted. This step is done in  $\Theta(n)$ .

**Step 2:** For each possible bitmask in both bins, calculate and remember the respective subsum (can be done by matrix multiplication Section 9.5.1). This step is in  $\Omega(2^{0.5n} n \log_2 n)$  if the negative and positive bins are equal in size and  $\Omega(2^n n \log_2 n)$  on the other extreme.

**Step 3:** Sort both bins. If step 3a can be done, this step will be a constant  $O(1)$ , else it will take  $\Omega(2^{n/2} \times \log_2(2^{n/2}) = \Omega(2^{n/2}n)$  and  $O(2^n n)$ .

**Step 3a:** Depending on the data set, the sort may be done inherently in step 2. For both bins, if the sum of the two smallest (in absolute value) is greater than or equal to the greatest absolute value of that same bin, a bitmask pattern as done in Table 9.2 can be done to produce a completely sorted array. In NEG from Table 9.2, the two smallest absolute values are  $\{-1, -0.9\}$  and the greatest absolute value is  $-1.1$ . Now,  $|-1 + -0.9| \geq |-1.1|$  so this set of weights can be sorted inherently. Omitting the negligible weights in step 1 allows more sets to be inherently sorted given this bitmask pattern. Furthermore, this algorithm was planned to only occur when the weights have approximately equal absolute values. These cases often allow for step 3a.

---

**Algorithm 8:** Step 4. See Table 9.2 for an example.

---

**Input:**

- POS, a bin of subsums for all possible positive weights with the respective bitmask table.
- NEG, a bin of subsums for all possible negative weights with the respective bitmask table.

**Output:** NodeSoP. A sum of products explaining the current node.

```

if sizeof(NEG) > sizeof(POS) then
    bins  $\leftarrow$  POS
    binl  $\leftarrow$  NEG
else
    bins  $\leftarrow$  NEG
    binl  $\leftarrow$  POS
NodeSop  $\leftarrow$  False
foreach (Bitmaski, subsumi)  $\in$  bins do
    Bitmaskn  $\leftarrow$  BinarySearch(binl, subsumi) /* BinarySearch
        returns the bitmask that corresponds to the subsum
        which is the closest absolute value in binl that is
        smaller than subsumi */*
    if Bitmaskn is null then
         $\downarrow$  continue
    foreach Bitmaskj  $\in$  Bitmask1 . . . Bitmaskn do
        product  $\leftarrow$  bins(Bitmaski)  $\cup$  binl(Bitmaskj)
        NodeSop  $\leftarrow$  NodeSop  $\vee$  product
return NodeSop

```

---

**Analysis of Algorithm 8** Let  $s$  be the size of  $bin_s$  and  $l$  be the size of  $bin_l$  where  $0 \leq s \leq 2^{\frac{n}{2}}$ ,  $2^n \geq l \geq 2^{\frac{n}{2}}$ , and  $s \times l = 2^n$ . Finding each  $Bitmask_n$  in step 4 is in  $O(s \log_2(l))$  which has the worst case when  $s = l$ . In terms of  $n$ , this makes the complexity  $O(2^{\frac{n}{2}} \log_2(2^{\frac{n}{2}})) = O(2^{\frac{n}{2}}n)$  to find each  $Bitmask_n$ . Unfortunately, adding each lower bitmask in the inner loop makes the algorithm  $O(sl) = O(2^n)$ . A hash table will not be helpful for this table since the search is for the closest value (represented by  $Bitmask_n$ ) and each bitmask corresponding to a value less than the closest value.

**Algorithm 8 Example** In Table 9.2,  $subsum_s$ 's (POS bin) first subsum  $s_1$  is zero which is paired with Bitmask1. Searching the NEG bin for the absolute value closest to  $s_1$  and still less than  $s_1$  yields Bitmask1, therefore Bitmask1 of POS unioned with Bitmask1 of NEG yields a total summation greater than or equal to zero—therefore this combination is a product in the sum of products representing the node ( $SoP_{node}$ ).  $subsum_s$ 's second subsum  $s_2$  is 1 (Bitmask2) that finds the closest, smaller absolute value in NEG bin at Bitmask2 so Bitmask2 of NEG unioned with Bitmask2 of POS is also a product in  $SoP_{node}$ . Additionally, each BitmaskN in NEG below Bitmask2 unioned with Bitmask2 of POS is also in  $SoP_{node}$ —here that only includes Bitmask1 of NEG. So far,  $SoP_{node} = 000000 + 001001 + 000001$  where the 000000 comes from the iteration of Bitmask1 in POS, and 001001 + 000001 comes from Bitmask2 in NEG.

To assert correctness (not needed in the algorithm—only for human understanding), add the respective subsums for each product in the  $SoP_{node}$  obtained so far:

$$\begin{aligned} 000000 &\rightarrow NEG(000) + POS(000) = 0 + 0 = 0 \geq 0 \\ 001001 &\rightarrow NEG(001) + POS(001) = -0.9 + 1 = 0.1 \geq 0 \\ 000001 &\rightarrow NEG(000) + POS(001) = 0 + 1 = 1 \geq 0 \end{aligned}$$

Table 9.2: An example of step two in Section 9.5.2 with the set of weights being  $\{1.2, 1.1, 1, -1.1, -1, -0.9\}$  and the bias constant  $B = 0$ .

| Weights  | NEG  |    |      | Negative Subsums<br>BitmaskN·NEG+B | POS |     |   | Positive Subsums<br>BitmaskN·POS+B |
|----------|------|----|------|------------------------------------|-----|-----|---|------------------------------------|
|          | -1.1 | -1 | -0.9 |                                    | 1.2 | 1.1 | 1 |                                    |
| Bitmask1 | 0    | 0  | 0    | 0                                  | 0   | 0   | 0 | 0                                  |
| Bitmask2 | 0    | 0  | 1    | -0.9                               | 0   | 0   | 1 | 1                                  |
| Bitmask3 | 0    | 1  | 0    | -1                                 | 0   | 1   | 0 | 1.1                                |
| Bitmask4 | 1    | 0  | 0    | -1.1                               | 1   | 0   | 0 | 1.2                                |
| Bitmask5 | 0    | 1  | 1    | -1.9                               | 0   | 1   | 1 | 2.1                                |
| Bitmask6 | 1    | 0  | 1    | -2                                 | 1   | 0   | 1 | 2.2                                |
| Bitmask7 | 1    | 1  | 0    | -2.1                               | 1   | 1   | 0 | 2.3                                |
| Bitmask8 | 1    | 1  | 1    | -3                                 | 1   | 1   | 1 | 3.3                                |

**Conclusion** This algorithm was promising because of the binary search in Algorithm 8 and only computing  $2^{0.5n}$  subsums in the best case. However,

even if we assume the best matrix algorithm possible for the best case in step 2 ( $\Omega(2^{0.5n}n \log_2 n)$ ) and a constant sort in step 3, step 4 will still make this algorithm's optimal scenario  $O(2^n)$ . The memory and time complexities of this algorithm are worse than  $\mathcal{B}$ .

# Chapter 10

## Empirical Complexity of $\mathcal{B}$

This chapter compares  $\mathcal{B}$ 's average complexity, worst-case complexity, and the alternative brute force's complexity in time and space. I derive the average complexity by performing many simulations on  $\mathcal{B}$  with a random array of weights with a uniform distribution. The empirical evidence is found by doing three regression fits:  $2^{bn}$ ,  $a \times 2^{bn}$ , and  $a \times 2^n$  where a and b are the constants to be found in the regression fits and n is the independent variable being tested (n is either the number of nodes or the time spent).

Since  $\mathcal{B}$  does a constant amount of work in each child node, the asymptotic time complexity is the node complexity. Moreover,  $\mathcal{B}$ 's structure saves the required subsum from the weight vector in each parent node. Not saving the subsums would cause a reoccurring addition over  $n$  weights inside the  $O(2^n)$  algorithm—yielding  $O(2^n n)$ . Instead,  $\mathcal{B}$ 's complexity is  $a \times 2^{bn}$ .

Future work can investigate the nature of neural network nodes and how close a uniformly-random distribution properly represents the average neural node. All regression fits are done with the SciPy Python library.

Notably, the computational time spent for  $\mathcal{N}$  (the parsing algorithm that employs  $\mathcal{B}$  many times) to approximate a neural network is dwarfed when comparing the time spent to construct the AIG using Mockturtle [5]. All experiments here only considered  $\mathcal{N}$ .

### 10.1 Node Complexity

This section is the best empirical evidence for  $\mathcal{B}$ 's average case of  $O(2^{0.5n})$  and  $\mathcal{B}$ 's worst-case being  $\theta(2^n)$ .

$\mathcal{B}$  only needs to remember the current path being traversed (memory of  $O(n)$ ), but the sum of products remembered for  $\mathcal{N}$  scales with  $\mathcal{B}$ 's. Therefore, the memory complexity of  $\mathcal{B}$  is its total nodes whose complexities are found to be in  $O(2^n)$  with an average of  $\Theta(2^{0.5})$ .

### 10.1.1 Average Node Complexity

After analyzing Figure 10.1, we see the best-fit regression for  $a \times 2^n$  is the worst fit of the three regression functions. The other two regressions ( $a \times 2^{bn}$  and  $2^{bn}$  for  $b \approx 0.5$ ) are the better fits for the data.

Table 10.1: Average node complexities of  $\mathcal{B}$

| Node Type   | $2^{bn}$                            | $a \times 2^{bn}$   | $a \times 2^n$                            |
|-------------|-------------------------------------|---|---|
| Leaves      | $\approx 2^{4.743 \times 10^{-1}n}$ | $\approx 1.870 \times 10^{-1} \times 2^{5.269 \times 10^{-1}n}$ | $\approx 4.362 \times 10^{-8} \times 2^n$ |
| Parents     | $\approx 2^{4.956 \times 10^{-1}n}$ | $\approx 6.184 \times 10^{-1} \times 2^{5.107 \times 10^{-1}n}$ | $\approx 8.548 \times 10^{-8} \times 2^n$ |
| Total Nodes | $\approx 2^{5.085 \times 10^{-1}n}$ | $\approx 7.859 \times 10^{-1} \times 2^{5.160 \times 10^{-1}n}$ | $\approx 1.291 \times 10^{-7} \times 2^n$ |

**Percent Increases** In Figure 10.2, the percentage increase from the average amount in the weight size prior is shown in a scatterplot. Since 10,000 out of the possible  $c \times 2^n$  samples are used for each weight size, there is an increasing variance as the weight array gets larger—increasing the samples in proportion to the exponentially increasing possibilities would likely reduce the change in variance. However, this would cause sampling to be exponentially more expensive on an already exponential algorithm.

In Figure 10.2, the median and means all show an approximate increase of 40%, which indicates the average case is approximately  $O(1.4^n)$ . This validates the average case of  $O(2^{0.5n})$  since

$$2^{0.5n} = (2^{0.5})^n \approx 1.4^n$$

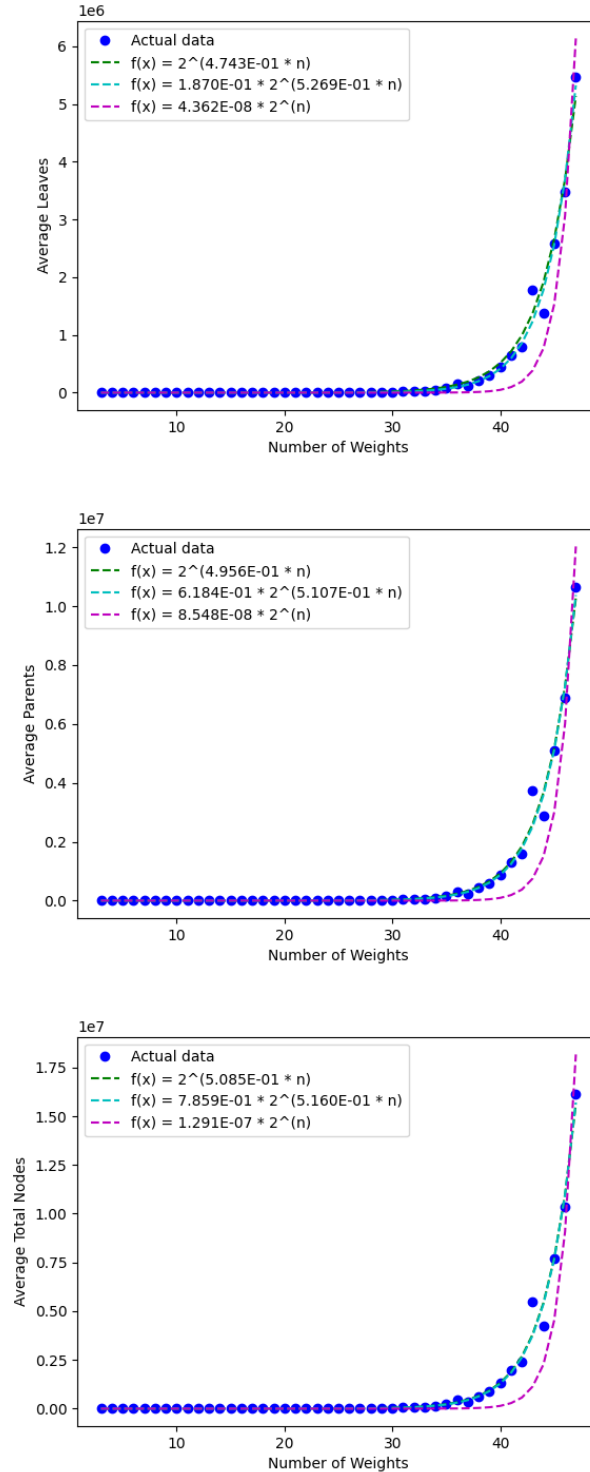


Figure 10.1: Scatter plots of  $\mathcal{B}$ 's average nodes with regression fits from Table 10.1.

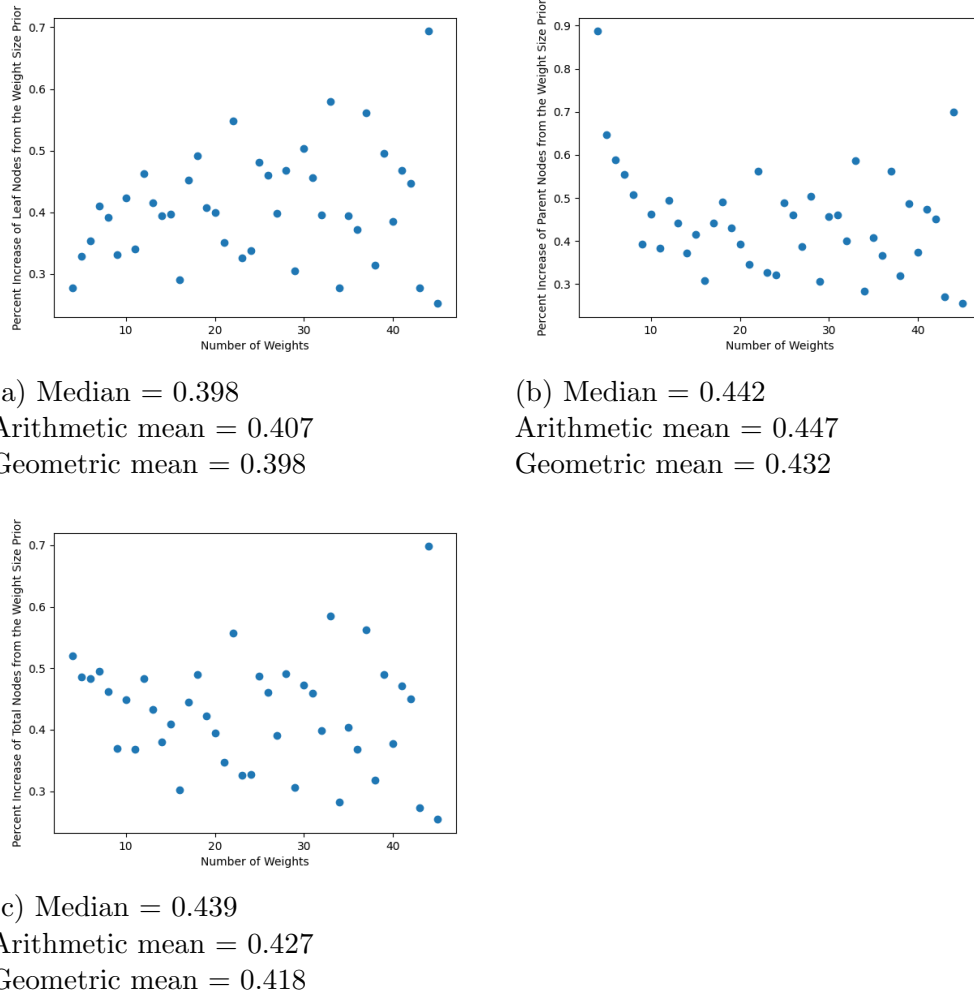


Figure 10.2: The average increases for the average node complexity using 10,000 samples for each weight. A value of 0.439 for  $\text{weight}_n$  means that  $n$  is 1.439 times greater than  $\text{weight}_{n-1}$ .

### 10.1.2 Worst-Case Node Complexity

Regression fits for the worst-case are shown in Table 10.2. The empirical evidence in Figure 10.3 strongly supports the theoretical analysis for  $\mathcal{B}$ 's worst case of  $O(2^n)$ . In Figure 10.4, we can see alternating increases (odd versus even weight array sizes). Despite the odd sizes being a smaller increase from the prior even size than vice versa, both appear to be asymptotic between 0.95 and 1 which indicates the complexity is  $O(2^n)$ .

Table 10.2: Worst-case complexities

| Node Type   | $2^{bn}$                            | $a \times 2^{bn}$   | $a \times 2^n$                            |
|-------------|-------------------------------------|---|---|
| Leaves      | $\approx 2^{8.615 \times 10^{-1}n}$ | $\approx 1.098 \times 10^{-1} \times 2^{9.813 \times 10^{-1}n}$ | $\approx 7.770 \times 10^{-2} \times 2^n$ |
| Parents     | $\approx 2^{8.976 \times 10^{-1}n}$ | $\approx 2.927 \times 10^{-1} \times 2^{9.642 \times 10^{-1}n}$ | $\approx 1.509 \times 10^{-1} \times 2^n$ |
| Total Nodes | $\approx 2^{9.201 \times 10^{-1}n}$ | $\approx 3.988 \times 10^{-1} \times 2^{9.699 \times 10^{-1}n}$ | $\approx 2.286 \times 10^{-1} \times 2^n$ |

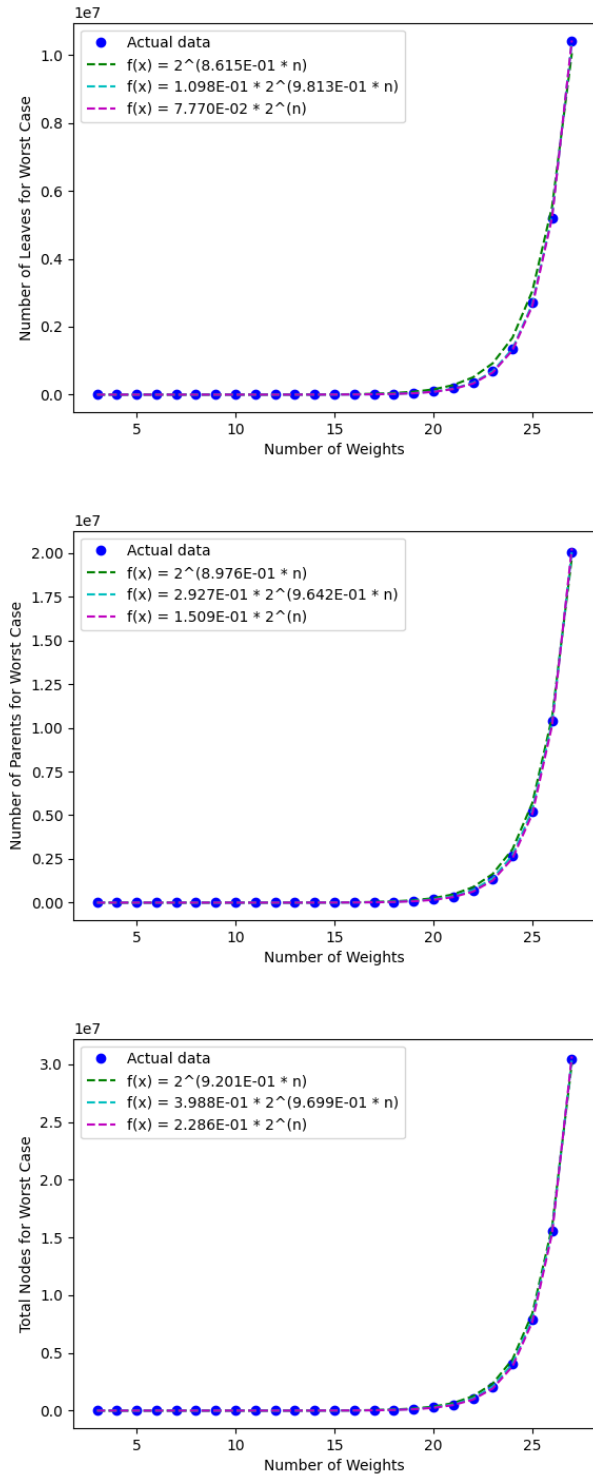


Figure 10.3: Scatter plots of  $\mathcal{B}$ 's node count in the worst-case with regression fits from Table 10.2.

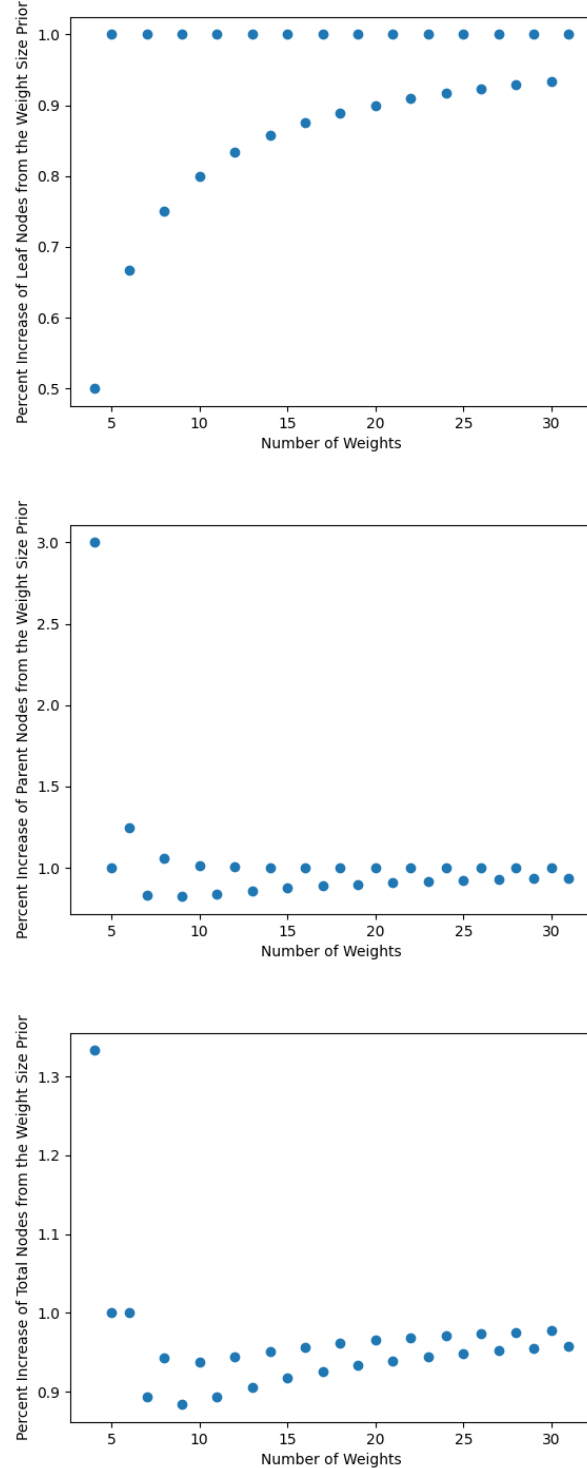


Figure 10.4: The percentage increase for the worst case. Following the structure of Figure 10.2, a value of 1.0 for weight<sub>n</sub> means that weight<sub>n</sub> had twice the amount of nodes as weight<sub>n-1</sub>.

### 10.1.3 Exhaustive Case

The exhaustive version of  $\mathcal{B}$  would be a binary tree that does not terminate early (see more information about  $\mathcal{B}$  in Section 9.2.2). By enabling early termination, the amount of total nodes in the worst case is about  $\frac{1}{9}$  of the exhaustive traversal of the tree. The exhaustive traversal ( $O(2^n)$ ) is also faster than the brute-force approach ( $O(2^n n)$ ) (see Section 10.2.3). Table 10.3 illustrates the speedup of  $\mathcal{B}$ 's worst cases over the exhaustive cases. The speedup (represented as percents) is found using the coefficient  $a$  from the  $a \times 2^n$  complexities in Table 10.2.

Table 10.3: The exact node complexity if  $\mathcal{B}$  always calculated every possibility (exhaustive case).

| Node Type   | Exhaustive Case | Percent of $\mathcal{B}$ 's Worst-case Node Complexities |
|-------------|-----------------|--|
| Leaf        | $2^n$           | 1287%  |
| Parent      | $2^n - 1$       | 663%   |
| Total Nodes | $2^{n+1} - 1$   | 875%   |

## 10.2 Time Complexity

These results further validate complexities hypothesized in Section 10.1 and give the brute force's complexity as a point of reference.

### 10.2.1 Average Time Complexity

Table 10.4 and Figure 10.5 use a uniformly random distribution to approximate the average case of  $\mathcal{B}$ . The problem of the average-case complexity here coincides with the average amount of minterms needed to express the linear combinations.

Table 10.4

| Percentile | $2^{bn}$                            | $a \times 2^{bn}$   | $a \times 2^n$                             |
|------------|-------------------------------------|---|--|
| 10th       | $\approx 2^{3.270 \times 10^{-1}n}$ | $\approx 6.754 \times 10^{-4} \times 2^{5.577 \times 10^{-1}n}$ | $\approx 4.252 \times 10^{-10} \times 2^n$ |
| 25th       | $\approx 2^{3.502 \times 10^{-1}n}$ | $\approx 1.429 \times 10^{-2} \times 2^{4.845 \times 10^{-1}n}$ | $\approx 8.438 \times 10^{-10} \times 2^n$ |
| 50th       | $\approx 2^{3.766 \times 10^{-1}n}$ | $\approx 1.224 \times 10^{-2} \times 2^{5.154 \times 10^{-1}n}$ | $\approx 1.964 \times 10^{-9} \times 2^n$  |
| 75th       | $\approx 2^{4.033 \times 10^{-1}n}$ | $\approx 7.447 \times 10^{-4} \times 2^{6.295 \times 10^{-1}n}$ | $\approx 4.743 \times 10^{-9} \times 2^n$  |
| 90th       | $\approx 2^{4.384 \times 10^{-1}n}$ | $\approx 2.043 \times 10^{-3} \times 2^{6.326 \times 10^{-1}n}$ | $\approx 1.439 \times 10^{-8} \times 2^n$  |

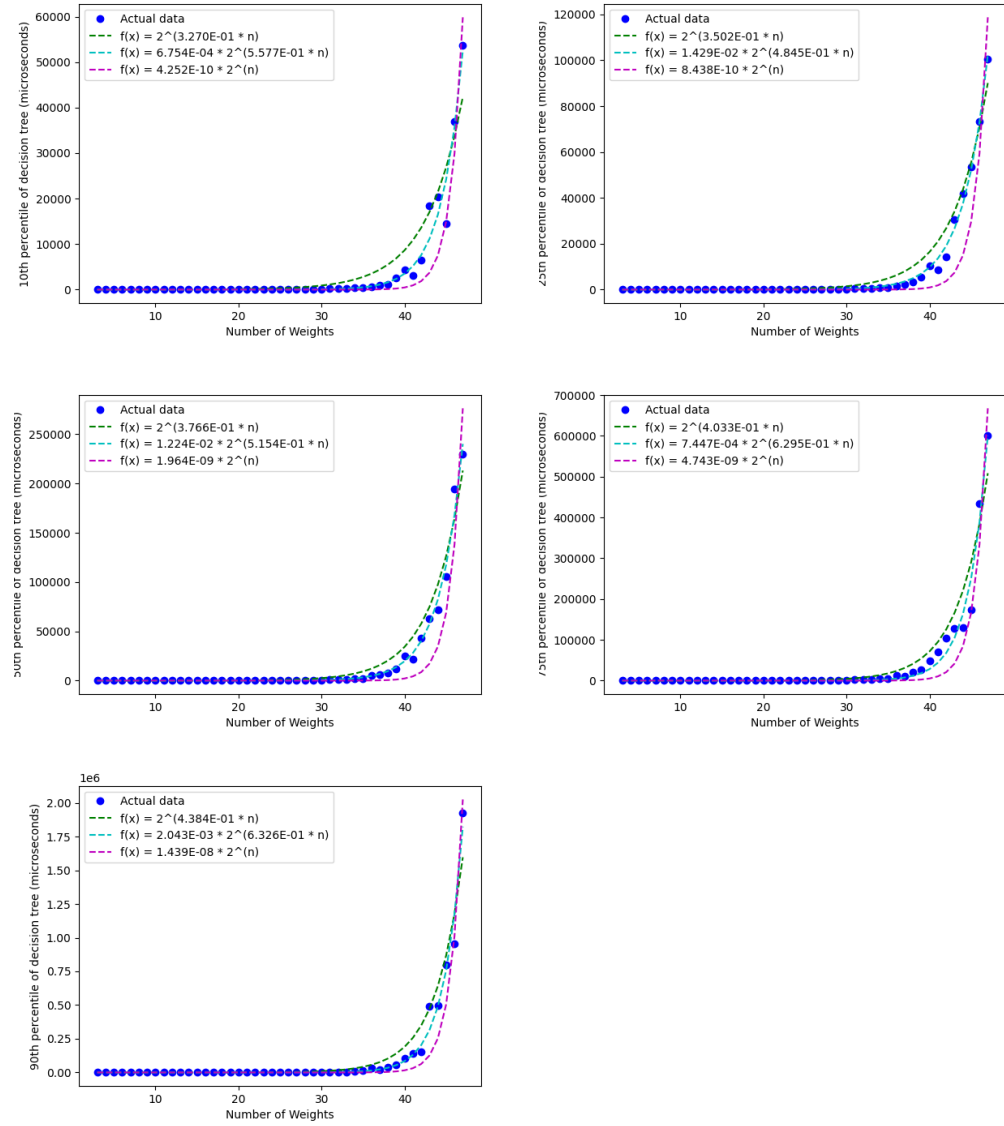


Figure 10.5: Scatter plots of recorded times for  $\mathcal{B}$ 's average case (random weights are used) with regression fits from Table 10.4.

### 10.2.2 Worst-Case Time Complexity

Table 10.5 and Figure 10.6 use weight arrays where each element has the same absolute value and the distributed between positive and negative bins are done as evenly as possible. Figure 10.6 shows that regressions of about  $2^n$  are the best fit. This confirms  $\mathcal{B}$ 's worst case of  $O(2^n)$ .

Table 10.5

| Percentile | $2^{bn}$                            | $a \times 2^{bn}$                                | $a \times 2^n$                            |
|------------|-------------------------------------|--|---|
| 10th       | $\approx 2^{7.316 \times 10^{-1}n}$ | $\approx 5.530 \times 10^{-3} \times 2^{1.014n}$ | $\approx 7.188 \times 10^{-3} \times 2^n$ |
| 25th       | $\approx 2^{7.317 \times 10^{-1}n}$ | $\approx 5.394 \times 10^{-3} \times 2^{1.016n}$ | $\approx 7.206 \times 10^{-3} \times 2^n$ |
| 50th       | $\approx 2^{7.319 \times 10^{-1}n}$ | $\approx 5.347 \times 10^{-3} \times 2^{1.016n}$ | $\approx 7.226 \times 10^{-3} \times 2^n$ |
| 75th       | $\approx 2^{7.321 \times 10^{-1}n}$ | $\approx 5.413 \times 10^{-3} \times 2^{1.016n}$ | $\approx 7.251 \times 10^{-3} \times 2^n$ |
| 90th       | $\approx 2^{7.325 \times 10^{-1}n}$ | $\approx 6.205 \times 10^{-3} \times 2^{1.009n}$ | $\approx 7.299 \times 10^{-3} \times 2^n$ |

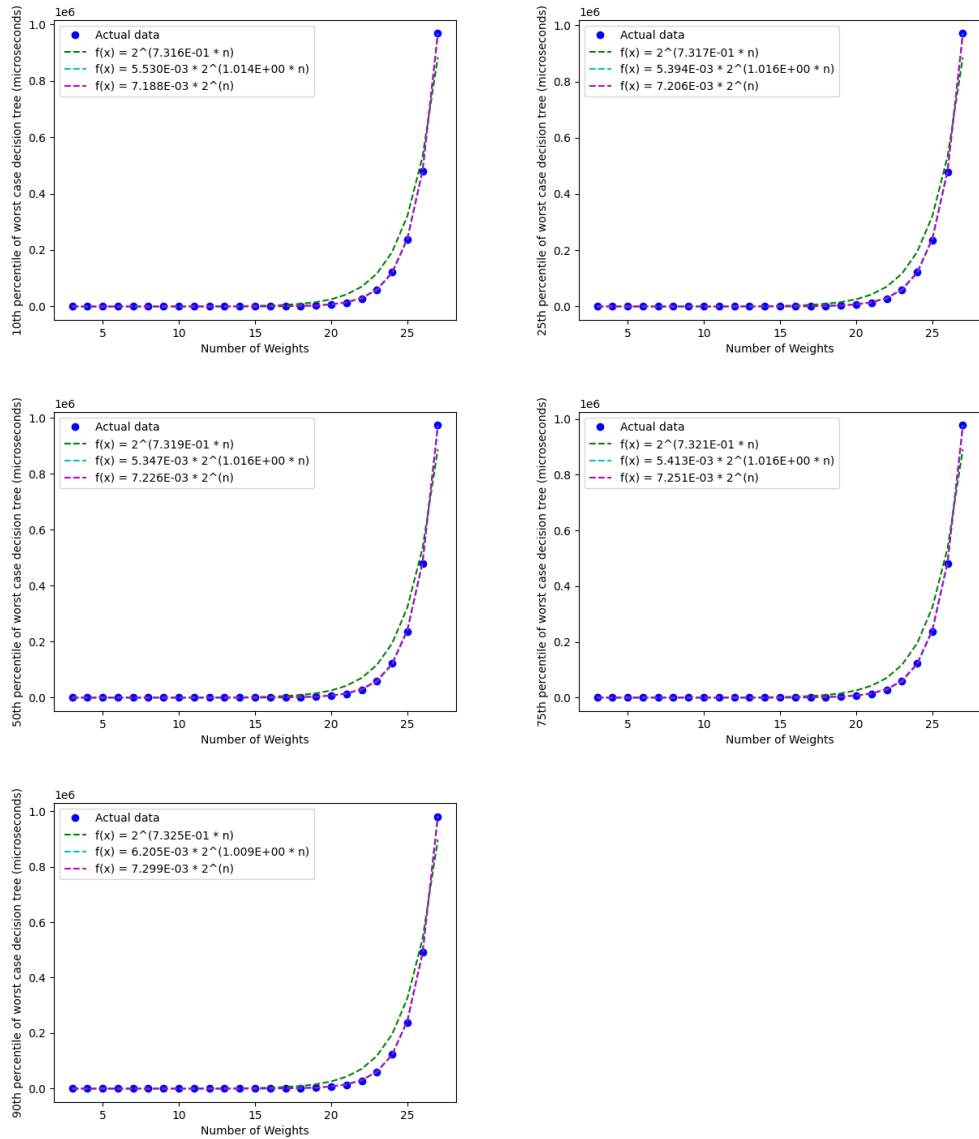


Figure 10.6: Scatter plots of times recorded for  $\mathcal{B}$ 's worst-case with regression fits from Table 10.5.

### 10.2.3 Brute-Force Complexity

Table 10.6 and Figure 10.7 approximates the complexity of a brute-force solution. The brute force solution is a simple recursive program that iterates over all  $2^n$  mask possibilities as shown in Section 10.2.3 and Section 10.2.3. Following the logic from Section 9.5.1, this algorithm has a complexity of  $O(2^n n)$ . However, the regressions are done in the same manner as the prior regressions as a control.

---

#### **Procedure initializeBruteForce**

---

**Input:**  $n$ , the number of weights.

**Output:**  $\text{productTable}$ , a sum of products describing the random weight array created.

```
/* Initialize random array. */  
randArr ← array(value=random_double, size=n);  
initMask ← array(value=false, size=n);  
productTable ← ∅;  
/* Let  $\theta_t = 0$  for this pseudocode. */  
if  $\text{initMask} \cdot \text{randArr}^T > \theta$  then  
    productTable ← productTable ∪ initMask;  
bruteForceIter(randArr, productTable, initMask, 0);  
return productTable
```

---

---

**Procedure** bruteForceIter

---

**Input:**

- randArr: an array of random weight values.
- productTable: the table of products.
- currentMask: the current bitmask.
- maskIter: tracks the current position in currentMask to update.

**Output:** Updates the productTable which is passed by reference.

```

if maskIter = currentMask.size() then
    return
    bruteForceIter(randArr, sopTable, currentMask, maskIter + 1);
    currentMask[maskIter] = true;
    if currentMask · randArrT > 0 then
        productTable ← productTable ∪ currentMask;
    bruteForceIter(randArr, productTable, currentMask, maskIter + 1);
return

```

---

Table 10.6

| Percentile | $2^{bn}$                            | $a \times 2^{bn}$   | $a \times 2^n$                            |
|------------|-------------------------------------|---|---|
| 10th       | $\approx 2^{8.833 \times 10^{-1}n}$ | $\approx 3.381 \times 10^{-1} \times 2^{9.468 \times 10^{-1}n}$ | $\approx 1.362 \times 10^{-1} \times 2^n$ |
| 25th       | $\approx 2^{8.867 \times 10^{-1}n}$ | $\approx 3.824 \times 10^{-1} \times 2^{9.430 \times 10^{-1}n}$ | $\approx 1.444 \times 10^{-1} \times 2^n$ |
| 50th       | $\approx 2^{8.947 \times 10^{-1}n}$ | $\approx 5.058 \times 10^{-1} \times 2^{9.347 \times 10^{-1}n}$ | $\approx 1.656 \times 10^{-1} \times 2^n$ |
| 75th       | $\approx 2^{9.057 \times 10^{-1}n}$ | $\approx 7.014 \times 10^{-2} \times 2^{1.061n}$                | $\approx 1.998 \times 10^{-1} \times 2^n$ |
| 90th       | $\approx 2^{9.086 \times 10^{-1}n}$ | $\approx 6.508 \times 10^{-2} \times 2^{1.068n}$                | $\approx 2.099 \times 10^{-1} \times 2^n$ |

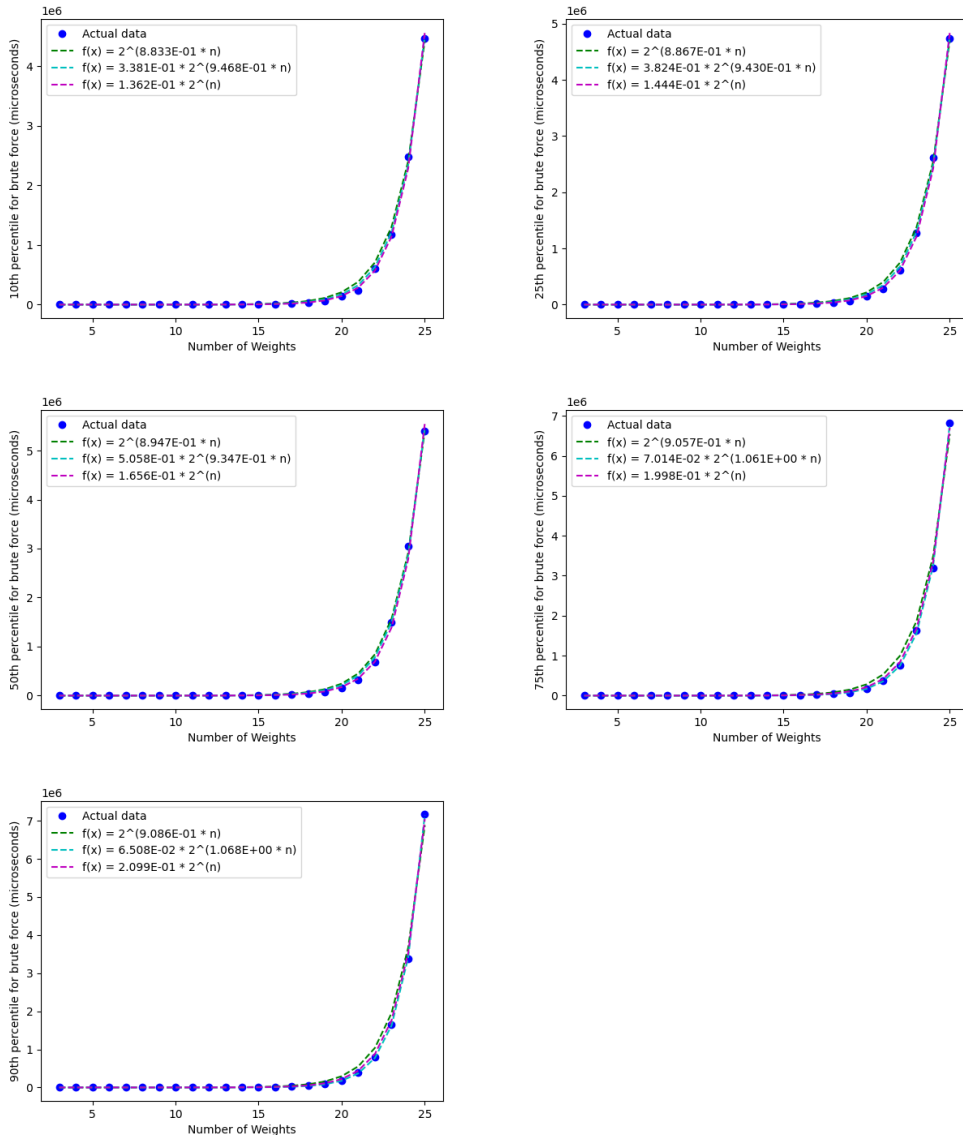


Figure 10.7: Scatter plots of the times recorded using the brute force approach with regression fits from Table 10.6.

### 10.2.4 Average, Worst, and Brute Time Ratios

While the average-case and the worst-case of  $\mathcal{B}$  and the brute force algorithm all have different complexities ( $O(2^{0.5n})$ ,  $O(2^n)$ ,  $O(2^n n)$ , respectively), the ratios are shown below to give an idea of how much quicker  $\mathcal{B}$  is for weight sizes 3 through 26. These ratios will only increase in favor of  $\mathcal{B}$  for greater weight sizes.

Table 10.7: The speedups for each complexity in the form  $a \times 2^n$ . Note:  $x : y$  is the ratio of how much faster  $y$  is than  $x$  so Worst-case:Average is the speedup of Average compared to the Worst-case.

| Percentile      | Worst-case:Average | Brute-force:Average | Brute-force:Worst-case |
|-----------------|--------------------|---------------------|------------------------|
| 10th            | $1.69 \times 10^8$ | $3.21 \times 10^8$  | 1.89                   |
| 25th            | $8.54 \times 10^7$ | $1.71 \times 10^8$  | 2.00                   |
| 50th            | $3.68 \times 10^7$ | $8.43 \times 10^7$  | 2.29                   |
| 75th            | $1.53 \times 10^7$ | $4.21 \times 10^7$  | 2.76                   |
| 90th            | $5.07 \times 10^6$ | $1.46 \times 10^7$  | 2.88                   |
| Geometric Mean  | $3.34 \times 10^7$ | $7.78 \times 10^7$  | 2.33                   |
| Arithmetic Mean | $6.24 \times 10^7$ | $1.27 \times 10^8$  | 2.36                   |

## 10.3 Conclusion

I have empirically determined  $\mathcal{B}$  (defined in Section 9.2.2) to have an average complexity (in the number of nodes and amount of time) of  $O(2^{0.5n})$  and a worst-case complexity (in the number of nodes and amount of time) of  $O(2^n)$ . In contrast, the brute-force approach has a time complexity of  $\Theta(2^n n)$ .

# Chapter 11

## Don't-Care Variables

In Boolean algebra, “don’t-cares” are variables that do not affect the output. For example, when predicting if it is going to rain tomorrow, the name of the weatherman is irrelevant and is considered a “don’t-care variable”.

Determining don’t-care variables is important in reducing the number of nodes that are represented in the final AIG, which is important in this thesis for the end goal of comprehensibility.

### 11.1 Red is Stop

First, let’s begin with a simple Boolean function. I use an example of the colors in a standard traffic light: red, yellow, and green. In this example, the yellow and green lights as input are irrelevant or ignored by the neural network—two don’t-care variables. Although I use three inputs, of which two are ignored, my point is to illustrate that any number of inputs can be ignored by a neural network if they do not contribute to the output and are thus “don’t-care variables.”

**RYG** RYG is a simple function with two don’t-care variables:

$$RYG(R, Y, G) = \neg R.$$

In other words, the function RYG takes in the input of R, Y, and G as input, but Y and G are irrelevant to the output of the neural network that returns the negation of R. As such, Y and G are don’t-care variables. Table 11.1 shows how a neural network can discover this relationship (simplified with

$\mathcal{N}$ ). See Figure 11.1a for the AIG representation of this table. Next, ABC further simplifies the function to Figure 11.1b.

Table 11.1: Every row is a product in the sum of products for each of the neural nodes trained on the RYG function in a  $3 \times 2 \times 1$  (excluding biases) neural network. The nodes are named as  $L\#X\#$  where the  $\#$  after L is the layer number and the  $\#$  after X is the node number of the layer. The input layer is L1. Since each node in L1 is activated when the input it represents is 1, L1 is boring and is not given a table.

| L2X1 |   |   | L2X2 |   |   | L3X1 |      |
|------|---|---|------|---|---|------|------|
| r    | y | g | r    | y | g | L2X1 | L2X2 |
| 0    | - | - | 0    | - | 0 | 1    | -    |
|      |   |   |      |   |   | 0    | 1    |

Theorem 11.1.1 translates Table 11.1 into the Boolean logic equivalent. Furthermore, Theorem 11.1.1 shows that  $\mathcal{N}$  is able to optimize away the y don't-care variable but not the g don't-care variable. Using simplification logic, we see that  $\mathcal{N}$  gave a correct formula and that g is optimized away.

$\mathcal{N}$  can only optimize away don't-cares that are immediately discarded in the next layer. Logic synthesis from ABC's simplification tool removes don't-care variables that are not immediately apparent [1]. See Table 11.1 for an illustration.

**Theorem 11.1.1.**  $\mathcal{N}$ 's approximation of the neural network (shown in Table 11.1) is equivalent to RYG.

*Proof.* First, convert Table 11.1 to Boolean functions.

$$L2X1 = \neg r \tag{11.1}$$

$$L2X2 = \neg r \neg g \tag{11.2}$$

$$L3X1 = L2X1 \vee \neg L2X1 \wedge L2X2 \tag{11.3}$$

Using substitution then simplification,

$$L3X1 = \neg r \vee \neg(\neg r) \wedge \neg rg \tag{11.4}$$

$$= \neg r \vee r \neg rg \tag{11.5}$$

$$= \neg r \vee 0 \tag{11.6}$$

$$= \neg r \tag{11.7}$$

□

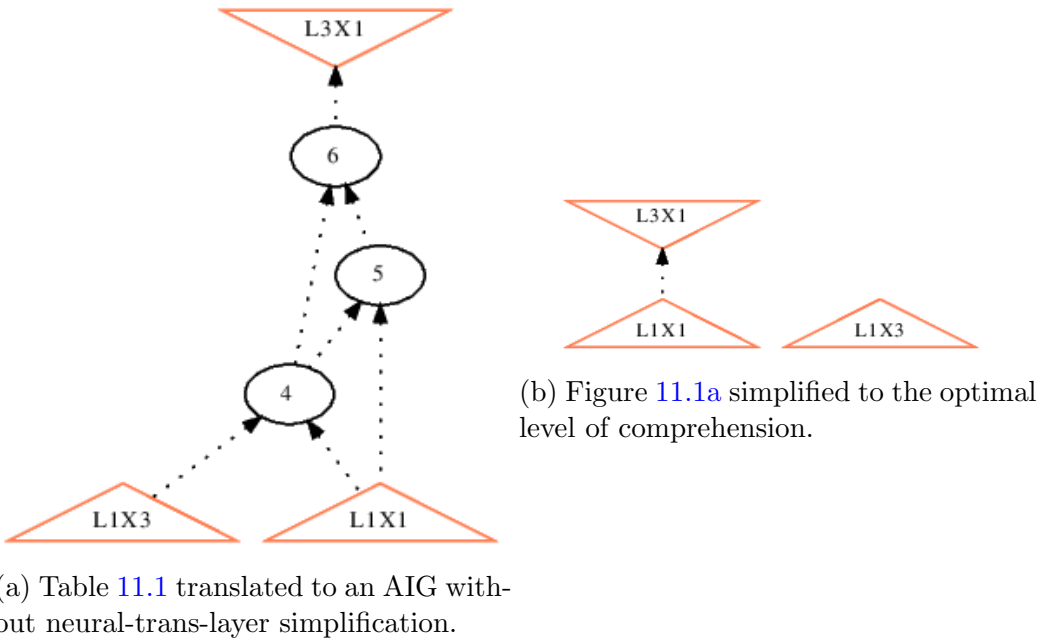


Figure 11.1: AIGs derived from Table 11.1. L1X1 is red and L1X3 is green.  $\mathcal{N}$  is able to optimize away L1X2 (yellow). This serves as a secondary proof that Table 11.1 is equivalent to RYG.

Table 11.1 shows the finished AIG that shows that the single input (L1X1 or “R”) is the only input needed and results in its negated input. Furthermore, this AIG is more comprehensible than any 4X2X1 neural network.

**Discussion** Interestingly, the neural network allowed for an impossible case of  $\neg r \wedge r$  in one of the products (see Equation (11.5)). This opens the door for future work in  $\mathcal{B}$ . Perhaps the scenario is possible before the binarization and this quasi impossibility can be used to achieve a better understanding of the neural network. Alternatively, this scenario is impossible, and future work could help  $\mathcal{B}$  skip these impossible scenarios. Another instance of  $\mathcal{B}$  including unneeded values is seen in Section 11.3.

## 11.2 Binarization and Limitations

### 11.2.1 Real to Binary Inputs

Before real-valued input is used, it must be cast to a Boolean value (binarized). Algorithm 9 defines how binarization is done in this chapter.

---

**Algorithm 9:** Binarization algorithm.

---

**Input:**

- $\hat{x}$ , some threshold.
- $I \in \mathbb{R}^n$ , the set of inputs in the real domain.

**Output:**  $I_{\text{binarized}} \in \mathbb{B}^n$ .

**forall**  $x \in I$  **do**

$$x \leftarrow \begin{cases} 0 & \text{if } x < \hat{x} \\ 1 & \text{otherwise.} \end{cases}$$

**return**  $I$

---

**Binarization Thresholds** Preliminary investigations tested four methods to obtain a threshold: median, mean, K-means with one centroid (took the centroid's value), and K-means with two centroids (took the average of the two centroid values). The mean threshold appeared to give the most accurate results. Future work can further analyze this threshold.

### 11.2.2 Illustrating the Limitations of Algorithm 9

Two limitations are identified in this section: binarized data sets that produce all possibilities and binarized data sets which do not accurately represent the original data.

#### HIGGS Data Set

Consider the HIGGS data set (a data set from particle physics that consists of real numbers) [52]. I split this set into high-level values (produced by functions) and low-level values (basic data used to compute the high-level features). One goal for publishing the HIGGS data set is to find better

functions that predict if the given data is noise or an important signal. One solution is to train and analyze a neural network.

**Neural Network Results** After applying the binarization algorithm in Algorithm 9 with the mean threshold, I got a 67% accuracy and 0.67 AUC by implementing a 28X24X24X1 neural network with the swish function activation (the majority class is 53%). Using real numbers and a far more intricate deep neural network, Baldi, Sadowski, and Whiteson managed to get 88% accuracy and 88 AUC in [52]. The AIG constructed from my 28X24X24X1 neural network (with binarized input) generated a file size too large (greater than 4GB) for ABC. So I am unable to use ABC’s simplification tools. Future work may apply maximum depth to  $\mathcal{B}$  as I did in Figure 11.7.

The loss in accuracy by binarizing the HIGGS data set can be better understood by looking at the binarized Iris data set in Section 11.2.2.

**A Simpler Neural Network** Since the 28X24X24X1 elicited an AIG too large for ABC to simplify, I tested a simpler neural network with fewer inputs.

I used Pearson correlation on the low-level values to approximate the five most promising inputs for a simple 5X4X4X1 neural network. Upon testing, I discovered the neural network performed poorly. After analyzing the data set, I found every one of the  $2^6$  possible Boolean combinations was present. See Table 11.2 for an example of every Boolean combination given two inputs.

| a | b | f(x) |
|---|---|------|
| 0 | 0 | 0    |
| 0 | 0 | 1    |
| 0 | 1 | 0    |
| 1 | 0 | 0    |
| 0 | 1 | 1    |
| 1 | 0 | 1    |
| 1 | 1 | 0    |
| 1 | 1 | 1    |

Table 11.2: A neural network cannot learn this function when reduced to this set, yet when trained on the original set the neural network biased towards the most instances of input/output pairs.

**AIGs From Uncertain Neural Networks** Furthermore, the resulting AIG's approximation of the simpler neural network had varying accuracy (about 50% to 90%). This is due to the activation outputs being around the binary threshold caused by the trained neural network's uncertainty. See Section 11.4 for more research into neural network certainty and resulting AIG approximations.

### Binarization Limits

Some features cannot be binarized without a sufficient loss of information. In this section, I will use the historic Iris data set from the early 1900s. The Iris data set is often used in statistics and machine learning education because of the simplicity of the data set. There are three Iris species in the data set: Virginica, Setosa, and Versicolor.

For example, notice how Virginica's sepal width (orange lines) in Figure 11.2 tends to be less than Setosa's but greater than Versicolor's sepal widths. Assume we wanted to create a binary class of "yes Virginica" or "not Virginica" and binarize the respective inputs. With Algorithm 9, we are allowed one threshold ( $\hat{x}$ ) for each input. Where should the  $\hat{x}$  for sepal width be? If  $\hat{x} = 3$ , then both 0 and 1 have approximately a  $\frac{1}{3}$  chance to represent Virginica's sepal width—this makes the sepal width input useless. A better solution is to place  $\hat{x}$  between Virginica and Versicolor ( $\hat{x} \approx 2.8$ ), then 1 will have about 50% chance of being Virginica and 0 will be not Virginica.

However, this problem is better solved if we gave sepal width more thresholds and more bits as done in Algorithm 10. Future work can expand on converting a real-valued input to multiple binary inputs (even greater than two) that can preserve essential information. Brudermueller et al. converted real-valued numbers to multiple binary inputs, but they did not minimize the number of bits needed per input [2].

---

**Algorithm 10:** Example of casting a real-valued input into multiple binary inputs.

---

**Input:**

- $I_s \in \mathbb{R}^n$ , the set of all sepal width inputs.
- $\hat{x}_1 = 2.8$ , the first threshold for sepal width.
- $\hat{x}_2 = 3.2$ , the second threshold for sepal width.

**Output:**  $I_{s:2-bit}$ , a set representing each element in  $I_s$  as a pair of bits.

```

 $I_{s:2-bit} \leftarrow \emptyset$ 
forall  $x \in I_s$  do
  if  $x < \hat{x}_1$  then
    |  $I_{s:2-bit} \leftarrow I_{s:2-bit} \cup \{00\}$ 
  else if  $x < \hat{x}_2$  then
    |  $I_{s:2-bit} \leftarrow I_{s:2-bit} \cup \{01\}$ 
  else
    |  $I_{s:2-bit} \leftarrow I_{s:2-bit} \cup \{10\}$ 
return  $I_{s:2-bit}$ 

```

---

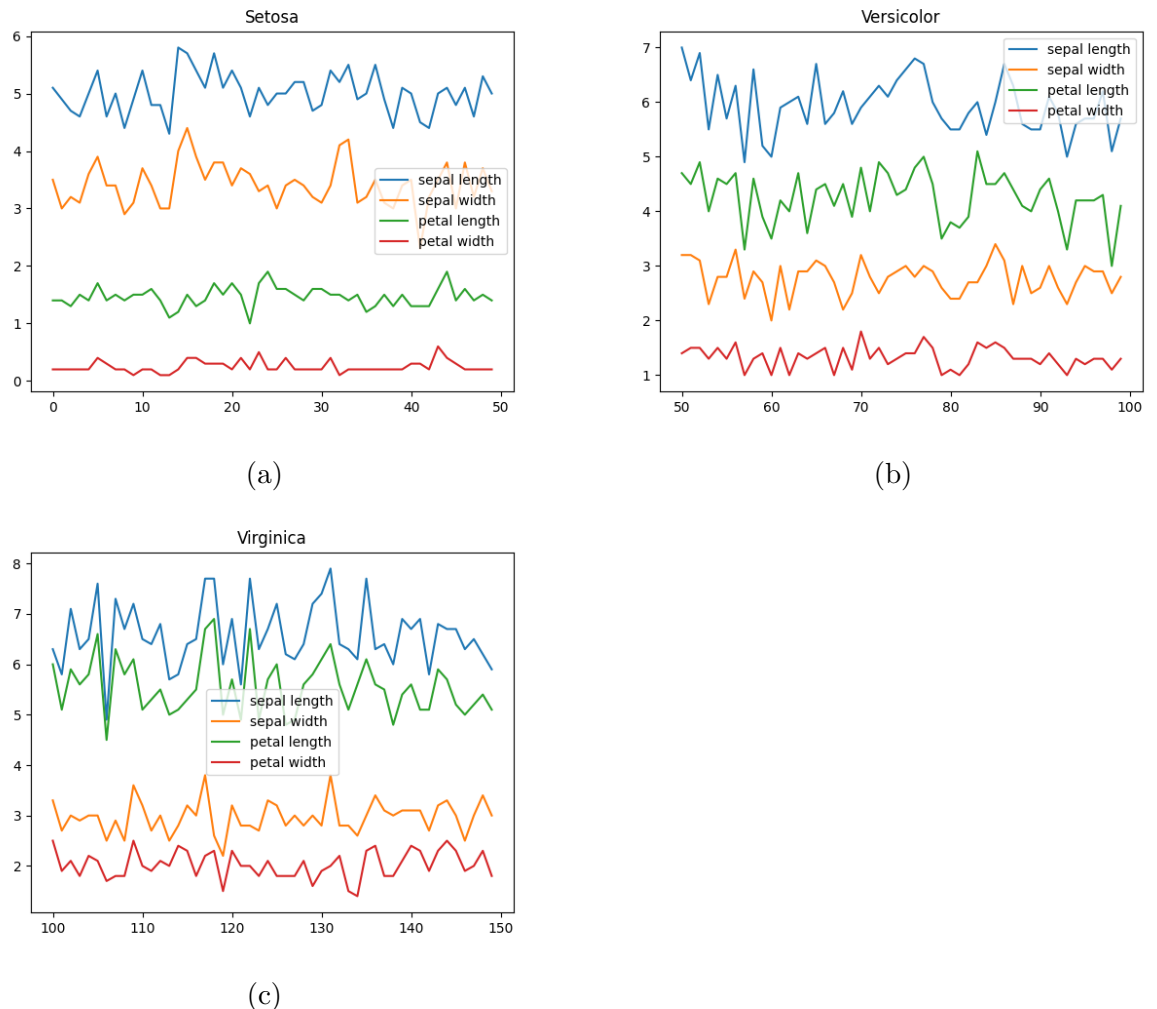


Figure 11.2: Line plots of the features for each class in the renown Iris data set.

Since Algorithm 9 cast the real-valued inputs into binary with a single pivot, the optimal data set for this algorithm consists of important inputs (inputs with the most weight in deciding classes) that are linearly separable—such as two clusters. Inputs that should not be determined by a single threshold will lose useful information (by definition) and should be discarded. This is why the future work of casting real-values to multiple bits is vital. Linearly separable relationships are the reason  $\mathcal{B}$  can binarize activation functions in Section 8.2.

Alternatively, one may train two neural networks—one that predicts Versicolor or Setosa, and the other predicts Versicolor or Virginica. To begin this second approach, copy the Iris data set into a second data set, erase all Virginica instances from the data set for the first neural network, and all Setosa rows from the other. Now, sepal width is linearly separable in both data sets. The first neural network is explored in Section 11.3.

## 11.3 Versicolor or Setosa

**Generalization Captured** I ran a 4X2X1 (bias nodes excluded) neural network several times on the Versicolor/Setosa binarized data set. Each neural network only differentiated in its initial randomized weights.

I will use a quadruple (sepal length, sepal width, petal length, petal width) or  $(n_1, n_2, n_3, n_4)$  to represent the inputs of the Iris data set with an epistemological commitment of  $\{0, 1, -\}$  which denotes {false, true, don't care}, respectively. Over 20 tests, the constructed AIG and the original neural network correctly predicts class 0 for inputs with  $(-, -, 0, 0)$  and class 1 for inputs like  $(-, -, 1, 1)$  (see Figure 11.3). Six of those eight possibilities are explicitly trained in the neural network (the six unique possibilities are shown in Table 11.3). Theorem 11.3.2 and Theorem 11.3.1 prove that the AIG correctly predicts these classes.

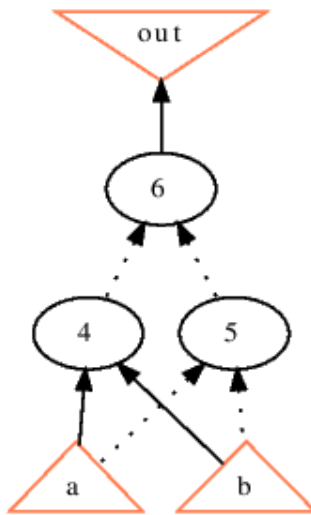


Figure 11.3: The optimally comprehensible AIG for the Versicolor or Setosa neural network. a is petal width and b is petal length. The comprehensibility is  $\frac{1}{9}$  (see Section 5.2.2).

| sepal length | sepal width | petal length | petal width | class |
|--------------|-------------|--------------|-------------|-------|
| 0            | 1           | 0            | 0           | 0     |
| 0            | 0           | 0            | 0           | 0     |
| 1            | 1           | 0            | 0           | 0     |
| 1            | 1           | 1            | 1           | 1     |
| 1            | 0           | 1            | 1           | 1     |
| 0            | 0           | 1            | 1           | 1     |

Table 11.3: All unique instances from the 100 rows left from excluding the Virginica class/feature combinations. Each input is binarized by the mean threshold (Section 11.2.1). Class 0 is Setosa and class 1 is Versicolor.

The network contains 4 logic nodes and 0 latches.

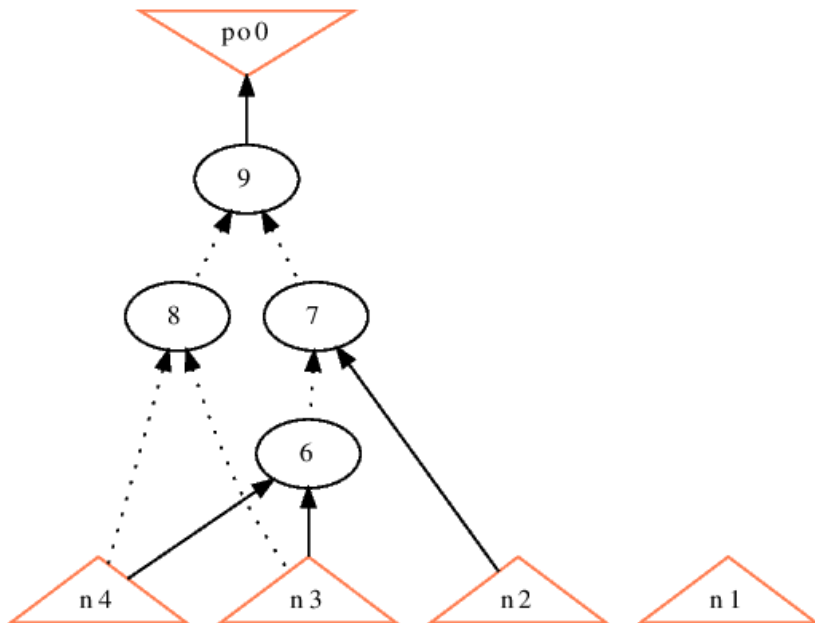


Figure 11.4: The AIG constructed by the weights given in Table 11.4;  $(n_1, n_2, n_3, n_4) = (\text{sepal length}, \text{sepal width}, \text{petal length}, \text{petal width})$ . From this, we can illustrate the neural network places heavy importance on homogeneous petal length/width pairs (see Theorem 11.3.1 and Theorem 11.3.2). Recall the simplified comprehensibility comparison outlined in Section 5.2.2. From this, the AIG has 3 inputs, 4 AND gates, and 4 NOT gates so the comprehensibility is quantified as  $\frac{1}{11}$ . The  $4 \times 2 \times 1$  neural network's inputs plus operations equals  $4 + 2(2 \times 4 + 1) + 1(2 \times 2 + 1) = 27$  and yields a comprehensibility of  $\frac{1}{27}$ . Since  $\frac{1}{11} > \frac{1}{27}$  the AIG is more comprehensible.

**Theorem 11.3.1.** *For the AIG in Figure 11.4, inputs that satisfy (-, -, 0, 0) must be class 0.*

*Proof.* Let  $(n3, n4) = (0, 0)$ . Then

$$Node_8 = AND(\neg n3, \neg n4) = 1 \quad (11.8)$$

In the binary AND operation, if any input is zero, then the result is zero.

$$Node_9 = AND(\neg Node_8, -) = 0 \quad (11.9)$$

The edge  $Node_9 \rightarrow po0$  does not negate so

$$Node_9 = po0 \quad (11.10)$$

□

**Theorem 11.3.2.** *For the AIG in Figure 11.4, inputs that satisfy (-, -, 1, 1) must be class 1.*

*Proof.* Let  $(n3, n4) = (1, 1)$ . Then

$$Node_8 = AND(\neg n3, \neg n4) = 0 \quad (11.11)$$

$$Node_6 = AND(n3, n4) = 1 \quad (11.12)$$

$$Node_7 = AND(\neg Node_6, -) = 0 \quad (11.13)$$

$$Node_9 = AND(\neg Node_8, \neg Node_7) = po0 = 1 \quad (11.14)$$

□

**Noise** While the AIG (Figure 11.4) accurately approximates the neural network for homogeneous petal length and petal width pairs, it is incorrect for inputs that the neural network is uncertain of (heterogeneous petal length and petal width values such as (-, -, 0, 1) or (-, -, 1, 0)). Given the data set, these heterogeneous pairs seem impossible or highly unlikely. It makes sense that the AIGs does not accurately predict these values since the neural networks are not even certain about them. Future work can consider the

```
Hidden node 1: -6.009057,2.0612597,-2.9449704,5.974104,6.9705567;
Hidden node 2: -5.9144406,1.9556314,-2.8650305,6.964409,5.840615
Output node: -12.945059,13.440295,13.615166
```

Table 11.4: An example of a 4X2X1 neural network that is certain for homogeneous sepal length/width values and uncertain for other inputs. Each of the hidden nodes's in-degree weights are ordered as bias, sepal length, sepal width, petal length, and petal width. The output node in-degree weights are ordered as bias, hidden node 1, hidden node 2.

input space with  $\mathcal{N}$  and omit the neural network relationships specifically for these unlikely inputs for a simpler AIG output.

Across several tests, the resulting AIG from the 4X2X1 neural network all articulated the homogeneous sepal length/width pairs with the predicted class correctly (see two more AIG examples in Figure 11.5 and Figure 11.6). The small neural network gave this relationship priority. Subtle and developing relationships in the large neural network occur inconsistently and are often not helpful. Furthermore, removing these subtle or developing relationships will help human comprehension. Figure 11.6 shows an example of the many developing or subtle relationships a large neural network may have. To remove these subtle or developing relationships, I recommend finding commonality among the several AIGs that approximate several different neural networks (an ensemble of AIGs). Section 11.4 is the first step to finding accurate (and relatively concise) AIGs for complicated neural networks by using ensembles.

Despite that the 4X2X1 neural network is uncertain for most of the heterogeneous petal length/width inputs, Section 11.4 shows that larger neural networks have room to predict heterogeneous pairs with greater certainty and elicit AIGs that correctly approximate the neural network (with about 95% accuracy).

The network contains 5 logic nodes and 0 latches.

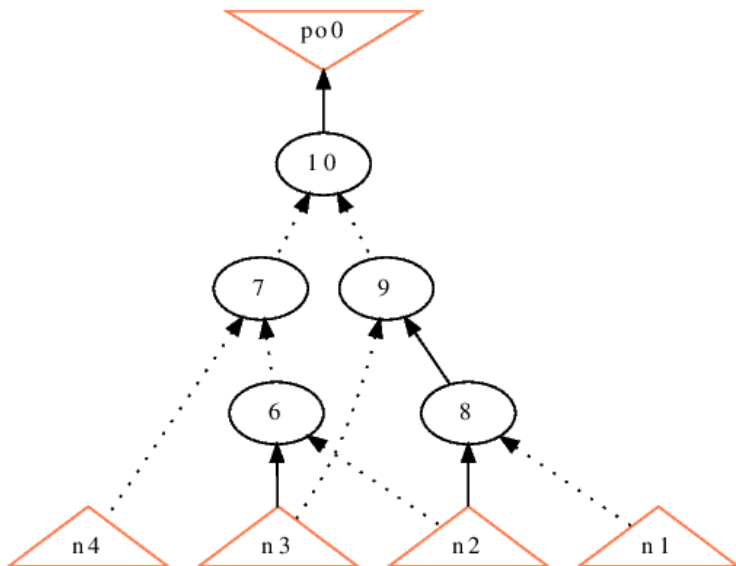


Figure 11.5: An AIG constructed from a separate neural network trained on the same data as the neural network that elicited Figure 11.4. We see that any input of homogeneous (n<sub>3</sub>, n<sub>4</sub>) pair is 100% accurate. This AIG has 4 inputs, 5 AND gates, and 7 NOT gates making the comprehensibility  $\frac{1}{16}$ . Figure 11.4 showed the 4X2X1 neural network's comprehensibility to be  $\frac{1}{27}$ . Since  $\frac{1}{16} > \frac{1}{27}$ , this AIG is more comprehensible than the neural network.

The network contains 141 logic nodes and 0 latches.

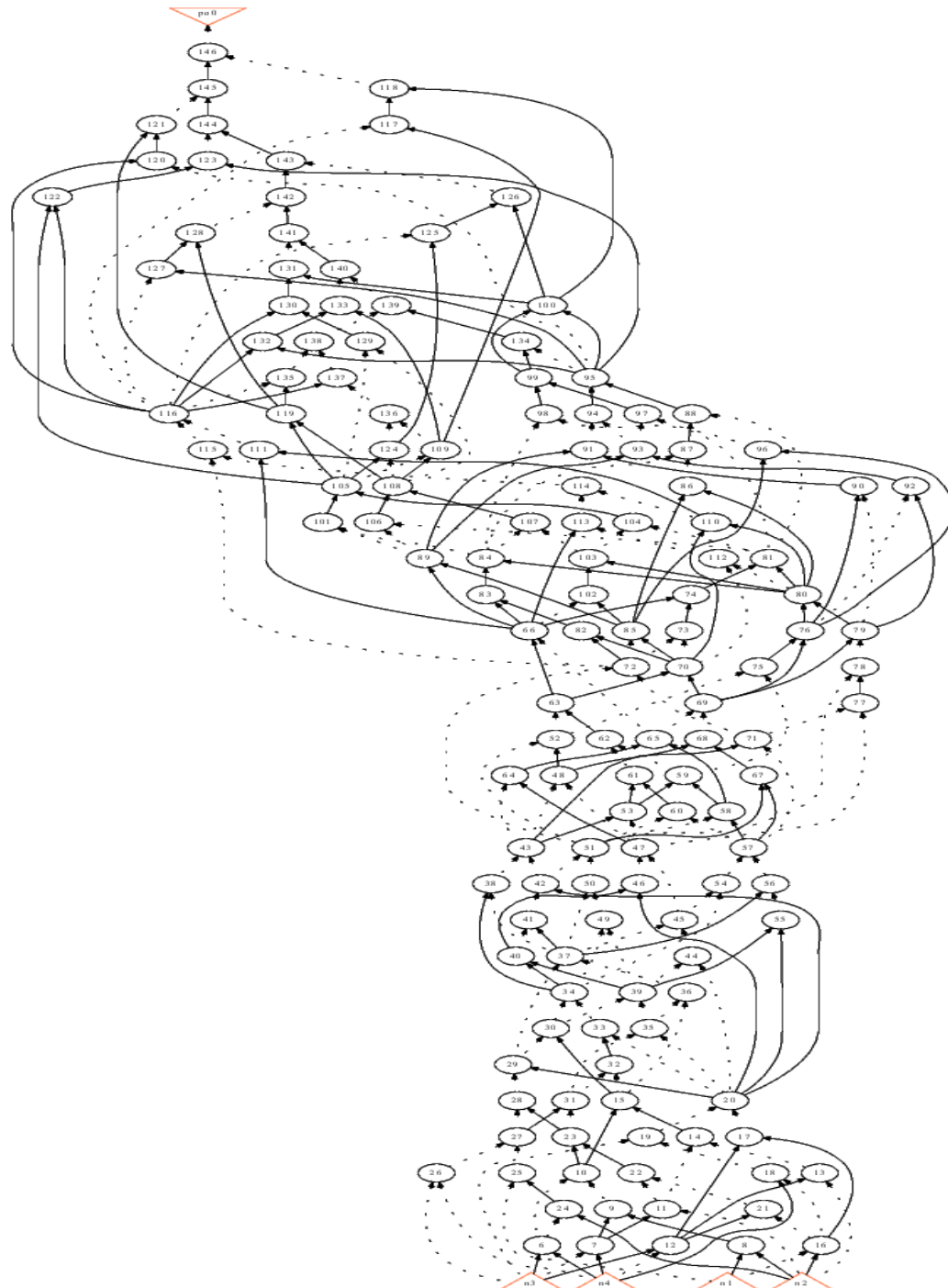
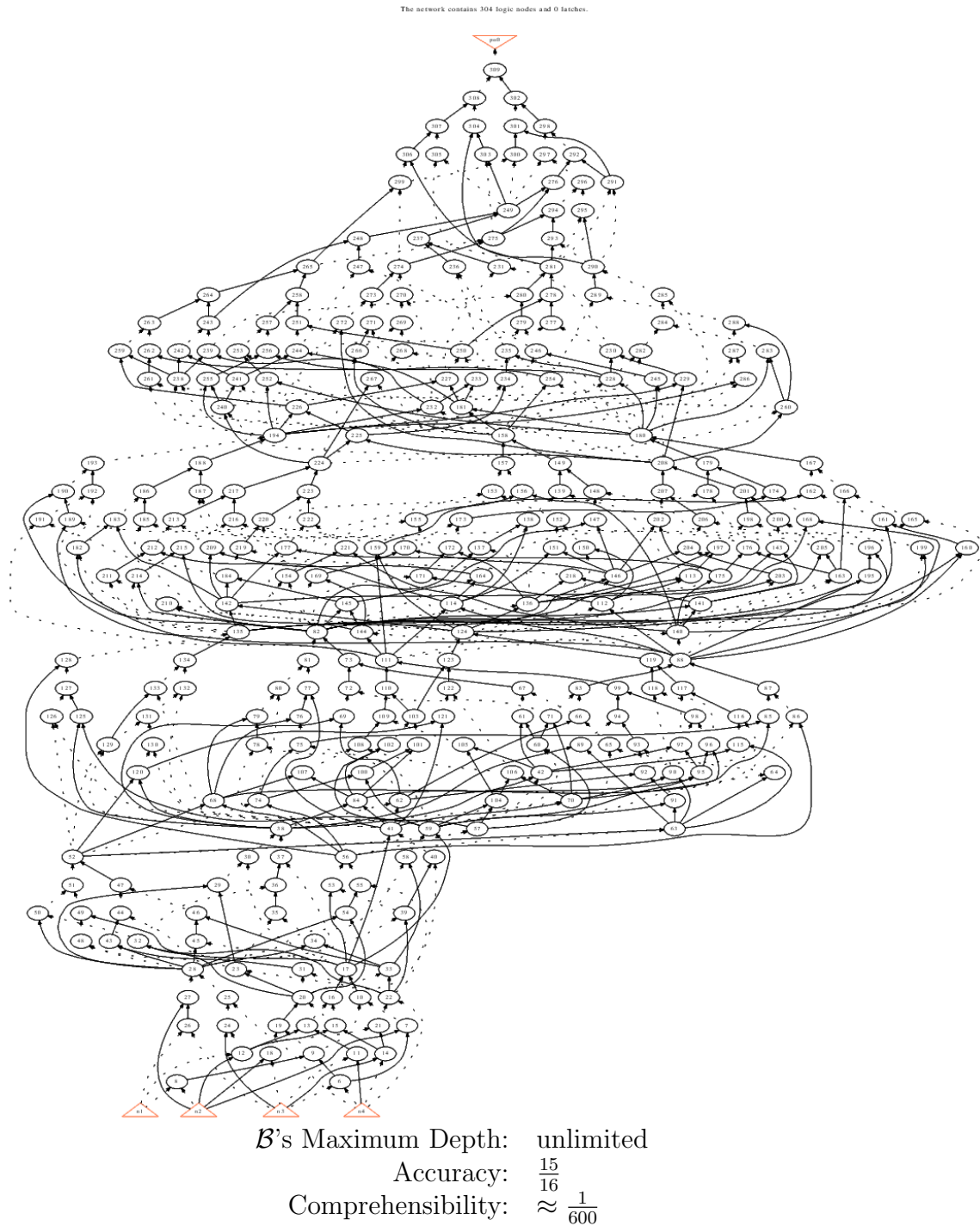


Figure 11.6: The AIG from a larger neural network ( $4 \times 5 \times 5 \times 5 \times 5 \times 1$  excluding biases) that was trained on the same data set eliciting Table 11.3. Like all other AIGs derived from neural networks trained on this data, homogeneous petal width/length pairs are perfectly construed. This AIG is more complicated due to the greater volume of subtle or developing relationships in the neural network. The neural network comprehensibility is  $\frac{1}{255}$  and this AIG's comprehensibility is  $\frac{1}{239}$ .

**On Complex Neural Networks** Sometimes  $\mathcal{N}$  produces an AIG less comprehensible than the neural network if we follow the neural-network-biased system presented in Section 5.2.2. For example, Figure 11.6's comprehensibility ranges between  $\frac{1}{44}$  and  $\frac{1}{551}$  on the seven neural-networks-to-AIGs tested. A better comprehensibility metric may consider the bits and complexity of operations; AIGs would almost certainly always win with this metric.

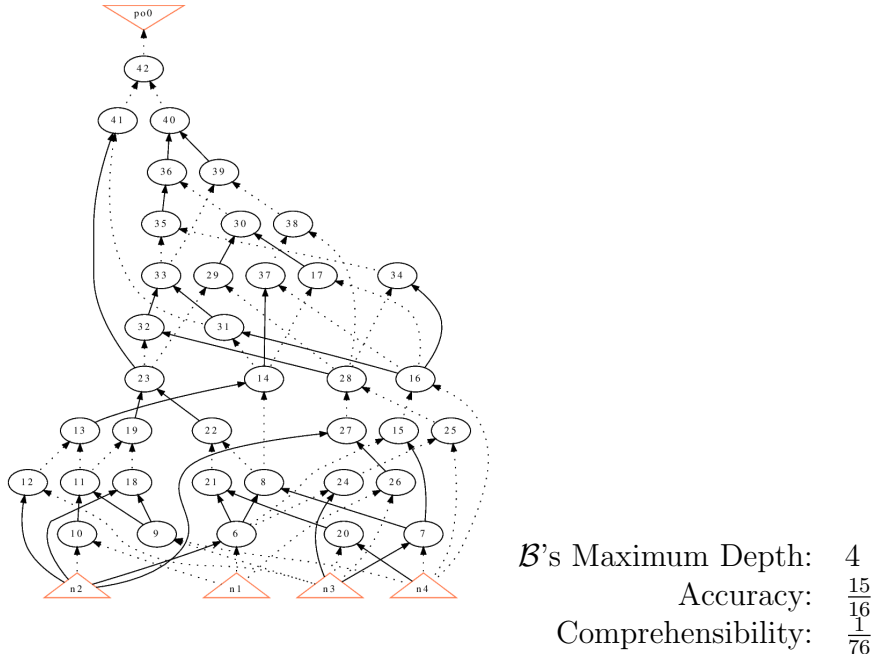
However, if we keep the neural-network-biased metric, the AIGs would most likely be more comprehensible if the noise from memorization in these AIGS is removed. For instance, if noise reduction in Figure 11.6 leaves only the homogeneous petal length and petal width pattern, then the AIG in Figure 11.6 would be improved to a comprehensibility of  $\frac{1}{9}$  (see Figure 11.3).

**Removing Noise** Using the maximum depth idea from Section 9.4.1, we can quickly remove much of the noise with no or little loss in accuracy (see Figure 11.7). Additionally, an ensemble can be used to further mitigate the noise. The next section explores the ensemble idea—future work can compile a single AIG from this ensemble.



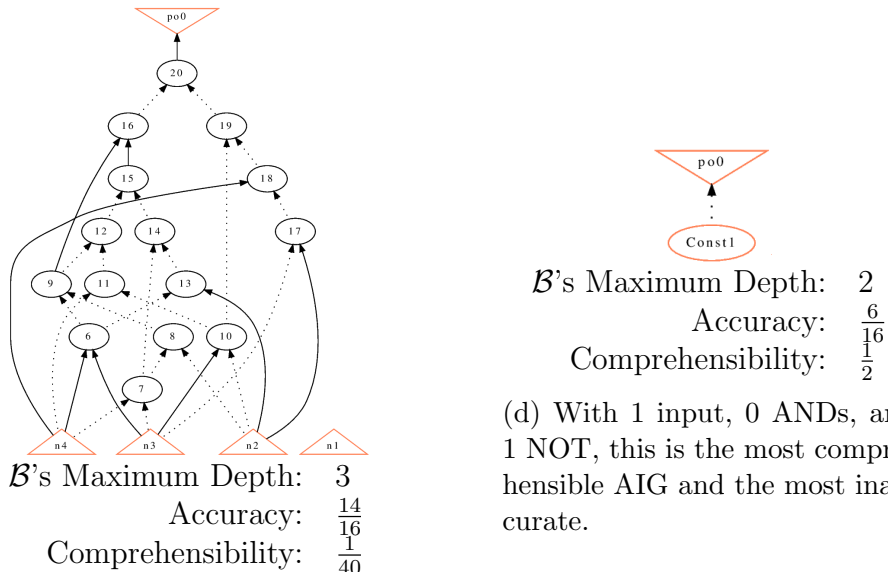
- (a) Using unlimited depth in  $\mathcal{B}$  (same as using a depth of five for this 4X5X5X5X5X1 neural network), this model has 4 inputs, 304 ANDs, and about 300 NOTs.

The network contains 37 logic nodes and 0 latches.



- (b) With 4 inputs, 35 NOTs, and 37 ANDs, this AIG is about eight times as comprehensible as Figure 11.7a.

The network contains 15 logic nodes and 0 latches.



- (c) With 3 inputs, 15 ANDs, and 22 NOTs, this AIG is about twice as comprehensible as Figure 11.7b.

Figure 11.7: AIG abstractions with varying maximum depths in  $\mathcal{B}$ .

## 11.4 Ensemble of Neural Networks and AIGs

This section investigates further mitigating the memorization problem of converting a single neural network to a single AIG. Preliminary results in Section 11.4.2 show that an ensemble is highly accurate and can successfully generalize. Furthermore, removing the noise from memorization will elicit a more concise and comprehensible AIG.

### 11.4.1 Developing and Subtle Relationships

The AIG is less accurate on input vectors when the neural network itself is uncertain. The nodes of the neural network are constantly developing relationships to minimize the network's loss. Of course, not all developing relationships become certain—some are consistently in an uncertain state. Probing the network out of an uncertain state can be done by providing it more information (more training data). During the network's search of relationships, some subtle relationships may find room to develop (especially in larger neural networks). These subtle relationships only slightly help with class prediction and often differ among neural networks. Removing the subtle or uncertain relationships with an ensemble would create an AIG that more accurately and comprehensibly represents the data set as seen by an ensemble of neural networks.

Figure 11.6 is an intricate AIG due to the memorization of many subtle and developing relationships found in the large neural network. In contrast, Figure 11.5 and Figure 11.4 represent smaller neural networks and fewer subtle and developing relationships that make the AIGs more comprehensible.

Since different neural networks have varying subtle and developing relationships, a fuzzy intersection of logic using an ensemble will extract generalized relationships. While Section 11.3 shows how a 4X2X1 neural network can articulate the feature combinations for prediction, this section uses two larger neural networks (4X3X3X1 and 4X8X8X8X8X8X1) to produce a realistic amount of noise (more subtle or developing relationships to articulate).

### 11.4.2 Neural Network and AIG Ensemble Accuracy

Table 11.6 and Table 11.7 show the average predictions for both neural networks and their respective AIGs. The values in the top row are the inputs tested. The columns are the average predictions from the neural network

Table 11.5: Summary for the two neural network ensembles of dimensions 4X3X3X1 (smaller) and 4X8X8X8X8X1 (larger) trained on the data set mentioned in Table 11.3.

| Epochs                         | 500    | 1000   | 2000   | 4000   | 8000   |
|--------------------------------|--------|--------|--------|--------|--------|
| Samples                        | 1000   | 1000   | 1000   | 750    | 500    |
| Average AIG Accuracy (smaller) | 0.9443 | 0.9604 | 0.9689 | 0.9740 | 0.9749 |
| Average AIG Accuracy (larger)  | 0.9486 | 0.9532 | 0.9511 | 0.9517 | 0.9554 |

trained on X epochs (found in the leftmost column) and the average predictions from the respective AIG. These tables indicate that the AIG ensemble accurately represents the ensemble of neural networks (given enough epochs).

In Table 11.3, the quadruple (sepal length, sepal width, petal length, petal width) on the top rows correspond to the symbols NN# and AIG# which are the neural network and AIG predictions on the respective quadruple. Conforming to previous tests, the training set for these neural networks had six unique inputs that correspond to the NN1, NN2, NN3, NN5, NN6, and NN7 inputs (Table 11.3 lists these unique inputs as well). That means NN4, NN8 (the only two homogeneous petal length/width pairs not trained on), and NN9 through NN16 (the heterogeneous petal length/width pairs) are all predicted from novel input (not in the training set).

Table 11.6: This table consists of average neural network (4X3X3X1) probabilities (listed under NN#) and average AIG approximations (listed under AIG#) given an input vector (sepal length, sepal width, petal length, petal width) (in the top rows). Interestingly, the pairs (NN11, AIG11) and (NN14, AIG14) have a negative correlation while Table 11.7 has no negative correlations. The negative correlation indicates that an AIG is less likely to correctly predict the neural network for this input vector despite that the neural network gave a more certain probability. Future work may investigate why this is.

|        | (0,0,0,0) | (0,1,0,0) | (1,1,0,0) | (1,0,0,0) | (1,0,1,1) | (1,1,1,1) | (0,0,1,1) | (0,1,1,1) |
|--------|-----------|-----------|-----------|-----------|-----------|-----------|-----------|-----------|
| Epochs | NN1       | NN2       | NN3       | NN4       | NN5       | NN6       | NN7       | NN8       |
| 500    | 0.17      | 0.12      | 0.15      | 0.46      | 0.87      | 0.84      | 0.85      | 0.71      |
| 1000   | 0.04      | 0.03      | 0.03      | 0.29      | 0.97      | 0.97      | 0.97      | 0.91      |
| 2000   | 0         | 0         | 0         | 0.08      | 1         | 1         | 1         | 0.99      |
| 4000   | 0         | 0         | 0         | 0         | 1         | 1         | 1         | 1         |
| 8000   | 0         | 0         | 0         | 0         | 1         | 1         | 1         | 1         |
| Epochs | AIG1      | AIG2      | AIG3      | AIG4      | AIG5      | AIG6      | AIG7      | AIG8      |
| 500    | 0         | 0         | 0         | 0.53      | 1         | 1         | 1         | 0.97      |
| 1000   | 0         | 0         | 0         | 0.23      | 1         | 1         | 1         | 1         |
| 2000   | 0         | 0         | 0         | 0.08      | 1         | 1         | 1         | 1         |
| 4000   | 0         | 0         | 0         | 0.02      | 1         | 1         | 1         | 1         |
| 8000   | 0         | 0         | 0         | 0.01      | 1         | 1         | 1         | 1         |
|        | (0,0,0,1) | (0,1,0,1) | (1,1,0,1) | (1,0,0,1) | (1,0,1,0) | (1,1,1,0) | (0,0,1,0) | (0,1,1,0) |
| Epochs | NN9       | NN10      | NN11      | NN12      | NN13      | NN14      | NN15      | NN16      |
| 500    | 0.65      | 0.21      | 0.56      | 0.83      | 0.83      | 0.55      | 0.65      | 0.21      |
| 1000   | 0.8       | 0.06      | 0.61      | 0.96      | 0.96      | 0.63      | 0.81      | 0.06      |
| 2000   | 0.92      | 0.01      | 0.68      | 0.99      | 0.99      | 0.68      | 0.92      | 0.01      |
| 4000   | 0.97      | 0         | 0.73      | 1         | 1         | 0.72      | 0.97      | 0         |
| 8000   | 0.98      | 0         | 0.72      | 1         | 1         | 0.73      | 0.98      | 0         |
| Epochs | AIG9      | AIG10     | AIG11     | AIG12     | AIG13     | AIG14     | AIG15     | AIG16     |
| 500    | 0.97      | 0.01      | 0.79      | 1         | 1         | 0.77      | 0.96      | 0.01      |
| 1000   | 0.96      | 0         | 0.74      | 1         | 1         | 0.77      | 0.96      | 0         |
| 2000   | 0.97      | 0         | 0.73      | 1         | 1         | 0.76      | 0.97      | 0         |
| 4000   | 0.96      | 0         | 0.73      | 1         | 1         | 0.71      | 0.95      | 0         |
| 8000   | 0.95      | 0         | 0.7       | 1         | 1         | 0.71      | 0.95      | 0         |

Table 11.7: Average neural network (4X8X8X8X8X8X1) probabilities and AIG approximations given inputs (sepal length, sepal width, petal length, petal width).

|        | (0,0,0,0) | (0,1,0,0) | (1,1,0,0) | (1,0,0,0) | (1,0,1,1) | (1,1,1,1) | (0,0,1,1) | (0,1,1,1) |
|--------|-----------|-----------|-----------|-----------|-----------|-----------|-----------|-----------|
| Epochs | NN1       | NN2       | NN3       | NN4       | NN5       | NN6       | NN7       | NN8       |
| 500    | 0.03      | 0.02      | 0.03      | 0.27      | 0.98      | 0.98      | 0.98      | 0.97      |
| 1000   | 0.01      | 0.01      | 0.01      | 0.22      | 1         | 1         | 1         | 0.99      |
| 2000   | 0         | 0         | 0         | 0.19      | 1         | 1         | 1         | 1         |
| 4000   | 0         | 0         | 0         | 0.16      | 1         | 1         | 1         | 1         |
| 8000   | 0         | 0         | 0         | 0.19      | 1         | 1         | 1         | 1         |
| Epochs | AIG1      | AIG2      | AIG3      | AIG4      | AIG5      | AIG6      | AIG7      | AIG8      |
| 500    | 0         | 0         | 0         | 0.68      | 1         | 1         | 1         | 1         |
| 1000   | 0         | 0         | 0         | 0.63      | 1         | 1         | 1         | 1         |
| 2000   | 0         | 0         | 0         | 0.62      | 1         | 1         | 1         | 1         |
| 4000   | 0         | 0         | 0         | 0.59      | 1         | 1         | 1         | 1         |
| 8000   | 0         | 0         | 0         | 0.56      | 1         | 1         | 1         | 1         |
|        | (0,0,0,1) | (0,1,0,1) | (1,1,0,1) | (1,0,0,1) | (1,0,1,0) | (1,1,1,0) | (0,0,1,0) | (0,1,1,0) |
| Epochs | NN9       | NN10      | NN11      | NN12      | NN13      | NN14      | NN15      | NN16      |
| 500    | 0.95      | 0.03      | 0.8       | 0.98      | 0.98      | 0.79      | 0.95      | 0.03      |
| 1000   | 0.98      | 0.01      | 0.84      | 1         | 1         | 0.84      | 0.99      | 0.01      |
| 2000   | 0.99      | 0         | 0.82      | 1         | 1         | 0.82      | 0.99      | 0         |
| 4000   | 0.99      | 0         | 0.81      | 1         | 1         | 0.84      | 0.99      | 0         |
| 8000   | 1         | 0         | 0.82      | 1         | 1         | 0.81      | 0.99      | 0         |
| Epochs | AIG9      | AIG10     | AIG11     | AIG12     | AIG13     | AIG14     | AIG15     | AIG16     |
| 500    | 1         | 0.01      | 0.92      | 1         | 1         | 0.92      | 1         | 0.01      |
| 1000   | 1         | 0.01      | 0.93      | 1         | 1         | 0.94      | 1         | 0.02      |
| 2000   | 1         | 0.01      | 0.91      | 1         | 1         | 0.91      | 1         | 0.01      |
| 4000   | 0.99      | 0.01      | 0.91      | 1         | 1         | 0.9       | 1         | 0.01      |
| 8000   | 1         | 0.01      | 0.92      | 1         | 1         | 0.91      | 1         | 0         |

Figure 11.8 and Figure 11.9 shows the distribution plots of AIG accuracy compared to the neural network predictions. These figures confirm that inaccuracies are more likely to occur when the neural network is uncertain (gives probabilities close to 50%). Since more training (epochs) causes neural networks to become more certain, the more trained networks yield more accurate AIGs. This training need not be enough to overfit the data. Table 11.7 and Table 11.6 shows the neural network correctly generalizes for 4000 epochs and Table 11.5, Figure 11.9, and Figure 11.8 show 4000 epochs make the neural network certain enough to yield highly accurate AIGs.

**Conclusion** In conclusion, an AIG ensemble derived from the neural network ensemble is more accurate than any single AIG. Furthermore, converting the AIG ensemble to a single AIG would help remove the intricacies of subtle and developing relationships—yielding a more comprehensible structure. Recall that using a maximum depth for  $\mathcal{B}$  removes much of the memorization noise (see Figure 11.7).

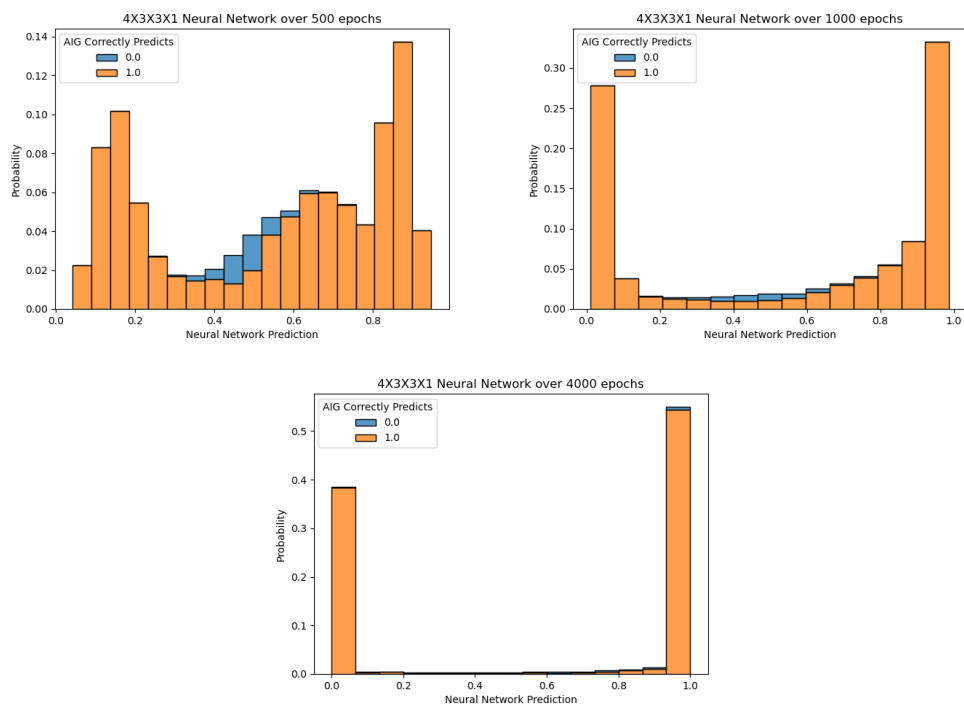


Figure 11.8: Distribution plots that shows the AIG's accuracy for all 16 inputs over all samples of the  $4 \times 3 \times 3 \times 1$  neural network for the respective number of epochs (shown in the title). The blue color denotes the portion of incorrect AIG predictions while the orange color shows the portion of correct AIG predictions. An AIG prediction is correct if it matches the neural network prediction.

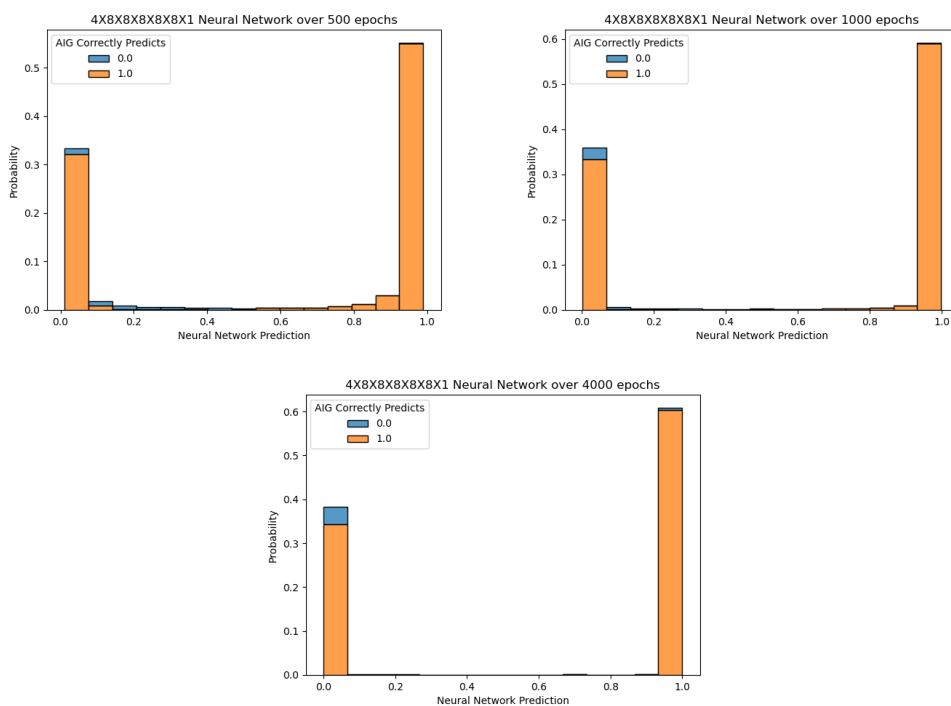


Figure 11.9: AIG approximations for the  $4 \times 8 \times 8 \times 8 \times 8 \times 1$  neural network following the standards mentioned in Figure 11.8.



## **Part IV**

## **Results**



# Chapter 12

## Results and Moving Forward

### 12.1 Conclusion

**Comprehension** In Chapter 5, I found that comprehensibility scales inversely proportional to the sum of inputs and operations. This thesis successfully translates neural networks (NNs) into the more comprehensible and-inverter graphs (AIGs)—with some loss in accuracy.

**NN to AIG** Chapter 8 found that the importance of each input (to a neural node) is the absolute value of the respective weight over the absolute sum of all weights.  $\mathcal{B}$  (Section 9.2.2) exploits this idea and implements a novel binary decision tree that computationally outperforms other decision trees for this specific problem.  $\mathcal{N}$  (Section 9.3) traverses the neural network in reverse order, skipping negligible neural nodes and implementing  $\mathcal{B}$  on other neural nodes.

#### Accuracy

**Lossy Translations** I found the accuracy of an AIG by comparing its predictions to NN predictions. The AIGs constructed by  $\mathcal{B}$  and  $\mathcal{N}$  are completely accurate on smaller neural networks that did not have room for extra noise (Chapter 7, Section 11.1). In Chapter 11, I discover that AIG predictions are accurate about half of the time for input vectors that the neural network had predictions at about 50% (uncertain predictions). This is likely due to the lossy abstractions of binarizing activation functions. Furthermore, these uncertain predictions are the developing or subtle relationships produced by

the neural networks. However, Section 11.4 shows that the AIGs produced by  $\mathcal{N}$  are highly accurate on average.

**Increasing Comprehensibility and Accuracy** Uncertain NN predictions are the primary cause of the AIG’s inaccuracy. This indicates the developing or subtle relationships cause some input vectors to yield inaccurate predictions. Furthermore, these developing or subtle relationships introduce memorization noise—decreasing the AIG’s comprehensibility. Consequently, I mitigate the AIG’s inaccuracies and incomprehensibility with a maximum depth in Figure 11.7. Potentially, ensembles can further generalize the AIG (see Section 11.4).

## 12.2 Future Work

**Pruning** Unnecessary intricacies arise when neural networks are larger than needed. Pruning the neural network before, during, and/or after training will mitigate bloated graphs such as Figure 11.6. See this brief survey for more information on neural network pruning: [53].

**Binary-Weight-Networks** Rastegari et al. found that binary neural networks (such as Binary-Weight-Networks and XNOR-Networks) often give sufficient results even with limited precision [54]. Simplifying these neural networks to AIGs would be straight forward and likely elicit results quicker and more accurately than networks with real-valued weights. A survey on binary neural networks was published by Qin et al. in 2020 [55].

**Input Space** Chapter 11 shows that capturing relationships for impossible inputs can heavily complicate the end product. To remedy this, one can remove the impossible or implausible instances from the AIG’s consideration. This can be done inside of  $\mathcal{N}$  or by amending the layered sum of products produced by  $\mathcal{N}$ . This idea could elicit a quicker algorithm and a more concise and accurate depiction of the neural network.

**Related Work** Brudermueller et al. reduced each hidden layer’s input space by using random forests or LogicNet to remove “unimportant” variables [2]. This technique also improved generalization. However, in Figure 11.7,

I found that omitting the smallest weights (using a maximum depth for  $\mathcal{B}$ ) greatly simplified and generalized the AIGs. My method is simpler and less computationally expensive than Brudermueller et al.’s.

**Dynamic Maximum Depth** A dynamic maximum depth can be used such that  $\mathcal{B}$  will not omit any weights for weight vectors like  $(-1,-1,1,1)$  and omit two weights for vectors like  $(-1,-1,0.02,0.01)$ . This will improve accuracy while minimizing noise and memorization. I illustrate constant maximum depth in Figure 11.7.

**Related Work Published After my Experiments** As mentioned in Section 6.3, Shi et al. [6] published an article that cited an algorithm [42] to approximate neural nodes with a time complexity better than  $\mathcal{B}$  ( $O(2^{0.5n}n)$  versus  $O(2^n)$ ). Additionally, Shi et al. mentions the fragility of neural networks and relates how robustness can be analyzed with the BDD produced by their algorithm, but they did not mention the memorization versus generalization problem cited by [2, 43] and seen in Section 11.2. In future work, I plan to investigate intersecting several AIGs from several trained neural networks to elicit generalization (see Section 11.4).

**AIG Ensemble** Section 11.3 shows that the final weights of neural networks could significantly differ despite that the training algorithm only changes its initial weight values. The commonality of the many AIGs over the trained neural networks appears to elicit generalization and are the paths that AIGs consistently and accurately represent from the original neural networks. Extracting this commonality will highlight the best relationships while omitting the more subtle or developing relationships (see Section 11.4 for supporting data). Furthermore, this will cause the AIGs to be more concise and comprehensible (Chapter 5).

**End Product** I chose AIGs due to their eminence in theoretical Boolean operations. Nevertheless, other graphs may be more comprehensible (e.g. majority-inverter graph ([20]) or binary decision diagrams (Section 4.1)).

**Satisfiability** This thesis introduces a new algorithm to approximate a neural network’s satisfiability of given properties.

**Multiple Outputs** One could binarize output functions such as softmax to approximate neural networks with multiple outputs. However, the AIG or other Boolean structure may give more than one answer per input.

**Comprehensibility Metric** The comprehensibility metric defined in Section 5.2.2 is heavily biased for the neural network. Future work can improve this metric to accurately represent the simpler AIG operations versus the neural network operations.

# **Part V**

# **Appendix**



# Appendix A

## Definitions

### A.1 Abbreviations

- $\mathcal{B}$ : the optimized, binary decision tree that approximates a neural node (Section 9.2.2).
- $\mathcal{N}$ : the algorithm that parses the neural network with  $\mathcal{B}$  in reverse (Algorithm 7).
- NN: neural network.
- LUT: lookup table.
- SoP: sum of products.
- AIG: and-inverter graph (Section 4.1).
- MIG: majority-inverter graph (Section 4.1).
- BDD: binary decision diagram (Section 4.1).
- $\mathbb{R}$ : the set of real numbers.
- $\mathbb{B} = \{0, 1\}$ : the Boolean set.
- $L\#_1 X \#_2$ : the  $\#_2^{th}$  node of the  $\#_1^{th}$  layer.
- $\#_1 X \#_2 X \cdots X \#_n$ : the ordered dimensions (excluding bias nodes unless otherwise stated) of an n-layered neural network starting with the input

layer's size ( $\#_1$ ). Example: 28X24X24X1 is a neural network with an input layer of size 28, two hidden layers of size 24 each, and an output layer with a size of 1.

## A.2 Mathematical Symbols

- $\leftarrow$ : assignment (read as “gets”).
- $\in$ : is an element of (read as “in”).
- $\cup$ : union.
- $\cap$ : intersection.
- $\wedge$ : and.
- $\vee$ : or.
- $\neg$ : not.
- $\mapsto$ : maps to.
- $\rightarrow$ : implies.
- $\longleftrightarrow$ : bi-implication (read as “if and only if”).
- $\forall$ : the universal quantifier (read as “for all”).
- $\exists$ : the existential quantifier (read as “there exists”).
- $\therefore$ : therefore.
- $\models$ : models (or satisfies).

## A.3 Complexity Symbols

- $O$ : Big-O notation—the asymptotic upper bound.
- $\Omega$ : Omega notation—the asymptotic lower bound.
- $\Theta$ : Theta notation—the asymptotic upper and lower bound.

## A.4 Vocabulary

- $N^{th}$ -order relationship: a loose definition conveying how nested the relationship is (see Chapter 5).
- Satisfiability: if some structure  $s$  holds for some property  $\phi$ , then this structure satisfies (models) the property. Formally,  $s \models \phi$ .



# Bibliography

- [1] R. Brayton and A. Mishchenko, “Abc: An academic industrial-strength verification tool,” vol. 6174, pp. 24–40, 07 2010.
- [2] T. Brudermueller, D. Shung, L. Laine, A. Stanley, S. Laursen, H. Dalton, J. Ngu, M. Schultz, J. Stegmaier, and S. Krishnaswamy, “Making logic learnable with neural networks,” 02 2020.
- [3] R. Guidotti, A. Monreale, F. Turini, D. Pedreschi, and F. Giannotti, “A survey of methods for explaining black box models,” *ACM Computing Surveys*, vol. 51, 02 2018.
- [4] R. Andrews, J. Diederich, and A. Tickle, “Survey and critique of techniques for extracting rules from trained artificial neural networks,” *Knowledge-Based Systems*, vol. 6, pp. 373–389, 12 1995.
- [5] M. Soeken, H. Riener, W. Haaswijk, E. Testa, B. Schmitt, G. Meuli, F. Mozafari, and G. De Micheli, “The EPFL logic synthesis libraries,” Nov. 2019. arXiv:1805.05121v2.
- [6] W. Shi, A. Shih, A. Darwiche, and A. Choi, “On tractable representations of binary neural networks,” 04 2020.
- [7] T. H. Abraham, “(physio) logical circuits: The intellectual origins of the mcculloch–pitts neural networks,” *Journal of the History of the Behavioral Sciences*, vol. 38, no. 1, pp. 3–25, 2002.
- [8] Minsky and Papert, *Perceptrons*. 1969.
- [9] D. E. Rumelhart, G. E. Hinton, and R. J. Williams, “Learning representations by back-propagating errors,” *nature*, vol. 323, no. 6088, pp. 533–536, 1986.

- [10] G. P. Zhang, “Neural networks for classification: a survey,” *IEEE Transactions on Systems, Man, and Cybernetics, Part C (Applications and Reviews)*, vol. 30, no. 4, pp. 451–462, 2000.
- [11] W. Liu, Z. Wang, X. Liu, N. Zeng, Y. Liu, and F. E. Alsaadi, “A survey of deep neural network architectures and their applications,” *Neurocomputing*, vol. 234, pp. 11–26, 2017.
- [12] E. Fiesler, “Neural network formalization,” tech. rep., IDIAP, 1992.
- [13] I. Goodfellow, Y. Bengio, and A. Courville, *Deep Learning*. The MIT Press, 2016.
- [14] D. P. Kingma and J. Ba, “Adam: A method for stochastic optimization,” 2017.
- [15] P. Ramachandran, B. Zoph, and Q. V. Le, “Searching for activation functions,” *CoRR*, vol. abs/1710.05941, 2017.
- [16] Y. LeCun *et al.*, “Generalization and network design strategies,” *Connectionism in perspective*, vol. 19, pp. 143–155, 1989.
- [17] Y. A. LeCun, L. Bottou, G. B. Orr, and K.-R. Müller, “Efficient back-prop,” in *Neural networks: Tricks of the trade*, pp. 9–48, Springer, 2012.
- [18] J. Hawkins, *On Intelligence: How a New Understanding of the Brain Will Lead to the Creation of Truly Intelligent Machines*. 2005.
- [19] W. Duch and N. Jankowski, “Survey of neural transfer functions,” *Neural Computing Surveys*, vol. 2, no. 1, pp. 163–212, 1999.
- [20] L. Amarú, P. Gaillardon, and G. De Micheli, “Majority-inverter graph: A novel data-structure and algorithms for efficient logic optimization,” in *2014 51st ACM/EDAC/IEEE Design Automation Conference (DAC)*, pp. 1–6, 2014.
- [21] A. Biere, K. Heljanko, and S. Wieringa, “AIGER 1.9 and beyond,” Tech. Rep. 11/2, Institute for Formal Models and Verification, Johannes Kepler University, Altenbergerstr. 69, 4040 Linz, Austria, 2011.
- [22] M. Vazquez-Chanlatte, “mvcisback/py-aiger,” Aug. 2018.

- [23] J. Qin, “Logic simulator for bench format.”
- [24] R. Descartes, *Rules for the Direction of the Mind*, vol. 1, p. 7–78. Cambridge University Press, 1985.
- [25] R. W. Weyhrauch, “Prolegomena to a theory of mechanized formal reasoning,” in *Readings in Artificial Intelligence* (B. L. Webber and N. J. Nilsson, eds.), pp. 173 – 191, Morgan Kaufmann, 1981.
- [26] J. Shlens, “A tutorial on principal component analysis,” *arXiv preprint arXiv:1404.1100*, 2014.
- [27] L. Deng, “The mnist database of handwritten digit images for machine learning research [best of the web],” *IEEE Signal Processing Magazine*, vol. 29, no. 6, pp. 141–142, 2012.
- [28] Y. Danilov and M. Tyler, “Brainport: an alternative input to the brain,” *Journal of integrative neuroscience*, vol. 4, no. 04, pp. 537–550, 2005.
- [29] E. B. Goldstein and J. Brockmole, *Sensation and Perception*. Cengage Learning, 2016.
- [30] C. A. Seger, “Implicit learning.,” *Psychological bulletin*, vol. 115, no. 2, p. 163, 1994.
- [31] G. A. Miller, “The magical number seven, plus or minus two: Some limits on our capacity for processing information.,” *Psychological review*, vol. 63, no. 2, p. 81, 1956.
- [32] S. Feferman, “Tarski’s conceptual analysis of semantical notions,” *New essays on Tarski and philosophy*, pp. 72–93, 2008.
- [33] C. Smorynski, “The incompleteness theorems,” in *Studies in Logic and the Foundations of Mathematics*, vol. 90, pp. 821–865, Elsevier, 1977.
- [34] W. Timberlake, “Behavior systems, associationism, and pavlovian conditioning,” *Psychonomic Bulletin & Review*, vol. 1, no. 4, pp. 405–420, 1994.
- [35] J. A. Fodor, Z. W. Pylyshyn, *et al.*, “Connectionism and cognitive architecture: A critical analysis,” *Cognition*, vol. 28, no. 1-2, pp. 3–71, 1988.

- [36] J. Sutton, *Philosophy and memory traces: Descartes to connectionism*. Cambridge University Press, 1998.
- [37] A. M. Turing, “On computable numbers, with an application to the entscheidungsproblem,” *Proceedings of the London mathematical society*, vol. 2, no. 1, pp. 230–265, 1937.
- [38] J. Nash, “Non-cooperative games,” *Annals of mathematics*, pp. 286–295, 1951.
- [39] C. F. Camerer, *Behavioral game theory: Experiments in strategic interaction*. Princeton University Press, 2011.
- [40] J. W. Weibull, *Evolutionary game theory*. MIT press, 1997.
- [41] S. Chatterjee, “Learning and memorization,” in *International Conference on Machine Learning*, pp. 755–763, 2018.
- [42] H. Chan and A. Darwiche, “Reasoning about bayesian network classifiers,” *arXiv preprint arXiv:1212.2470*, 2012.
- [43] S. Chatterjee and A. Mishchenko, “Circuit-based intrinsic methods to detect overfitting,” *arXiv preprint arXiv:1907.01991*, 2019.
- [44] N. Eén and N. Sörensson, “An extensible sat-solver,” in *International conference on theory and applications of satisfiability testing*, pp. 502–518, Springer, 2003.
- [45] M. W. Moskewicz, C. F. Madigan, Y. Zhao, L. Zhang, and S. Malik, “Chaff: Engineering an efficient sat solver,” in *Proceedings of the 38th annual Design Automation Conference*, pp. 530–535, 2001.
- [46] E. Goldberg and Y. Novikov, “Berkmin: A fast and robust sat-solver,” *Discrete Applied Mathematics*, vol. 155, no. 12, pp. 1549–1561, 2007.
- [47] F. Pedregosa, G. Varoquaux, A. Gramfort, V. Michel, B. Thirion, O. Grisel, M. Blondel, P. Prettenhofer, R. Weiss, V. Dubourg, J. Vanderplas, A. Passos, D. Cournapeau, M. Brucher, M. Perrot, and E. Duchesnay, “Scikit-learn: Machine learning in Python,” *Journal of Machine Learning Research*, vol. 12, pp. 2825–2830, 2011.

- [48] J. Ellson, E. Gansner, L. Koutsofios, S. North, G. Woodhull, S. Description, and L. Technologies, “Graphviz — open source graph drawing tools,” in *Lecture Notes in Computer Science*, pp. 483–484, Springer-Verlag, 2001.
- [49] S. Han, J. Pool, J. Tran, and W. J. Dally, “Learning both weights and connections for efficient neural networks,” 2015.
- [50] R. Raz, “On the complexity of matrix product,” in *Proceedings of the thiry-fourth annual ACM symposium on Theory of computing*, pp. 144–151, 2002.
- [51] J. Alman and V. V. Williams, “A refined laser method and faster matrix multiplication,” 2020.
- [52] P. Baldi, P. Sadowski, and D. Whiteson, “Searching for exotic particles in high-energy physics with deep learning,” *Nature communications*, vol. 5, no. 1, pp. 1–9, 2014.
- [53] D. Blalock, J. J. G. Ortiz, J. Frankle, and J. Guttag, “What is the state of neural network pruning?,” 2020.
- [54] M. Rastegari, V. Ordonez, J. Redmon, and A. Farhadi, “Xnor-net: Imagenet classification using binary convolutional neural networks,” in *European conference on computer vision*, pp. 525–542, Springer, 2016.
- [55] H. Qin, R. Gong, X. Liu, X. Bai, J. Song, and N. Sebe, “Binary neural networks: A survey,” *Pattern Recognition*, vol. 105, p. 107281, Sep 2020.

# Jarren Briscoe MSCS thesis

Final Audit Report

2021-01-29

|                 |  |
|-----------------|--|
| Created:        | 2021-01-29                                     |
| By:             | Christel Grange-Hicks (cgrangehicks@weber.edu) |
| Status:         | Signed   |
| Transaction ID: | CBJCHBCAABAAokZQn6WP25zqdz7hpBaG9iLVDtAaaJNx   |

## "Jarren Briscoe MSCS thesis" History

-  Document created by Christel Grange-Hicks (cgrangehicks@weber.edu)  
2021-01-29 - 7:19:12 PM GMT- IP address: 137.190.250.81
-  Document emailed to Jarren Briscoe (jarrenbriscoe@mail.weber.edu) for signature  
2021-01-29 - 7:20:51 PM GMT
-  Document emailed to Brian Rague (brague@weber.edu) for signature  
2021-01-29 - 7:20:51 PM GMT
-  Document emailed to Robert Ball (robertball@weber.edu) for signature  
2021-01-29 - 7:20:52 PM GMT
-  Document emailed to Kyle Feuz (kylefeuz@weber.edu) for signature  
2021-01-29 - 7:20:52 PM GMT
-  Email viewed by Kyle Feuz (kylefeuz@weber.edu)  
2021-01-29 - 7:29:10 PM GMT- IP address: 66.102.6.104
-  Document e-signed by Kyle Feuz (kylefeuz@weber.edu)  
Signature Date: 2021-01-29 - 7:29:22 PM GMT - Time Source: server- IP address: 38.94.240.75
-  Email viewed by Jarren Briscoe (jarrenbriscoe@mail.weber.edu)  
2021-01-29 - 7:40:56 PM GMT- IP address: 66.249.84.124
-  Email viewed by Brian Rague (brague@weber.edu)  
2021-01-29 - 7:56:46 PM GMT- IP address: 66.249.84.122
-  Document e-signed by Brian Rague (brague@weber.edu)  
Signature Date: 2021-01-29 - 7:57:17 PM GMT - Time Source: server- IP address: 137.190.160.74
-  Email viewed by Robert Ball (robertball@weber.edu)  
2021-01-29 - 8:43:07 PM GMT- IP address: 66.249.84.104



Adobe Sign

-  Document e-signed by Jarren Briscoe (jarrenbriscoe@mail.weber.edu)  
Signature Date: 2021-01-29 - 9:01:27 PM GMT - Time Source: server- IP address: 104.200.131.108
-  Document e-signed by Robert Ball (robertball@weber.edu)  
Signature Date: 2021-01-29 - 9:20:11 PM GMT - Time Source: server- IP address: 174.23.189.16
-  Agreement completed.  
2021-01-29 - 9:20:11 PM GMT



**Adobe Sign**